Distribution Agreement

In presenting this thesis or dissertation as a partial fulfillment of the requirements for an advanced degree from Emory University, I hereby grant to Emory University and its agents the non-exclusive license to archive, make accessible, and display my thesis or dissertation in whole or in part in all forms of media, now or hereafter known, including display on the world wide web. I understand that I may select some access restrictions as part of the online submission of this thesis or dissertation. I retain all ownership rights to the copyright of the thesis or dissertation. I also retain the right to use in future works (such as articles or books) all or part of this thesis or dissertation.

Signature:

_____ _____

Eric Salgado Date

Novel Cancer Therapeutics from Bench to Bedside

By

Eric Salgado
Doctor of Philosophy

Graduate Division of Biological and Biomedical Sciences
Molecular and Systems Pharmacology

Hyunsuk Shim, Ph.D.
Advisor

Rita Nahta, Ph.D.
Committee Member

Mala Shanmugam, Ph.D.
Committee Member

Sumin Kang, Ph.D.
Committee Member

Accepted:

Lisa A. Tedesco, Ph.D.
Dean of the James T. Laney School of Graduate Studies

Date

Novel Cancer Therapeutics from Bench to Bedside

By

Eric Salgado
B.S./B.S.CHEM, The University of Georgia, 2013

Advisor: Hyunsuk Shim, Ph.D.

An abstract of
a dissertation submitted to the Faculty of the
James T. Laney School of Graduate Studies of Emory University
in partial fulfillment of the requirements for the degree of
Doctor of Philosophy
in the Graduate Division of Biological and Biomedical Sciences,
Molecular and Systems Pharmacology
2018

Abstract

Novel Cancer Therapeutics from Bench to Bedside

By: Eric Salgado

Drug discovery and development from bench to bedside is a challenging endeavor, whereby 1 in about 5000 compounds which show initial promise actually succeed as a therapeutic. This multistep process consists of: target and hit discovery, hit-to-lead optimization, pharmacological and toxicological preclinical testing, and finally, human clinical trials. In order to provide a solid, broad training experience to lay the foundation for a career in drug development in industry, the work illustrated here highlights research performed at each phase of drug development. The three major targets selected for this work include: aromatase, CXCR4, and histone deacetylases.

After appropriate target selection, drug design becomes the next major endeavor. Pre-existing results supported that an *in silico* approach would be an efficient route for the development of a novel generation of aromatase inhibitors for breast cancer. *In silico* studies revealed key mechanistic similarities between existing therapies with that of our novel chemical scaffold. Furthermore, computational studies suggested a novel residue, Ser478, which may be exploited for further drug design. A second screening approach, virtual high throughput screening, was used for the development of novel anti-inflammatory CXCR4 modulators, given the flexibility of the CXCR4 binding site and from previous pharmacophore analyses. Upon identifying virtual hits, compounds were systematically screened via various preclinical assays and a comprehensive SAR study was conducted which revealed key differences in compound structure versus CXCR4 inhibitory activity.

Given the widely recognized roles and signaling pathways of both aromatase and CXCR4, attention was focused on the third target, histone deacetylases, and in particular, elucidating the mechanism of action of histone deacetylase inhibitors (HDACi's). Mechanistic *in vitro* and *in vivo* studies revealed that in a cancer cell line, HDACi's partly exert their function through the inhibition of HDAC9; in turn, suppressed HDAC9 levels restore levels of tumor suppressor miR-206, which negatively regulates invasion and angiogenesis. Finally, Phase I and ongoing Phase II clinical trials assessing the role of the HDACi belinostat in combination with standard of care in glioblastoma patients is summarized. This work provides the basis for the various methodologies required for a career in drug development in the pharmaceutical industry.

Novel Cancer Therapeutics from Bench to Bedside

By

Eric Salgado
B.S./B.S.CHEM, The University of Georgia, 2013

Advisor: Hyunsuk Shim, Ph.D.

A dissertation submitted to the Faculty of the
James T. Laney School of Graduate Studies of Emory University
in partial fulfillment of the requirements for the degree of
Doctor of Philosophy
in the Graduate Division of Biological and Biomedical Sciences,
Molecular and Systems Pharmacology
2018

Acknowledgements

I will forever be indebted to various individuals that have played integral roles in their support of my completion of the Doctor of Philosophy degree. First and foremost, I would like to thank my advisor, Dr. Hyunsuk Shim, for her unwavering support and endless hours of mentoring that she devoted towards the success of my graduate career. What I valued the most about my time in the Shim lab was the versatility in the scope of research that I was able to perform and how flexible she was in ensuring that I became adequately prepared for various career alternatives as a PhD scientist. Thank you, Dr. Shim, for my development as a cancer researcher.

I also would like to extend my gratitude to my dissertation committee, Drs. Rita Nahta, Sumin Kang, and Mala Shanmugam for challenging my views and always providing valuable insight towards my dissertation work. Given the interdisciplinary nature of my dissertation, they found ways to seamlessly connect the various themes in my work and helped ensure that I stayed on track with my experiments.

Finally, I would like to thank my parents, Gloria and Eric, and grandmother, Nubia, because I would certainly not be the man I am today without their care, compassion, and trust in me. I will become the first in my entire family to receive a doctoral degree from an American institution as a first-generation Latin-American. I come from a modest childhood in the suburbs of Jackson Heights, Queens, New York, a predominantly Hispanic suburb, where unfortunately education was not a reality for many. My parents and grandmother have always stressed the importance of an education and have always been there to celebrate all of the awards and accomplishments that I have amassed throughout my educational career. Their unconditional love and support for me in all aspects of my life is something I will always cherish and for that, this doctoral degree is especially dedicated to the three of them. Los amo, Mami, Papi, y Mita, hoy y siempre.

Table of Contents

List of Figures

Chapter 1

Chapter 2

Chapter 3

Chapter 4

Chapter 5

List of abbreviations

IP	Intellectual property
LDH	Lactate dehydrogenase
HTS	High-throughput screening
siRNA	small interfering RNA
SAR	Structure Activity Relationship
PDB	Protein database
RT-PCR	Reverse transcriptase polymerase chain reaction
MMTV	Mammary tumor virus long terminal repeat
FDA	Food and Drug Administration
IND	Investigational New Drug Application
MTD	Maximum Tolerated Dose
NDA	New Drug Application
ER	Estrogen Receptor
AI	Aromatase Inhibitor
AIAA	Aromatase-Inhibitor associated anthralgia
SERM	Selective estrogen receptor modulator
AR	Androgen receptor
NSAID	Nonsteroidal anti-inflammatory drugs
GI	Gastrointestinal
COX	Cyclooxygenase
PG	Prostaglandin
CXCR4	C-X-C chemokine receptor type 4
SDF-1	Stromal-derived-factor-1
CXCL12	C-X-C chemokine ligand 12
vHTS	Virtual high-throughput screening
FRESH	FRagment-based Exploitation of modular Synthesis
PI3K	Phosphoinositide 3-kinase
TNBC	Triple negative breast cancer
HDAC	Histone deacetylase
HDACi	Histone deacetylase inhibitor
VEGF	Vascular endothetlial growth factor
HAT	Histone acetyltransferase
ATDC	Ataxia telangiectasia group D-complementing protein
PR	Progesterone receptor
HER2/neu	Human epidermal growth factor receptor 2
miRNA	microRNA
GBM	Glioblastoma
sMRI	Proton spectroscopic MRI
RT	Radiation therapy
OS	Overall survival
SAHA	Suberanilohydroxamic acid
sMRI	Proton spectroscopic magnetic resonance imaging
IRB	Institutional Review Board
IHC	Immunohistochemistry
NAWM	Normal appearing white matter
IDS-SR	Inventory of Depressive Symptoms-Self Report
PFS	Progression free survival

Chapter 1

Scope of Drug Discovery & Development Research: An Outline

1.1. Natural products as the initial source of therapeutic relief and a driver for small-molecule discovery

The use of exogenous substances as an intervention to cure human diseases has long been documented across various early Chinese, Indian, Babylonian and Egyptian civilizations. These ancient civilizations quickly discovered that certain herbs and plants harbored medicinal properties, that, while their mechanisms of action remained unknown, somehow alleviated certain complications of human diseases. Resins of *Boswelia* trees were exploited for their antiseptic properties; essential oils and alkaloid plants exhibited anti-hypertensive properties, and soothing balms were effective at alleviating skin complications. Many therapeutic formulae encrypted in Egyptian hieroglyphics have since been translated and are remarkably still in use today (1). Natural products remained the sole source of deriving therapeutic benefit prior to the advent of medicinal and synthetic chemistry in the nineteenth century, which allowed for precise analytical techniques capable of identifying bioactive compounds in natural samples.

One of the most fundamental discoveries that laid the foundation for drug discovery research was the isolation and characterization of morphine from opium by Sertürner in 1806. This vastly revolutionized the field of therapeutics and paved the way for the first class of alkaloid drugs that were subsequently developed throughout the early 1800s (2). Theories then developed that described chemical structure and bonding eventually gave rise to modern organic and medicinal chemistry, and in 1869, Crum-Brown and Fraser postulated that “it is obvious that there must exist a relation between the chemical constitution and the physiological action of a substance” (3). These ideas dramatically shifted the drug discovery paradigm due to the fact that scientists were now able to identify and isolate specific compounds responsible for eliciting the desirable effects in certain natural products.

Natural products continue to play a significant role in drug development; a meta-analysis highlighted that roughly 49% of 175 FDA-approved cancer therapeutics from the 1940s to the end of 2014 were either direct natural products or natural product derivatives (4). However, as analytical laboratory techniques have evolved to elucidate distinct biological structure and function, scientists have exploited these structures to design semi-synthetic or purely synthetic compounds that may better compliment the target protein compared to their fully natural counterparts. While advancements in medicine have made it possible to design such eloquent, diverse chemical scaffolds capable of targeting most, if not all conditions, one must keep in mind that not all may qualify as viable therapeutics, even if they display high affinity and specificity for the desired target. Thus, there exists a stringent set of procedures that must be followed in order to successfully maneuver a promising lead from discovery to the clinic.

1.2. Brief summary of the traditional drug discovery and development process

Statistically speaking, there is a 0.02% chance that a compound which showed initial promise will actually translate into a successful therapeutic. The drug discovery and development process has proven to be a very costly and timely endeavor; on average, it takes nearly 15 years to progress an experimental drug from bench to market. Out-of-pocket costs accrued throughout this 15 year journey amount to about $1.4 billion, a number that continues to rise (5). While there is no singly defined path in drug discovery, there have been significant paradigm shifts due to scientific advancement that affect how a particular therapeutic may proceed from the bench to the clinic. Prior to the mid 80's, drug discovery research was primarily chemistry focused rather than target-driven; in other words, once a lead compound was obtained (generally natural product derived), structure-activity relationship (SAR) studies were conducted in attempt to optimize the lead structure into a more promising therapeutic. This procedure required an intricate collaboration between the synthetic chemists responsible for the design of the compounds and the biomedical researchers conducting the SAR studies (6).

Throughout the next two decades, there were two significant scientific contributions that paved the foundation for the next generation of drug discovery research: high-throughput screening (HTS) methodology and the human genome project. Collectively, these two efforts have shifted drug discovery research which now allow for target-driven lead identification by the massive simultaneous screening on the order of hundreds of thousands of compounds. The early stages of HTS can be traced to the late 1980's, when companies such as Pfizer would use 96-well plates and reduced assay volumes of about 50-100uL to screen approximately 800 compounds per week. By 1989, this number increased nearly 9-fold to about 7200 compounds per week (7). Technological advancements made it possible for the automated, massive parallel screening of compounds for the identification of leads. Completed in April of 2003, the human genome project

successfully identified for the first time the approximately 3 billion base pair sequence of the human race (8). Data from this project revealed an approximate 20,000 to 25,000 genes that are encoded within the human genome and thus, revealed a vast number of "druggable" targets that could potentially be linked to certain diseases. Therefore, not only did researchers have the means to automatically filter through thousands of compounds to obtain leads, they also had insight from the human genome project as a guide to know the biological targets worth pursuing.

It is important to note that while HTS screening has vastly improved the drug screening process, HTS is not always required for the identification of such hits. Depending on the information that is known *a priori* about the target, scientists may already have an idea in terms of the pharmacophore that they are interested in and thus, would bypass the massive HTS process and may instead focus on optimizing the lead structure(s). The rest of this chapter will aim to summarize the drug discovery and development process, beginning from the identification of lead compounds and going to Phase IV clinical trials and subsequent FDA approval of the therapeutic. The figure on the following page highlights the key steps that are involved in this process.

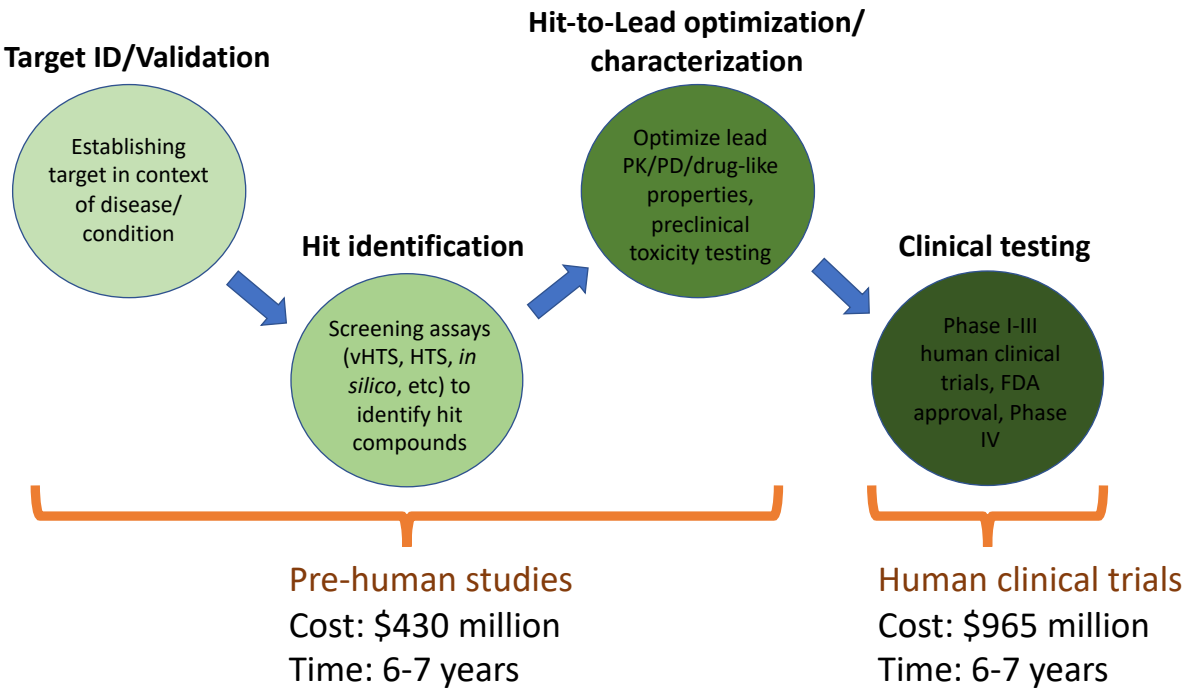

Figure 1.1. Brief schematic of the drug discovery and development process. Each circle corresponds to a different phase of drug development. It is important to note that the time and money spent in each phase is not equal and varies between phases. A study from Tufts Center for the Study of Drug Development in 2016 showed the rising out-of-pocket cost of bringing a therapeutic from bench to market over the previous decade and is now estimated to be around 1.4 billion dollars (5).

1.2.1. Target Identification/Validation

A "target" is a broad term that can simply be defined as any biological entity (i.e. nucleotides, proteins, polysaccharides, lipids) that harbors a property that renders it "druggable," due to its relevance to a given disease or condition. Not only should the target be druggable, it should also be safe, efficacious, and meet clinical and commercial standards. A study in 2011 defined a druggable target as one that "is accessible to the putative drug molecule, be that a small molecule or larger biologicals and upon binding, elicits a biological response which may be measured both *in vitro* and *in vivo*" (9). While all biological entities have the potential of being a target, the vast majority of currently prescribed drugs target proteins (10). Two reasons account for this phenomenon: it is extremely challenging to design specific, potent, and non-toxic drugs for the other three classes of macromolecules, and because most successful protein-targeting drugs exploit their active site and tend to compete with its endogenous ligand for binding (11). While specificity and toxicity issues may still arise by targeting proteins, the chances of such problems arising are generally smaller than with the other classes of macromolecules. Nonetheless, appropriate target identification and validation in the context of its relevant disease is critical for providing rationale for the drug discovery effort.

Previous analyses have advocated that target selection is one of the most important facets of drug discovery; in fact, a study highlighted that approximately 30-40% of experimental drugs fail because of inappropriate target selection (12). With advancements in scientific technology and communication, the number of identifiable and reliable targets has increased dramatically due to various data mining approaches. Data mining is a bioinformatics approach that involves the complex filtering of targets through a combination of literature databases, microarray data mining, and statistical and computational algorithms to identify candidate targets (13). The biomedical literature database MEDLINE/Pubmed has become the most popular means of sharing peer-

reviewed scientific content, containing over 18 million literature abstracts. If a research group has *a priori* knowledge or interest about a target, they can simply enter key words or phrases into the database and all previously published content about the target will be readily available. Microarray data may sometimes be regarded as a "fishing expedition" approach, where one may either perform unsupervised clustering, which involves searching for genes exhibiting similar expression patterns, or supervised classification, where one can search for genes distinguishable between tissue types (e.g. cancerous vs normal) (13). Efforts from either of these approaches may then become integrated where aggregate data such as proteomic data, meta analyses, protein-protein interactions may all become conglomerated to produce a series of therapeutic targets or diagnostic markers.

Once identified, any drug target must then be evaluated and validated for its potential therapeutic applicability towards its relevant disease. Some of the most common approaches involve functional studies, whereby genetic knockdown, knockout, or, any modulators such as antibodies or small molecule drugs (if available) can demonstrate whether or not it has a phenotypic consequence in the relevant biological system. For instance, if data mining approaches revealed a potential growth factor involved in an oncogenic proliferative pathway, then a small-interfering RNA (siRNA) specific for that growth factor can be introduced in an *in vitro* system to confirm that this growth factor does indeed regulate proliferation. One other popular validation tool would be a transgenic mouse model which has the target gene either mutated or knocked out entirely. This offers a unique advantage in that it involves whole, live animals and any phenotypic endpoint may be measured indefinitely, especially if the endpoint is one that may take longer to be observed. One recent example using a transgenic mouse model was a study by Yuan et al in 2018 where they showed that transgenic mice which overexpressed the human form of the enzyme aldose reductase (AR) showed impaired atherosclerosis regression in diabetic mice, demonstrating

the role of the enzyme in the disease (14). The importance of target validation to its disease in both *in vitro* and *in vivo* models instills confidence for the drug discovery project moving forward.

After having established a promising target, a review by Gashaw et al in 2011 outlined additional properties that should be ideally be met to rationalize a target in drug discovery, which include, but are not limited to: (i) having a favorable "assayability" suitable for high throughput screening (will be discussed in detail in a later section); (ii) target expression is discrete and not ubiquitious; (iii) identifying a disease/target specific biomarker to assess therapeutic efficacy; (iv) knowledge of potential adverse effects via genetic mutation studies and/or knockout mice studies; (v) intellectual property (IP) rights on the given target (15). Discrete tissue expression is favored in any drug discovery project in order to minimize potential side effects that the therapeutic might elicit. Furthermore, in most cases, monitoring therapeutic efficacy may not always be as obvious, especially in preclinical mice *in vivo* or in human clinical trial studies; thus, identifying a disease specific or target-specific biomarker would be instrumental in assessing the therapeutic potential of the target-modifying drug. A classic example of a liver biomarker used to assess liver function is the enzyme lactate dehydrogenase (LDH) – LDH is normally expressed within the liver; however, in the event of liver injury, LDH levels in serum become elevated and can easily be detected (16-19). Not only should a target have a reliable means of measuring therapeutic efficacy, the target should also have a predicted side effect profile, either from knockout mice studies or genetic mutation studies. Finally, while IP rights may not necessarily be required to pursue a target in drug discovery, having the intellectual and scientific freedom to conduct original research will ensure that no competitor will seize control of the target and thus, prevent the shift of potential revenue to another research group.

1.2.2. Hit identification

Upon successfully establishing and validating an appropriate target for drug discovery,

efforts then become focused to identify lead compounds which show preliminary promise that may be pursued further. A hit compound is a loosely defined term that refers to any compound which demonstrates the desired activity in a screening assay which can then be recapitulated upon retesting (9). Several different screening strategies exist which allow for precise identification of hit compounds; however, the type of screening paradigm that a research team might pursue oftentimes depends on *a priori* knowledge about the target and/or previous hits. The following section will focus on those strategies that were employed in the original work that contributed to the writing of this dissertation, which include: high-throughput screening (HTS) and *in silico* virtual drug design.

1.2.2.1. High-throughput screening

HTS has received considerable widespread popularity over the past two decades and involves the use of automated systems to simultaneously screen massive amounts of compounds in a relatively short period of time. This parallel compound screening is usually done in multi-well plates where each well acts as a separate system to test one of the several compounds to be screened. Not only can HTS methodologies screen large quantities of compounds without human intervention, due to the miniaturization of these systems, only a remarkably minute amount (i.e. micrograms) of each compound is needed to screen for activity (20). A successful HTS procedure should have the following components optimized prior to its execution: (i) suitably arrayed compound libraries; (ii) an appropriate assay that has been configured for automation; (iii) robots suitable for performing the automated assays; (iv) a computerized system for handling and storing the data (21).

Selection of a suitable compound library may either be unguided (i.e. can screen random compounds with diverse chemical scaffolds to identify any promising preliminary leads) or the

research team might have some general knowledge for the pharmacophore(s) that will guide the HTS effort. The evolution of compound libraries in drug discovery stems from the 19th century where natural product extracts and synthetic dyes were among the first classes of chemicals used to identify drug targets. It became increasingly apparent that these strategies alone could not provide a robust framework to screen on the other of thousands to hundreds of thousands of compounds in a given HTS screening. Therefore, natural product extracts and synthetic dyes soon became replaced with synthetically derived compounds (22). Pharmaceutical firms were the source of the first chemical library collections available for HTS as some companies had archival collections of synthesized compounds suitable for library screening. These early libraries were generally unsuccessful as many of these compounds harbored poor physicochemical properties. This lead to an increased awareness that each library member should possess "lead-like" qualities. As a result, smaller, more focused libraries with the potential for optimization were developed and are still ongoing today (22). A research group can purchase diverse scaffolds of interest from firms who specialize in generating robust, eloquent libraries.

Selection of an appropriate assay that has been optimized for automated screening becomes the next major hurdle. Intuitively, the type of assay employed largely depends on the biology of the target and whether the functional consequence of manipulating the target can be precisely identified and/or quantified. The use of reporter genes in HTS assay development has emerged as a popular means for compound screening because it provides a visual and quantitative means for measuring compound efficacy. A couple of the most commonly used reporter genes include, but are not limited to, the luciferase gene derived from fireflies (23) and green fluorescent protein gene derived from the jellyfish Aequorea victoria (24). These reporter genes may either be transiently transfected into an appropriate model cell line or may be permanently integrated into the genome of the appropriate cell line that usually overexpresses the target of interest via a lentivirus. It is

imperative that the reporter gene is fused either directly downstream of regulated activation sequences of DNA such as promoters (if measuring transcriptional activity), or directly downstream of the protein coding sequence of the target. This ensures that any fluorescent visualization that is generated in the cell system is attributed solely to either activation or inhibition of the target (23, 24). Furthermore, because these two reporter genes are not found in mammals, there is no endogenous activity that can be measured and thus, there is low background noise and the signal measured becomes substantially reliable.

As previously mentioned, the goal of HTS is to provide an automated means for screening massive compound sets that could not otherwise be done manually. Therefore, the research group must also ensure that they have the robotic machinery capable of performing as well as storing the data as each assay is completed. Technological advancements have allowed for machines to perform a variety of automated tasks such as diluting and dispensing chemicals to appropriate wells. Common bench procedures such as centrifugation and well rinsing pose a significant challenge and should be avoided in an automated HTS effort. Ideally, an assay should be optimized so that only a minimal number of steps are needed for assay execution. The best case scenario would be one in which the assay can be run on a single well with the only manipulation being a simple injection of the sample to be tested (21). Finally, given the vast number of chemical libraries and compounds to be tested, there must exist an electronic means that is powerful enough to store and manage the data that is being collected after every round of screening. It should be organized in a way that allows for the research group to not only readily identify compounds that achieved a certain threshold, but also categorize the data in terms of chemical scaffolds and laterally assess the efficacies of the compounds within each scaffold.

1.2.2.2. in silico virtual drug design

While HTS continues to remain as the gold standard for early-stage drug discovery in the pharmaceutical industry, some of its limitations may deter its applicability in certain drug discovery efforts. For instance, HTS is usually not only very costly, it is also very time-demanding and requires for the group to either have the robotics capable of performing the task or have a high throughput screening core at their institution. Therefore, there has been an increasing use of rational, structure-based drug design (i.e. *in silico* virtual drug design) via computational methods (25). Arguments in favor of *in silico* virtual screening claim that this is a more efficient way than traditional drug discovery efforts because it aims to understand the molecular basis of the target in context to its disease. Thus, scientists using this methodology might get a much more profound understanding of the critical interactions involved in both ligand-target binding as well as drug-target binding at the atomic level. Because *in silico* methodologies are exclusively computationally based, the costs associated with this screening method are far less substantial than with HTS (25). However, it is important to note that a crystallized X-ray structure of the target must exist or else *in silico* drug design cannot be possible.

Two of the most common approaches in *in silico* drug design include virtual screening and *de novo* drug design. Virtual screening involves taking large virtual libraries of drug-like compounds and computationally screening hundreds of thousands of compounds against the protein target of interest. Usually, these compounds are commercially available, and those who have favorable predicted drug-protein interactions may then be ordered for subsequent testing. *De novo* drug design entails developing a thorough understanding of the target and exploiting its active site to design structurally novel molecules that may bind potently to the target. Indeed, structure-based drug design has enjoyed recent success in drug discovery efforts, and in some cases, the hit rates were shown to be greater than with HTS (26, 27). Thus, the feasibility and applicability of *in silico* drug design proves to be an invaluable asset in the realm of drug discovery research. Figure

1.2 on the following page summarizes the general procedures involved in any *in silico* drug discovery project.

The first major step in a virtual screening project involves pre-processing the 3D structure of the target (usually X-ray crystal structure). There is an online repository of solved protein 3D structures in the protein data bank (https://www.rcsb.org/) that is the most common way of accessing this information. Careful consideration of the appropriate protein dataset must be employed because in some cases, there might be more than one, if not several, solved, crystallized structures. These structures may all differ in the resolution with which the protein structure was solved as well as any ligand(s) that may have co-crystallized with the target of interest. After choosing and downloading the most feasible protein database (PDB) file, once it is visualized on a docking software (such as Schrodinger Maestro), it will then need to be refined so that it most accurately represents a physiologically relevant structure. PDB datasets typically only displays heavy atoms (i.e. non-Hydrogen atoms) as well as water molecules, cofactors, activators, ligands, and metal ions associated with the target. Furthermore, this crude PDB file usually gives no insight on residue ionization and tautomeric states. Thus, there are several protein preparation algorithms that help address these issues to more accurately represent the target *in vivo* (28). Moreover, it is

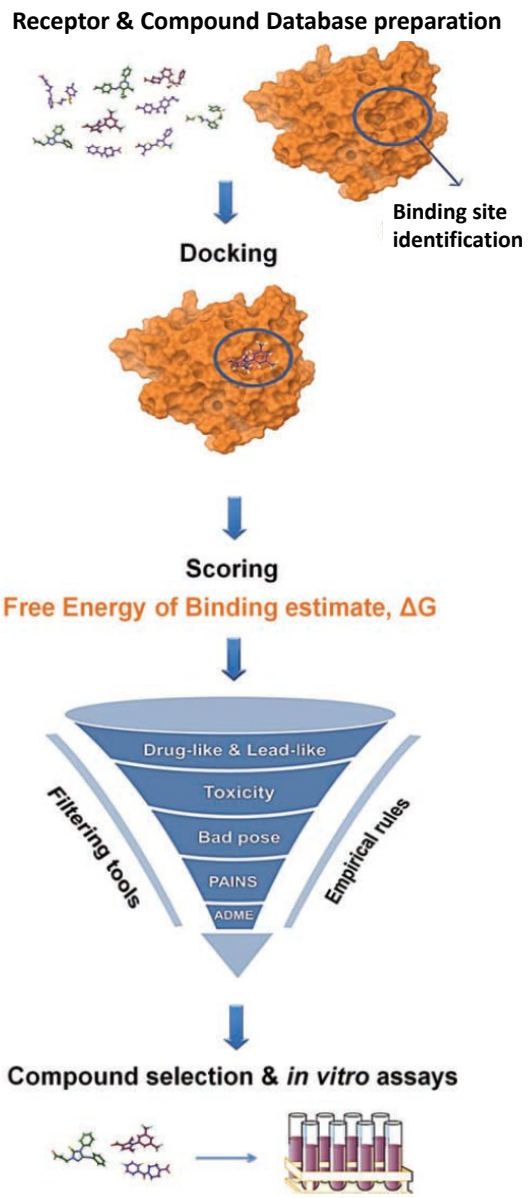

Figure 1.2. Workflow for a typical virtual screening protocol. Both the target and ligand need to first be pre-processed and optimized prior to screening. Computational software such as Schrodinger Maesto and Glide will virtually screen compounds against the target and assign them docking scores which is indicative of their predicted potencies. After filtering for drug-like and favorable ADMET properties, those selected compounds will then be subject to laboratory testing. Adapted by permission from Bentham Science Publishers: *Curr. Top. Med. Chem.* Lionta et al., copyright (2014).

imperative that the research team identifies the target binding site in order for the docking software to screening ligands against that binding site.

After the target has been processed and optimized for docking and the binding site has been identified, the next major goal is selecting a suitable virtual library for screening. Approaches that a research team may employ might depend on whether virtual screening or *de novo* drug design is desired. Generally, virtual screening is the preferred method of choice if there is no *a priori* information on pharmacophores or structure sets. Ideally, it is not advisable to dock huge compound collections (i.e. "blind docking") because it is highly computationally demanding and results in an unreasonable amount of compound sets for filtering. Thus, a research team should focus on a smaller subset of compounds that might already harbor drug-like properties with a favorable toxicity profile. For instance, the publicly available online application Chembioserver is a tool that specializes in filtering and selecting small molecules that possess these qualities (29). If *de novo* virtual design is employed, then there might likely be a rationale for the research group to focus on a particular subset of compounds to be screened. One example would be if the research team is interested in designing small molecules that are analogs of the endogenous ligand; since the endogenous ligand obviously binds well to the target, designing analogs structurally similar to its ligand may allow for efficient perturbation of the system. Nonetheless, with the employment of either approach, all compounds that will be subject to screening must be optimized and processed as well to represent chemically relevant 3D structures. This includes having realistic bond lengths, formal charges, and be devoid of solvent molecules and counter ions (30, 31). Collectively, these efforts will ensure that both the target and the compounds will be chemically and structurally optimized for docking.

Upon successful ligand and target optimization, docking becomes the next major endeavor. A number of docking programs have been developed for this purpose, such as Glide and LigandFit

(32, 33). Generally speaking, docking is the process of generating predicted protein-ligand poses for every screened compound and scoring their poses so that they can be rank-ordered and compared with the other compounds in the dataset. Docking programs employ a variety of different scoring functions that can be modified to most accurately quantify the sum of interactions between the ligand and target. Some of these scoring functions include: (i) force field-based functions that take the sum of the strength of all intermolecular van der Waals, electrostatic interactions and hydrogen bonding between all ligand-target atoms to generate a binding free energy; (ii) empirical scoring functions which place more of an emphasis on the unique types of interactions between the ligand and target; and (iii) knowledge-based functions, which use statistical observations of known receptor-ligand complexes to generate an approximated free-binding energy for the ligand and target (34). While these scoring functions provide a quantitative means to rank order compounds, a research team should proceed with caution as scoring alone may fail to correctly rank different compounds (35). Instead of relying solely on rank-ordering compounds based on their docking scores, a research team instead may analyze the docking poses generated for each compound; they may take two compounds that are similarly structured that may differ in predicted binding energy to identify the reason for this drop in predicted binding, whether it be steric clashes to the target, or an unfavorable ligand conformation. To help circumvent issues in ligand-target scoring, Ravindranathan et al have developed a physics based scoring function that has shown to correlate better with affinity data with the advent of MM-GBSA scoring. (36).

Finally, once ligand-target poses have been generated, rank-ordered, and analyzed for feasibility/practicality, additional filters must be incorporated to select for those compounds which possess drug-like properties that show favorable ADMET properties, such as obeying the Lipinski rule of five (i.e. molecular weight less than 500 g/mol, H-bond donors less than 5) (37). It is only after all of these steps have been completed that there should finally exist a subset of compounds

(i.e. hits), from either HTS, virtual screening or *de novo* drug design, that may then be synthesized and subject to preclinical testing which showed favorable *in silico* characteristics. The following section will discuss the next phase in drug development, which involves hit-to-lead optimization in the preclinical setting.

1.2.3. Hit-to-Lead optimization/characterization

Following a successful HTS or *in silico* approach in identifying candidate hit compounds, a rigorous evaluation of those hit compounds must be carried out to determine those who will progress as lead compounds. As one might expect, in carrying out massive parallel HTS screenings and/or virtual screening, there is the possibility of obtaining false-positive hits, which may hinder the drug discovery effort moving forward (38). A review by Keseru et al in 2006 highlighted three different approaches that might be employed to selectively filter for promising leads: (i) hit evolution; (ii) bioisosteric replacements; and (iii) hit fragmentation, or any combination of these (39). Hit evolution involves analyzing the core structure of the hit compound(s) and synthesizing analogs of those compounds which might have different substitution patterns. These analogs are then subject to various affinity screening assays to identify analogs that might have similar or perhaps improved K_d values. Initial SAR results conducted from these studies then serve as a catalyst for further medicinal chemistry efforts and in the generation of lead-like compounds. The principle of bioisosteres aims for the improvement of stability, membrane permeability and pharmacokinetic properties of hit compounds and entails replacing functional groups with those of similar size, hydrophobicity, and electronegativity that still retain biological activity. The phenomenon of bioisosteric replacement for lead optimization has proven successful for many drugs against diseases such as T-cell leukemia, malaria, and Alzheimer's disease (40). Hit fragmentation, as its name implies, is generally applied towards hits of high molecular weight and

involves structurally decomposing the compound into subsets to identify promising fragments with minimum pharmacophores. Once these fragments have been established, they can then be used as starting points for fragment expansion and developing better lead-like compounds (39).

At this point in the drug discovery effort, there should exist a specific subset of compounds that have been filtered from HTS and/or *in silico* hits that progress as lead compounds. It is important to note that the process of hit discovery-lead generation/testing is not unidirectional and oftentimes can be an iterative process. Compounds which initially showed promise as leads may prove to be unsuccessful upon subsequent testing and thus, might entail the research team to retract and begin anew. Nonetheless, once a series of candidate leads have been proposed, the next step requires for subsequent optimization and characterization in relevant model systems. As previously mentioned, the goal of HTS and *in silico* virtual screening approaches is to simply identify compounds which have shown preliminary promise via a crude screening protocol. There is usually limited information about specific mechanisms of action of the lead compounds and it is here where pharmacological and toxicological studies must be performed to formally characterize the lead compound(s) potential for progression into human studies. While assays on purified proteins have become the standard for detecting potent compounds, little information is known about how perturbation of the target in a model system might be affected at the cellular and organismal levels. Thus, characterization of the lead compounds is also essential in whole cell and *in vivo* systems in order to better predict how the lead compound might perform in humans (41).

Preclinical studies at the *in vitro* level mainly aim to demonstrate specific macromolecules (i.e. DNA, RNA, protein) that are perturbed by introduction of the lead compound. Common techniques used include, but are not limited to: (i) reverse-transcriptase polymerase chain reaction (RT-PCR) to assess lead impact on gene transcription; (ii) western blot analyses to evaluate impact on protein expression and/or downstream pathway activation or inhibition; (iii) functional assays

(i.e. kinase assays) to determine how the lead compound might intervene in the target's ability to perform its cellular function. Information about dosing is also comprehensively evaluated as this will be essential for *in vivo* studies and human clinical trials moving further. Generally, there is also a functional assay that is measured to correlate biochemical changes to cellular phenotypes, such as cell viability or tumor infiltration (42). Not only should the pharmacological mechanisms be elucidated in these studies, there should be methods to assess for potential adverse effects of the lead compounds. The types of toxicological tests might vary depending on the proposed mechanism of action of the lead compound. Generally speaking, drug-induced liver injury is the most common cause of toxicity (and the reason of withdrawal of drugs from the market) (43). Thus, one universally recognized method for measuring toxicity is by using a hepatocyte screening system. Since hepatocytes (i.e. liver cells) are the primary site for xenobiotic metabolism, information such as drug-drug interaction, metabolite formation and drug toxicity can all be evaluated in this type of screening (44). Results from the various *in vitro* screening assays may provide sufficient evidence to progress the lead into *in vivo* studies.

One of the main reasons that many lead compounds are first screened in cells is because of the costs associated with animal experiments, in addition to ethical concerns about freely experimenting on animals without a significant rationale to back up those studies (45). However, results from *in vivo* studies prove to be invaluable in preclinical research as this becomes our best predictor of how the lead compound might be tolerated in humans. Information such as the route of administration, half-life, bioavailability that could not otherwise be done in *in vitro* experiments are done in *in vivo* experiments (46). Mice and rats are among the most popular types of animals used in such studies due to their relative ease of manipulation and rate of reproduction. As one might expect, the *in vivo* model that is used should be as closely similar to a human model as possible. There are several types of mouse models that involve either genetic or immune

intervention which may better recapitulate the relevant human system: (i) transgenic mice; (ii) implantation of human xenografts into immune-deficient mice; (iii) orthotopic implantation (47).

Transgenic mouse models offer a unique advantage in that it allows for the *in vivo* development of a relevant human disease state that can be modeled in immunocompetent mice. Using breast cancer as an example, there are several oncogenic targets that are typically amplified in breast cancer: c-myc, cyclin D1, and ErbB-2, among others (48). Typically, these genes are fused with a strong tissue specific promoter such as the mammary tumor virus long terminal repeat (MMTV) and results in mammary adenocarcinomas which can be tracked through time to observe the effects of gene overexpression on tumor progression (49). However, some of the limitations with the use of transgenic mouse models include limited metastasis, loss of estrogen receptor positivity throughout tumor progression and the length of time required for the mice to develop tumors upon conception (47). A second common type of mouse model is a xenograft mouse model, in which human tumor cells are transplanted either under the skin or directly into the organ type in which the tumor originated. However, it is important to note that these tumor xenografts are typically only readily accepted in immunocompromised mice. Arguments in favor of this type of *in vivo* model claim that it is a better predictor of therapeutic efficacy given that the tumors are of human origin and not of mice (50). The last type of model, orthotopic implantation, involves the injection of a relevant human cell line into immunocompromised mice. Unlike a transgenic mouse model, orthotopic mouse models are commonly used to assess metastasis inhibition formed by a malignant tumor type (such as the triple negative MDA-MB-231 breast cancer cell line) that is injected into mice, typically into the fat pad. Furthermore, the costs associated with orthotopic models are generally lower than with the previous two mouse models (51). Thus, there exists a variety of *in vivo* options at the disposal of the research team and oftentimes, more than one model

type is used that more reliably assesses how the lead compound performs in a fully intact biological system.

1.2.4. From cells to humans: clinical trials

It is only after a candidate lead compound has undergone rigorous *in vitro* and *in vivo* testing that it may proceed into human clinical trials. At this point, the drug candidate should have sufficient evidence supporting its rationale as a viable therapeutic, which includes, but are not limited to: (i) showing selective binding to the target receptor site; (ii) eliciting the desired functional response of the target molecule; (iii) demonstrate adequate bioavailability and biodistribution in eliciting the desired response(s) in animals and humans; (iv) pass formal toxicity testing in animals (46). In order for a candidate drug to enter clinical studies, it must be approved by a regulatory agency, respective to the country in which clinical testing will be conducted, that exhibits substantial and dominant control over the requirements for drug testing and subsequent approval. The regulatory agency which oversees clinical trial studies in the United States is the Food and Drug Administration, or the FDA. By law, any research or medical entity who seeks to conduct clinical trials for an experimental drug must file a Notice of Claimed Investigational Exemption for a New Drug (IND) for approval. An IND application contains information about the synthesis, composition, and storage of the drug candidate, all necessary pharmacodynamic and pharmacokinetic cellular and animal therapeutic and toxicity testing, as well as the plans for the clinical trial (52). Once an IND application is filed, the FDA has 60 days to determine whether it intends to file or reject it. It is only after IND approval has been granted through the FDA that clinical studies may proceed. IND approval is considered by many a significant milestone in the drug development process because it is the first time that the drug candidate will ever be tested in humans (46). The following sections will summarize the three different phases in clinical trial

development prior to FDA approval: Phases I-III, followed by FDA review and approval, and finally, Phase IV studies.

1.2.4.1. Phase I clinical trials

Phase I clinical trials are the first instance in which the candidate drug is tested in humans. As such, the FDA places a heavy emphasis on preserving the safety of the clinical trial participants, and this becomes the major endpoint to be assessed in this phase, even before assessing drug efficacy (53). The number of participants in this clinical trial phase is remarkably smaller than in subsequent phases (i.e. about a dozen). The maximum tolerated dose (MTD) is the dose that a patient may receive before experiencing dose-dependent toxicity and is the critical endpoint measured in this clinical trial phase via various possible statistical designs (54). One example of the prototypic Phase I study design is the 3+3 design; a cohort of three patients are selected and receive a starting dose that is considered to be safe based on animal toxicological data. If none of the three patients in this starting cohort experience dose-limiting toxicity, then three more patients are selected and treated at the next higher dose level. If one of the patients experiences toxicity, then three more patients will be selected and will receive the drug at the same dose. These dose escalation studies continue until at least two patients in a cohort of three to six people experience dose-limiting toxicities. Once this dose has been determined, then it is used as a guide to conduct Phase II studies, and is usually the dose just below the observed dose-limiting toxicity (53).

1.2.4.2. Phase II clinical trials

Phase II clinical trials, a continuation of Phase I studies, incorporates a larger cohort than

those utilized in Phase I studies and are designed to assess several therapeutic endpoints such as safety and pharmacokinetics/pharmacodynamics. Furthermore, additional endpoints such as optimal dose determination and frequency and routes of administration may be determined that are used as guidelines for subsequent Phase III clinical trials. Ultimately, the major objective of a Phase II study is to determine whether a drug candidate has sufficient biological activity against the disease to warrant further study (55). A few ways that efficacy may be demonstrated in this clinical trial phase might include, but are not limited to: (i) comparing the candidate drug with previously known interventions for the given disease state; (ii) exploring different dosing arms (i.e. treatment groups); (iii) randomization. Phase II clinical studies tend to be underpowered to reliably establish efficacy (due to the relatively small number of participants) and thus, this phase is often said to be exploratory in nature. Upon completion of these initial exploratory phases, a meeting between the investigators and the FDA is usually held to discuss the feasibility of progressing onto phase III clinical studies (56).

1.2.4.3. Phase III clinical trials

As previously mentioned, the primary objectives of the two exploratory phases of clinical trials are to assess drug safety (Phase I) and preliminary efficacy/dosing regimens (Phase II), which are both essential for transition into phase III clinical trials. Phase III clinical trials are often referred to as "comparative efficacy trials" or "pivotal trials" because it is here where the candidate drug is studied in a large enough cohort (typically from 300-3000 participants, dependent on the study design) to demonstrate and confirm efficacy, as well as highlight any common adverse effect incidences (57). It is important to note, however, that, based on the statistical principle of Hanley's "Rule of 3," with a clinical study of 300-3000 participants, an adverse effect rate of no less than 1

in 100 persons might only be observed; thus, a final clinical trial Phase, Phase IV studies, are also conducted to establish rarer adverse events that may not be detected in Phase III clinical trials (58).

Two of the most common types of Phase III trials include comparative efficacy trials and equivalency trials. In a comparative efficacy trial (sometimes referred to as "placebo-controlled trials"), the efficacy of the drug candidate is compared to that of a control treatment in the form of a placebo (59). On the other hand, the goal of an equivalency trial is to determine whether the candidate drug is comparable to the accepted standard of care. It is important to note that a placebo is not typically included in this study design and only directly compares the trial drug with the accepted drug (60). Because one of the major goals of Phase III studies is to carefully assess candidate drug efficacy, balance in treatment allocation becomes a primary objective. Randomization has proven to be an effective way to reduce the possibility of cofounding variables, as well as any potential biases between treatment groups. Using simple randomization as the most common example, this process assigns subjects to treatments arms on the basis of random allocation, such as a coin toss (61). In addition to randomization, stratification offers yet another means of reducing biases in treatment arms by balancing arms by prespecified characteristics (such as age group or gender). This prevents a scenario in which simple randomization might have been employed that coincidentally results in a disproportionate amount of people of one age group in one treatment arm versus another (62). Furthermore, single and/or double blinded Phase III studies might be carried out because this may help reduce subjective biases when analyzing clinical data. Singly blinded studies are those in which the study participant does not know their respective treatment arm, whereas the study participant as well as the investigator are both unaware of treatment status in doubly blinded studies (63). Collectively, these approaches ensure that the data is collected, analyzed, and interpreted in an objective, unbiased manner.

Most Phase III clinical trial analyses are conducted as "intention-to-treat" analyses, where subjects are assessed based on the initial treatment assignment given via randomization, regardless of what treatment they may have received (otherwise known as the "analyzed as randomized" rule). This method is the preferred analytical method for clinical studies in that it helps eliminate selection bias by preserving randomization. By preserving randomization, the effect of confounders becomes negligible and the difference in outcomes can more reliably be attributed to therapeutic intervention by the candidate drug (57).

1.2.4.4. FDA review & approval

If the results from clinical trial Phases I-III look promising, then the clinical study team may file an application for FDA approval of the candidate drug. This application, the New Drug Application (NDA), includes: (i) all experimental data concerning the drug; (ii) information about manufacturing; (iii) quality control and assurance; (iv) complete product description (i.e. chemical formula, specifications, pharmacodynamics/pharmacokinetics); (v) indications; (vi) labeling; (vii) proposed risk evaluation (64). Once an NDA has been submitted, the FDA will have 60 days to decide if they will file the application. Upon review, FDA reviewers will evaluate the clinical data and will require that there be "substantial evidence" of drug safety and efficacy, according to the Federal Food, Drug, and Cosmetics Act (64). This review process typically occurs within 180 days of submission of a complete application. If the FDA decides to approve the NDA application, the candidate drug will have legal authority to manufacture and market the drug for human use. However, the candidate drug may be approved under circumstances, in which a post-approval Phase IV clinical study may be done to validate efficacy and utility of the candidate drug (64).

1.2.4.5. Phase IV clinical trials

Phase IV clinical trials occur after the drug has been approved by the FDA, and thus, are often referred to as "post-marketing" studies. As previously mentioned, Phase IV clinical trials might be required for some drugs by the FDA for several reasons, with some of the most common being: (i) identify less common adverse reactions, and (ii) evaluate cost and drug effectiveness in diseases, populations, or doses different from the original study population. The number of study participants are typically well into the thousands and in doing so provides the statistical power necessary to detect side effects that are otherwise rare to observe (57).

1.2.4.6. Concluding remarks

Overall, drug discovery and development is a timely and costly endeavor. The following chapters will discuss several aspects of drug discovery and development utilized towards the writing of this dissertation: *in silico* drug design (Chapter 2), vHTS screening (Chapter 3), determining mechanism of action (Chapter 4), and finally, Phase I & II clinical trial studies (Chapter 5). This broad, interdisciplinary scope of research is essential to provide the skillset for a rewarding career in the drug development pharmaceutical industry.

Chapter 2

Fundamentals of drug design: an *in silico* approach in the development of novel aromatase inhibitors for post-menopausal, estrogen dependent breast cancer

2.1. Abstract

Upon target validation, hit discovery becomes the next major phase of the drug development process. Several approaches exist in identifying such hits, and the work presented in this chapter highlight an *in silico* approach to identifying a novel class of aromatase inhibitors. Indeed, traditional therapies aiming to limit breast cancer tumor growth via ER related pathways, such as aromatase inhibitors (AIs), have been highly efficacious in diminishing tumor volume. However, aromatase-inhibitor associated anthralgias (AIAA) present as the major cause of patient withdrawal from AI therapy in as many as 20-30% of AI-patients. While the aromatase enzyme has been intensely studied and targeted for several decades, the aromatase crystal structure was not solved until 2009. Herein, we report an *in silico* approach to better understand the aromatase active site in hopes of unraveling mechanisms that link AI-drug class (reversible AIs such as letrozole vs irreversible AIs such as exemestane) to side-effects. We used semiquantitative IC50 data from a library of 32 androstenedione analogs to construct a preliminary SAR model. From this model, we selected three analog pairs with predicted differing mechanisms of action and revalidated their activities via the aromatase radiometric release assay to quantify aromatase inhibition. AI inhibition studies did not demonstrate any significant difference in activity with respect to anticipated mechanisms of action. However, we did observe a significant difference in activity between two of our analogs, HDDG-046 and HDDG-026 that only differ by a two carbon chain proceeding the terminyl alkynyl group at the C6-position. Docking studies revealed a shared 3D pharmacophore between letrozole and two of our exemestane-like analogs, which suggests that letrozole may partially mimic the endogenous steroidal androstenedione scaffold. Furthermore, our docking studies highlighted a particular residue, Ser478, lining the channel region which may be exploited for further AI development. Overall, while there was no observed correlation in

anticipated mechanism of action vs activity, our docking studies highlighted a novel residue which might provide benefit for the next generation of improved AIs.

2.2. Background

Breast cancer continues to be one of the deadliest types of cancers seen in women; it is estimated that over 230,000 women will be diagnosed with invasive breast cancer this year, with over 40,000 expected fatalities (65). Typically, most of the common treatments offered for breast cancer patients involve abrogating ER signaling in ER+ tumors: selective estrogen receptor modulators (SERMs) or aromatase inhibitors (AIs) (66). While SERMs are considered to be effective antiestrogens, they also exhibit tissue-specific partial agonism which has been associated with increased risk of hernias, stroke and endometrial cancer (67-70). AIs, on the other hand, have garnered considerable interest as effective antiestrogens; aromatase, a cytochrome P450 enzyme (CYP19A1), is responsible for the rate limiting conversion of androgens to estrogens, providing the ER substrate supply. The enzymatic process involves three oxidation steps with the aromatization of the steroidal A ring being the last step, hence its name (71). Currently, the third generation AIs letrozole and anastrozole (nonsteroidal, reversible AIs), as well as exemestane (steroidal, irreversible AI) have shown clear superiority over conventional therapies such as SERMs and have applications in the metastatic, adjuvant, and neoadjuvant settings (72).

However, although they are better tolerated than SERMs and have been improved from previous generations, there are noteworthy risks associated with each AI that has critical implications on patient quality of life and adherence. Letrozole has been shown to inhibit drug metabolizing cytochrome P450's such as CYP2A6, CYP2B6, and CYP2C19, while exemestane can act as a weak ER agonist and a potent androgen receptor (AR) agonist (73, 74). Furthemore, anastrozole inhibits CYP1A2 and CYP2C9 (75). The cytochrome P450 superfamily of enzymes is

largely known for its role in the metabolism of various endogenous and xenobiotic substrates. Due to the current AI's cross-reactivities with certain P450's, this implicates drug-drug interactions, an undesirable characteristic given the patient population (76). Moreover, AI-induced side effects, such as osteoporosis and AIAA, can be so severe that up to 20-30% of patients have to discontinue from therapy, which is an alarming statistic given the efficacy of these compounds (77-81).

Interestingly, when cross-compared in the clinic, all third generation AI's display distinct side-effect profiles; for instance, the nonsteroidal AI letrozole was shown to reduce plasma estrogen levels by 88-98%, whereas the steroidal AI exemestane reduced plasma estrogen levels by a modest 52-72% (82, 83). However, letrozole has been shown to reduce basal cortisol levels while increasing aldosterone levels; these effects were not observed with exemestane (84, 85). Moreover, the rate of bone demineralization was significantly less with exemestane administration in ovariectomized rats when compared to letrozole (86); clinical tests have also shown a greater preference for exemestane in preventing these effects. Whether these side-effects can be attributed to the compound's mechanism of action (i.e. reversible vs irreversible binding), potency, or selectivity remain unknown.

A potential barrier to discovering more selective, tolerable AIs might be that no crystal structure of aromatase had been solved until 2009. Thus, all aforementioned therapies lacked a reliable structural basis for generating supportive and predictive *in silico* data. Indeed, a crystal structure and *in silico* drug design is not mandatory for a drug discovery effort; however, it would surely garner an appreciation for the aromatase active site and explore ways to exploit its active site. Upon crystallization and analysis of the aromatase active site, Ghosh et al discovered that unlike most P450's, aromatase possesses a small, compact binding site that is not easily flexed by ligand binding. The several hydrophobic and polar residues surrounding the active site exquisitely complement the steroid backbone, supporting the enzyme's high specificity. Moreover, the C4-

and C6- positions of the androgen directly face the channel entry site (87). Therefore, synthesizing analogues bearing substituents at those positions can potentially provide for highly specific AIs. Finally, because both androgen aromatization and exemestane-induced irreversible inactivation occurs via the steroidal A ring, we are able to readily convert a compound's anticipated mechanism of action by directly manipulating the chemistry governing the steroidal A ring. More specifically, exemestane's steroidal A ring structure adopts a 1,4-diene conformation which is critical in its role as an irreversible substrate (88). We can thus design analogs that have differing saturation profiles in the A ring which will allow for that mechanical "switch" in action via novel C-H functionalization techniques currently being developed by our collaborators (89).

In this study, we took advantage of a library of 75 androstenedione analogs previously synthesized by our collaborators; semiquantitative data from crude antiaromatase assay experiments were collected for roughly 32 compounds, in which a preliminary SAR report was generated. We selected three interesting scaffold pairs which showed distinct activity cliffs (i.e. two compounds with similar structures, yet with a noticeable difference in activity) and focused on pairs which had variable A ring stereochemistry which we hypothesized would have differing mechanisms of action. Upon revalidation via the radiometric release assay for measuring aromatase inhibition, we were unable to construct an appropriate docking model to account for the discrepancies in activity. However, other docking models suggested that two of our analogs, in addition to letrozole, share 3D pharmacophores and essentially act as bioisosteres in the aromatase active site. Furthermore, we revealed a key residue, Ser478, that lines the channel entry site that may be exploited for further development as this residue is within hydrogen bonding distance of a triple bond substituent of one of our best hit compounds.

2.3. Materials and Methods

Generation of preliminary SAR report from semiquantitative data

Out of a focused chemical library of 75 potential AIs, 32 of them were crudely tested using the aromatase radiometric release assay, which will be explained in detail in the following section. We began by assigning these compounds semi-quantitative IC50 values based on their activities relative to the C6-alkynyloxy-derivatives published by our group (90). This was done to perform a first-pass structure activity relationship (SAR) analysis to identify trends on activity versus compound structure. We clustered compounds by chemical similarity into four distinct scaffolds and explored "activity cliffs" to select the most interesting compounds having diverse R-groups for *in silico* and biological testing. In this manner, activities across different scaffolds can be compared and "activity cliffs," which are two compounds that have nearly identical structures yet have a significant difference in activity.

Radiometric release assay for measuring aromatase inhibition

The radiometric aromatase release assay is the gold standard to measure aromatase activity (91). The main substrate that is used is a tritium-radiolabeled androstenedione molecule which is specifically radiolabeled at the C2- position. Upon aromatization, the tritium atom becomes displaced from the molecule and is incorporated into a molecule of water; therefore, direct aromatase activity can be readily detected by measuring the amount of tritiated water formed via a scintillation counter. For this assay, the AC-1 cell line was used, which is an MCF7-derived cell line kindly donated by the Angela Brodie laboratory. AC-1 cells were first plated in steroid-free media (Improved MEM, Life technologies) supplemented with charcoal-stripped serum (Atlanta Biologicals) in six-well plates at 60-70% confluency. 24h later, the cells were then washed twice with PBS, scraped and placed into microcentrifuge tubes containing a cocktail essential for assay

execution: 1% Bovine Serum Albumin (Sigma), 67mM KPO_4 at a pH of 7.4, and 2.0 uM progesterone (Sigma). Cells in this cocktail were then subject to sonification (Fisherbrand Model 100 Sonic Dismembrator) at a setting of "3" and were sonicated via three 5 second pulses that were separated by 6 second interval rest periods. Upon cell lysis, the suspended cell lysate was then incubated with the test compounds at 37 degrees Celsius for 6 hours at concentrations of 10 nM, 50 nM, 100 nM, 500 nM, and 1uM. After drug preincubation, cells were then treated with 1uM [3H]-androstenedione (Fisher Scientific) and 12mM NADPH (Sigma) at 37 degrees Celsius for approximately 18h to activate aromatase present in the cell lysate. Cells were then washed with 5% trichloroacetic acid (Sigma), spun down, and the supernatant was then extracted with chloroform. The top aqueous layer was transferred into a fresh tube and was further extracted with dextran coated charcoal (Sigma) to completely remove remaining unreacted tritiated androstenedione. This purified tritiated water solution was then placed into scintillation tubes and tritium activity was detected via a scintillation counter.

***in silico* docking/scoring analyses**

For the docking studies, a combination of the Maestro ligand/protein preparation wizard and the Glide docking software were utilized. We downloaded refined aromatase 3D structures expressed in breast/adipose tissue and complexed with small molecular inhibitors (PDB codes 4GL5, 4GL7, and 4KQ8, http://www.rcsb.org). First, the proteins were optimized with the Protein Preparation Wizard (Maestro, Schrodinger) software; extraneous molecules bound near the active site that may perturb results (e.g. water molecules, cofactors) were removed and a standard physiological environment (i.e. pH 7.4) were simulated. The OPLS3 force field was selected for all docking studies with XP sampling as the main scoring function for pose generation. Upon protein optimization, the ligand preparation tool was then used to generate our ligands suitable for

docking. Flexible ligand sampling was employed in achieving ligand-protein poses for all compounds. To verify our docking model, we first superimposed the poses generated by our software with that of the crystallized complex obtained from the database (data not shown). After validating our docking model, selected molecules were then docked, and Glide docking scores were generated for each ligand-protein pose and compared to each other.

MTT assay for growth inhibition

Compounds were tested for their antiproliferative potential via the MTT assay. AC-1 cells were incubated in steroid-free media (Improved MEM media, Life Technologies) for three days prior to plating. The following day, cells were seeded into 96-well plates at a concentration of 5,000 cells/well and treated with conditioned media containing either control (DMSO), the AI letrozole (Selleckchem USA), or the test compounds in increasing concentrations (0.001nM – 10 nM). The cells were washed with PBS and supplemented with fresh conditioned media every three days; on the ninth day after plating, the MTT assay was run via MTT assay kit (Promega).

Statistical Analyses

Two-way ANOVA was used to compare the effects of aromatase inhibition (factor 1: dose, factor 2: compound).

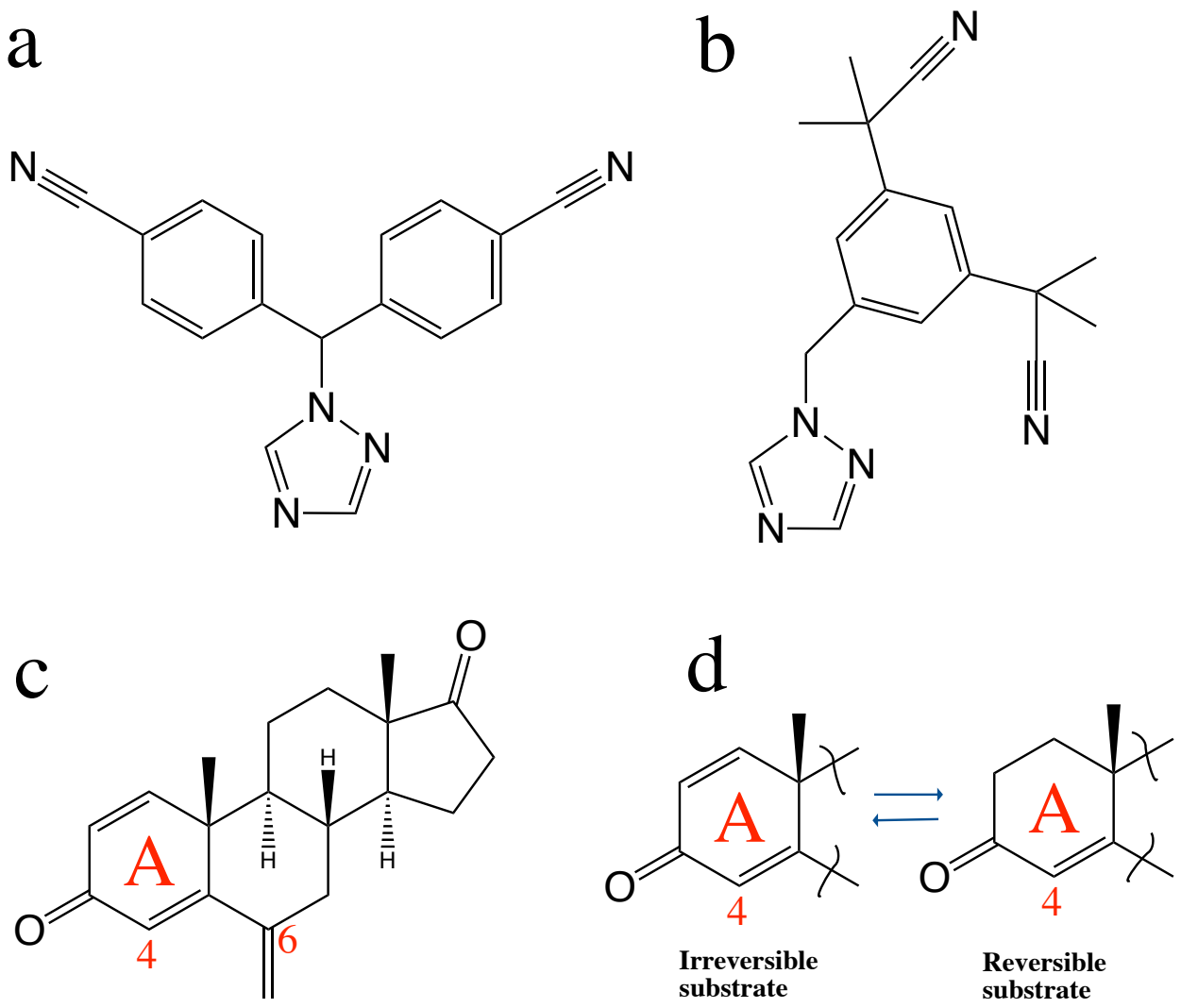

Figure 2.1. Structures of current third generation aromatase inhibitors (AIs): (**a)** nonsteroidal AI letrozole; (**b**) nonsteroidal AI anastrozole; (**c**) steroidal AI exemestane. The steroidal A ring, as well as the C4- and C6- positions, respectively, are depicted in (**c**), and are key regions for further exploitation in this study. (**d**) illustrates the hypothetical mechanical "switch" that allows for novel analog design to characterize reversible vs irreversible AI inhibition.

2.4. Results

Generation of first-pass SAR report

As previously mentioned, a series of 6-alkynyloxy-androstenedione derivatives were comprehensively studied and characterized in a previous collaboration by one of our collaborators with another group (90). However, a series of about 75 different androstenedione derivatives were synthesized and it was only this limited subset that was studied in great detail. Thus, as a starting point, we took advantage of crude preliminary data for about 32 of these compounds that were screened via the radiometric release assay (data not shown). From this crude data, we assigned semi-quantitative IC50 values which were cross-referenced to the published data in the publication previously described. Finally, from this semi-quantitative IC50 data, we generated a first pass structure activity relationship (SAR) report to identify interesting scaffolds with so-called "activity cliffs" that could be re-evaluated and studied further (**Fig. 2.2**). Results from **Fig 2.2** revealed several activity cliff clusters which demonstrated a notable difference in activity although possessing similar structures: (i) HDDG-026 (IC50: 4uM) & HDDG-046 (IC50: 11.8 nM) (**Fig 2.4a**); (ii) HDDG-043 (IC50: 2.2uM) & HDDG-050 (IC50: 5 nM) (**Fig 2.4b**); (iii) HDDG-016 (IC50: 40uM) & HDDG-041 (500 nM) (**Fig 2.4c**). The purpose of this preliminary SAR report was to have a focused compound set to utilize to not only revalidate their activities in our laboratory, but to also use *in silico* docking methods to justify the discrepancy in activity.

Validation of crude preliminary activity via aromatase radiometric release assay

Crude aromatase inhibition data enabled the generation of a first pass SAR report, which was used as a prioritization tool to reveal which compound sets demonstrated interesting activity cliffs to then retest in our laboratory. However, prior to this step, the radiometric release assay was

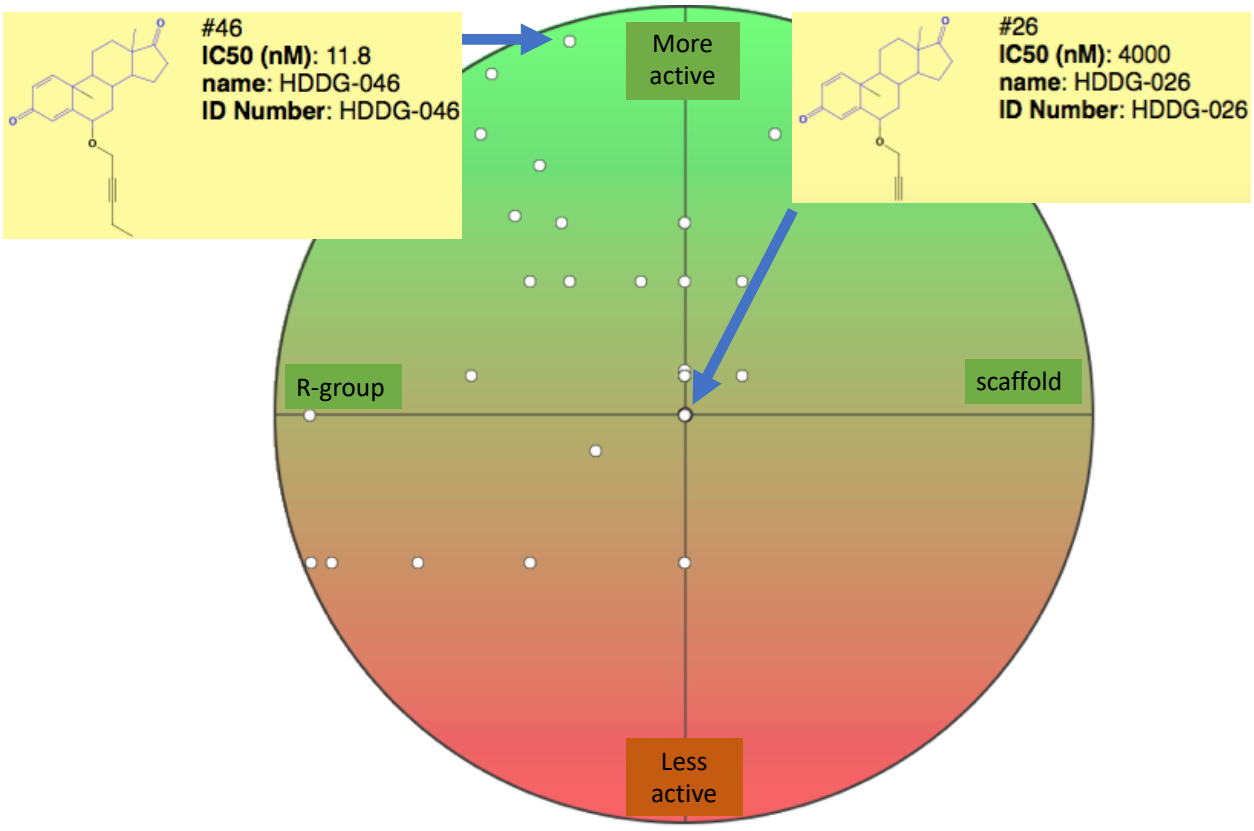

Figure 2.2. First pass SAR report reveals "activity cliffs" and identifies compound sets for further exploration. IC50 data was semi-quantitatively assigned to 32 compounds (i.e. dots) which had crude aromatase inhibition data based on published IC50 data for other compounds within the same library. An arbitrary molecule is positioned at the center of the cross-hairs, and the remaining compounds are plotted above and below the reference molecule, depending on whether the activity is greater or less, respectively. Molecules plotted to the left of the reference compound have the same scaffold (i.e. steroidal structure), and the distance indicates the extent to which R-groups differ. From this data, a first pass SAR report was generated, and compound pairs which showed activity cliffs (i.e. two closely structured compounds with a notable difference in activity) were selected and prioritized for further characterization. An example of an activity cliff between two closely related compounds, HDDG-026 and HDDG-046, are illustrated above.

first conducted on three currently known AI's: second-generation AI formestane, and third generation AI's letrozole and exemestane (**Fig 2.3**). As shown on **Fig 2.3** on the following page, letrozole proved to be the most potent compound with an IC50 value of 6.6nM, followed by exemestane with an IC50 value of 39.81nM, and lastly, formestane, with an IC50 value of 1uM. These values coincide well with accepted literature IC50 values for these compounds and instill credibility in subsequent screening assays for our focused compound set (92).

The first compound set that was retested were compounds HDDG-046 and HDDG-026 (**Fig 2.4a**). As shown in **Fig 2.4a**, both compounds possess nearly identical structures, with the only difference being the lack of a two-carbon chain preceding the terminal alkynyl group at the C6- position in HDDG-026. Subsequent radiometric testing showed that HDDG-046 exhibited a nearly 4-fold difference in potency compared to HDDG-026 with IC50 values of 72.4 nM and 316.3 nM, respectively; in other words, aromatase inhibition was enhanced with the inclusion of a two-carbon chain. The second set of screened compounds included HDDG-050 and HDDG-043 (**Fig. 2.4b**). The key difference between these two compounds lies in the A-ring stereochemistry; while they both possess a hydroxyl group at the C3-position, as opposed to a ketone group, the double bond configuration is also different: HDDG-050 adopts a 3,5-diene configuration whereas HDDG-043 adopts a 1,3,5-triene configuration. This has an impact on the 3D shape of the steroidal structure as the extra double bond in HDDG-043 renders it more planar than its HDDG-050 counterpart. Thus, these two compounds placed a bigger emphasis on the role of the steroid stereochemistry rather than the constitutents branching from them. Radiometric analyses revealed that compound HDDG-050 displayed a nearly 10-fold diference in potency compared to HDDG-043, with IC50 values of 100 nM and 1uM, respectively. Finally, the third compound set that was tested included compounds HDDG-016 and HDDG-041. Once again, the only difference

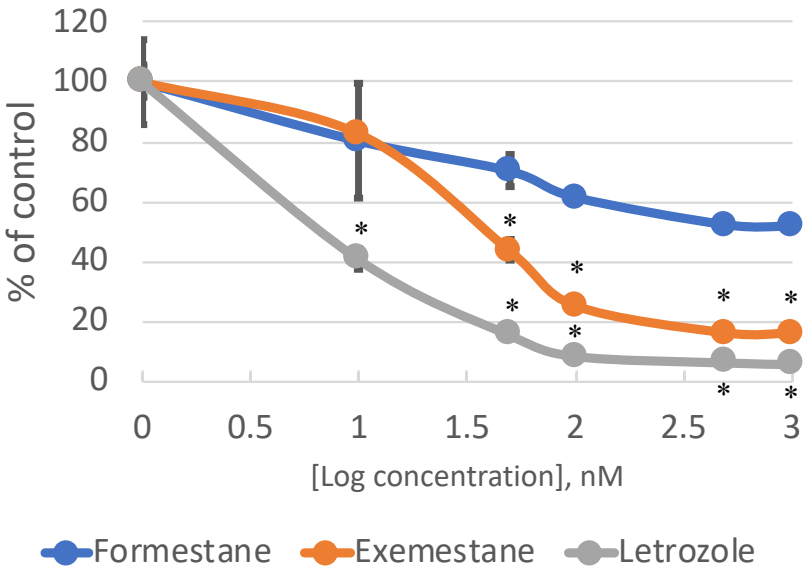

IC50 values:
Formestane: 1uM
Exemestane: 39.81 nM
Letrozole: 6.6 nM

Figure 2.3. Radiometric release assay demonstrates robust, reliable method for quantifying aromatase inhibition in AC-1 cells. The radiometric release assay was conducted on three known AI's: second generation AI formestane, and third generation AI's exemestane and letrozole in AC-1 cells. IC50 values were then calculated by measuring the concentration at which 50% of inhibition was achieved for all three compounds and are reported above. Error bars indicate SEM (* $P < 0.05$).

a

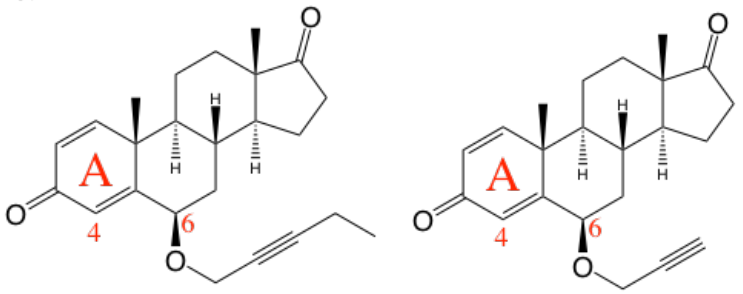

HDDG-046 HDDG-026

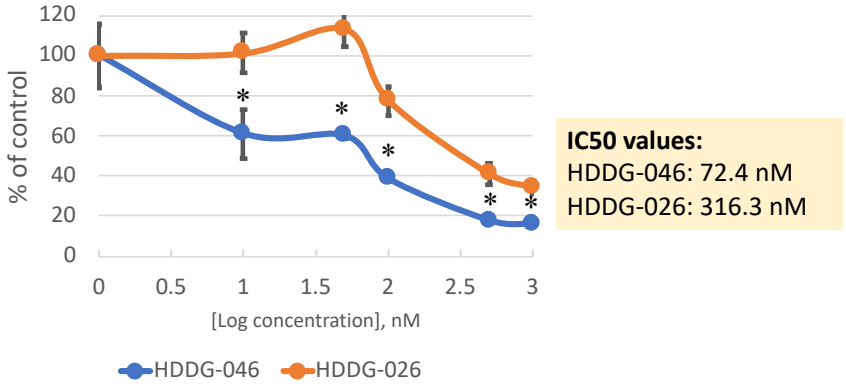

IC50 values:
HDDG-046: 72.4 nM
HDDG-026: 316.3 nM

b

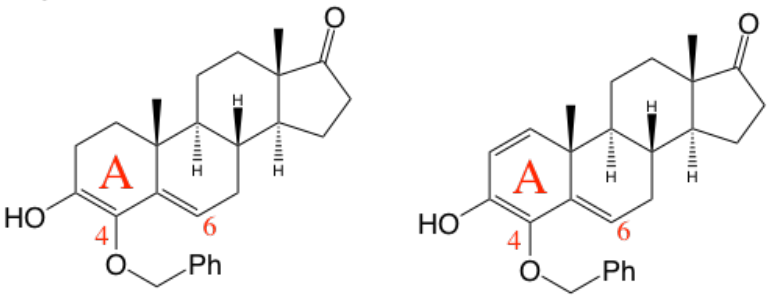

HDDG-050 HDDG-043

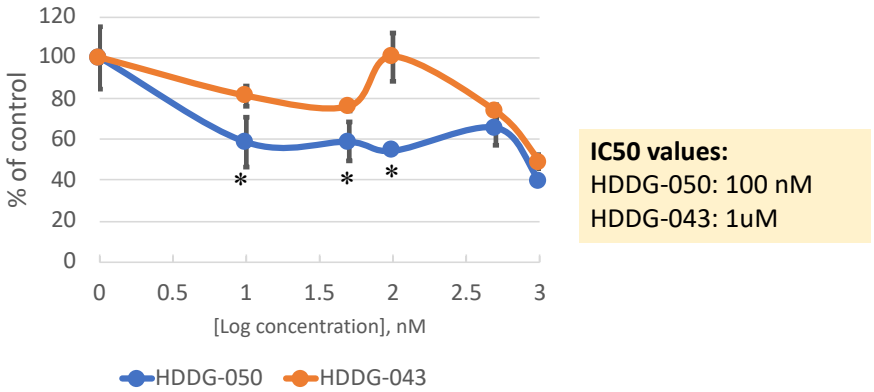

IC50 values:
HDDG-050: 100 nM
HDDG-043: 1uM

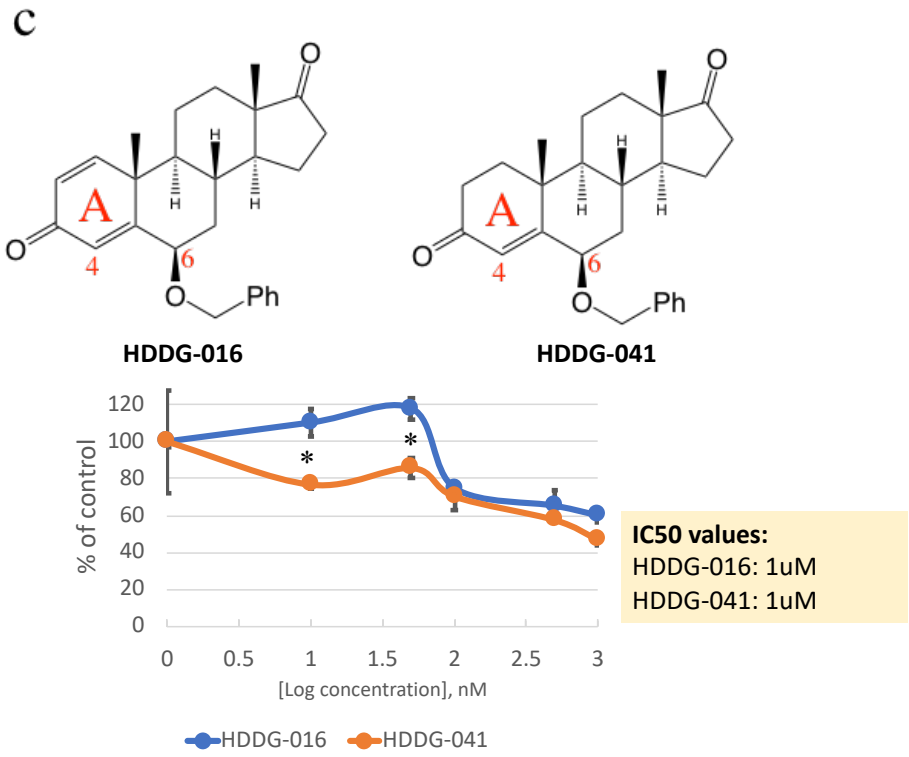

Figure 2.4. Radiometric release assay demonstrates notable differences in activity with respect to certain scaffolds. Data from the first pass SAR report in Fig. 2.3 was used to screen compound pairs which showed preliminary differences in activity while possessing similar structures: (**a**) HDDG-046 & HDDG-026; (**b**) HDDG-050 & HDDG-043; (**c**) HDDG-016 & HDDG-041. IC50 values were calculated by determining the concentration at which 50% of inhibition was achieved. Activities are normalized to percent of control, and error bars indicate SEM. Experiments were run in triplicate. (* $P < 0.05$).

between these two compounds lie in their A-ring stereochemistry. In this case, while both of these compounds possess a keto group, compound HDDG-016 employs a 1,4-diene configuration whereas HDDG-041 adopts a 4-ene configuration. These differences are noteworthy in that HDDG-016 is predicted to be an irreversible inhibitor, whereas HDDG-041 is predicted to be a reversible inhibitor (88). Thus, this compound set might provide a mechanical basis for discrepancies in aromatase inhibition. However, it was observed that both of these compounds were equally ineffective at inhibiting aromatase, with calculated IC50 values at nearly 1 uM, well below the targeted potency range. Moreover, when docking studies were performed to justify the differences in activities reported for each compound set, there was no model that could rationalize these differences (**Fig. S2.1**).

Docking of letrozole, HDDG-046 and HDDG-058 highlights shared 3D pharmacophores

In order to better understand the biology governing the aromatase active site for further exploitation, letrozole, along with compounds HDDG-046 and HDDG-058 were all docked into the aromatase protein via the Maestro Schrodinger and Glide docking software. After the ligands and active site were primed for docking, the best predicted binding poses were generated and all three ligands were superimposed on one another to account for how these molecules might be binding into the aromatase active site. As shown in **Fig 2.5** on the following page, the three molecules orient themselves into the active site in such a way that allows for letrozole to partially mimic the steroidal androgen structure. The cyanobenzyl moiety may essentially act as a bioisostere for the keto group in the steroidal structure, whereas the imidazole group in letrozole is aligned in similar fashion to the five-carbon cyclic D-ring in HDDG-046 and HDDG-058. Furthermore, docking scores predicted that all three compounds should harbor similar potencies,

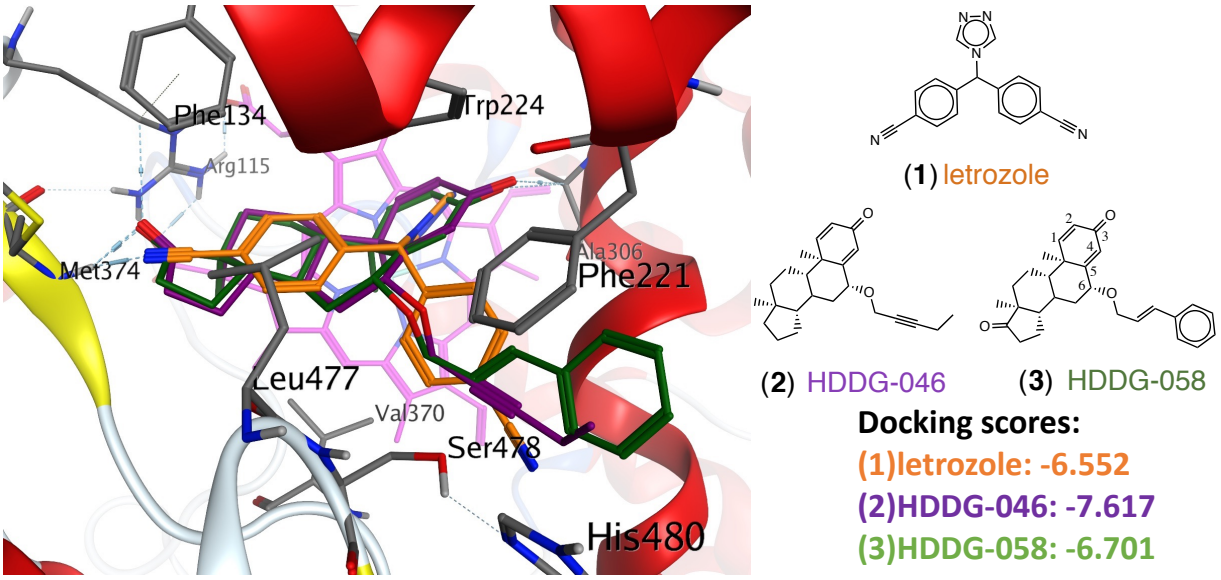

Figure 2.5. Docking data suggests letrozole, along with steroidal analogs HDDG-046 and HDDG-058, all share 3D pharmacophore with respect to aromatase active site binding. Letrozole (orange), along with compounds HDDG-046 (purple) and HDDG-058 (green) were all docked into the aromatase active site and docking scores were generated which reflect the predicted sum of interactions between the ligands and the residues aligning the aromatase active site.

as reflected by the similarity in docking scores. When an MTT assay was performed on these three compounds to evaluate their anti-proliferative potential (**Fig. 2.6**), all compounds exhibited a dose dependent decrease in cell viability at subnanomolar concentrations, which supports the predicted binding activities illustrated in **Fig 2.5**.

X-ray crystallographic data reveals novel residue, Ser478, that may play a role in drug binding

Fortunately, when the aromatase crystal structure was solved, the Ghosh group responsible for this discovery were able to crystallize aromatase in complex with several different ligands that are readily available in the PDB database. One of these crystallized structures includes the aromatase protein in complex with HDDG-046, one of the hits obtained in our preliminary screening. When this file was downloaded and analyzed from the PDB database (PDB code: 4GL7), we observed that the triple bond partially comprising the C6-substituent of compound HDDG-046 was within hydrogen bonding distance to a residue lining the channel, Ser 478, through which the endogenous substrate must travel to reach the heme active site (**Fig 2.7**). The approximate distance between this triple bond and the Ser478 residue lining the entry channel is about 2.5 angstroms, which supports its potential role in ligand binding to aromatase. Furthermore, this Ser478 residue is also highlighted in the predicted binding poses of HDDG-046 and HDDG-058 (**Fig 2.**5) and demonstrate that both of these compounds are also predicted to display interactions with this residue. Taken together, experimental as well as predictive docking studies provide the rationale for Ser478 as a means for enhancing aromatase inhibition.

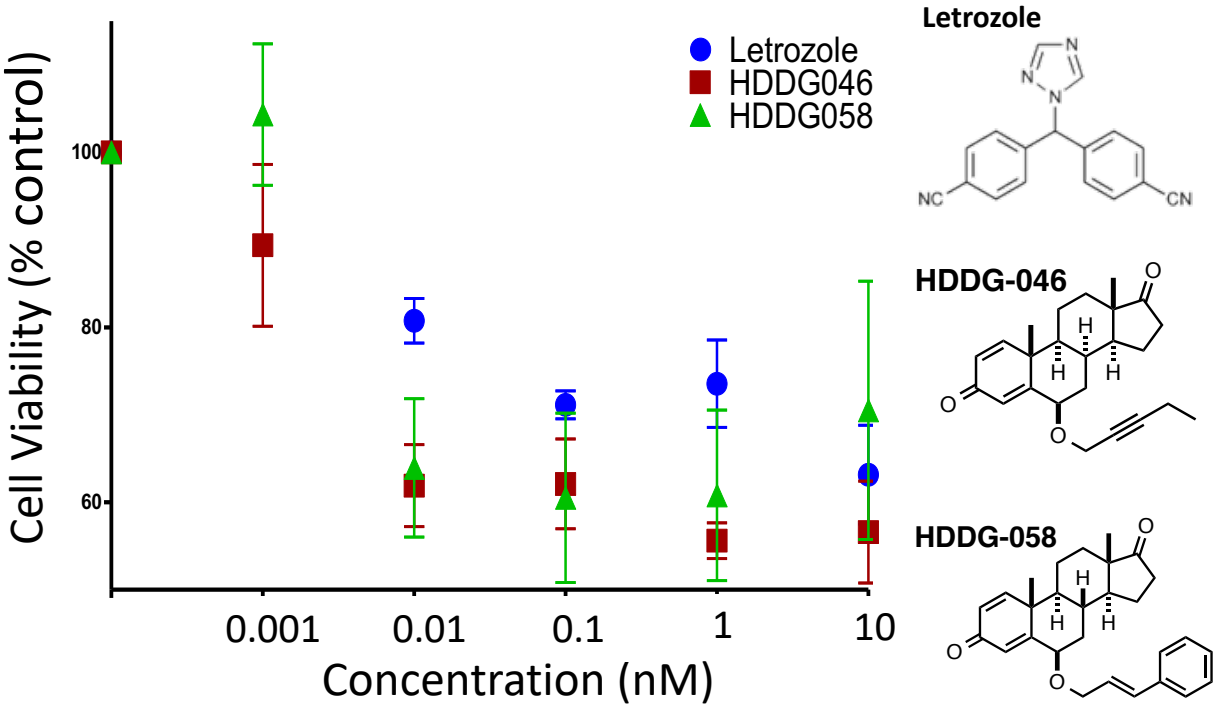

Figure 2.6. Anti-proliferative data suggests that steroidal analogs HDDG-046 and HDDG-058 are as efficacious as letrozole in limiting cancer cell proliferation. An MTT assay was performed on AC-1 cells and were treated with either vehicle (DMSO), letrozole, HDDG-046, or HDDG-058 over a course of 9 days. Data is represented as percentage of control, and error bars reflect SEM. Experiments were conducted in triplicate.

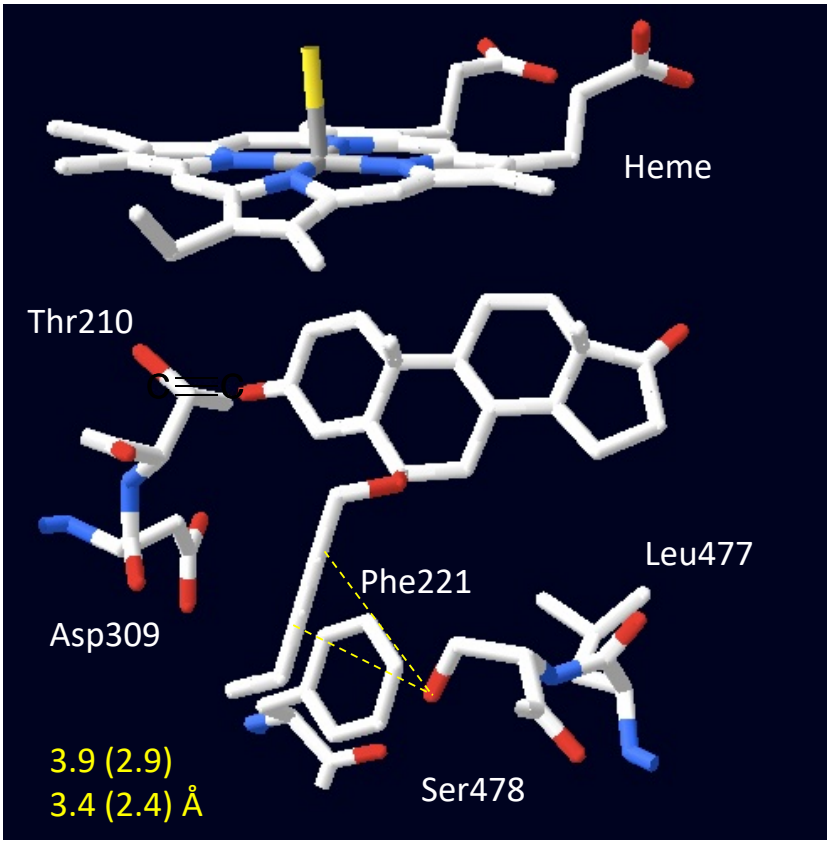

Figure 2.7. Existing X-ray crystallographic data highlights novel residue, Ser478, implicated in drug-protein interactions. When an X-ray crystal structure of aromatase in complex with compound HDDG-046 was downloaded and analyzed from the PDB database (PDB code: 4GL7), it was observed that the triple bond in the C6- substituent of the HDDG-046 compound was within predicted hydrogen binding distance to Ser478, a residue lining the aromatase channel entry site. The predicted distance between these two moieties was approximately 2.5 angstroms, well within the range for a potential hydrogen bonding interaction. Only the aromatase active site (i.e. heme), along with critical residues are shown for simplicity.

2.5. Discussion

In this study, we took advantage of a library dataset of 75 androstenedione-like compounds that had previously been synthesized by our medicinal chemistry collaborators. A previous study by our collaborators focused on a particular subset within their compound library, notably the 6-alkynyloxy class of compounds (90). Thus, there remained a multitude of previously uncharacterized compounds at our disposal which we were able to use as diagnostic markers to probe the aromatase active site. Instead of blindly screening compounds from this library, we gathered crude preliminary data on about 32 of these compounds and generated a first pass SAR report to denote differences in activity with respect to similarly structured compounds, or so-called activity cliffs. The SAR report revealed three pairs of compounds which were then investigated further to re-evaluate their anti-aromatase efficacies. The three pairs were unique in that they each had a distinct difference in chemical structure relative to the other two pairs: in the first pair (**Fig 2.4a**), the only distinction is in the lack of a two-carbon chain preceding the terminal C6-substituted alkynyloxy group; the second set of compounds (**Fig 2.4b**) had a key difference in the A-ring stereochemistry comprising the steroidal backbone; finally, the third set of compounds (**Fig 2.4c**) also had a key difference in the A-ring stereochemistry. However, what is noteworthy about this last set of compounds is the lack of the double bond in the B steroidal ring that is present in the second set of compounds. This is instrumental to our mechanistic analyses due to the fact that it was predicted that HDDG-016 would act as an irreversible inhibitor, whereas HDDG-041 would act as a reversible inhibitor, based on the overall steroidal stereochemistry in this compound set.

When these three compound sets were subject for revalidation via the radiometric release assay, it was observed that in the first set, HDDG-046 was nearly four times more potent than its HDDG-026 counterpart (IC50 values of 72.4 nM and 316.3 nM, respectively), whereas in the second set, HDDG-050 was 10 times more potent than HDDG-043 (IC50 values of 100 nM and 1

uM, respectively). The third set of compounds, HDDG-016 and HDDG-041 were both inert compounds, with IC50 values of 1 uM for both analogs. However, despite these notable differences in activity for each compound series, docking analyses failed to reveal differences in predicting binding modes that would have accounted for such differences in activity (**Fig. S2.1**). It was anticipated that the previous experimental data, supplemented with revalidation efforts from our group, would have provided biological evidence to construct and give credence to docking models that would have accounted for these differences. While the semiquantitative data that was used to construct the first pass SAR reports did not exactly coincide with our aromatase inhibition data, a couple of the trends did align, such as HDDG-046 and HDDG-050's superiorities over their analog counterparts. Nonetheless, docking efforts were unsuccessful at justifying these discrepancies in activity. Docking data generated poses for each compound set that were strikingly similar to their analog counterpart; in other words, docking suggested that each compound should interact in a similar fashion to their analogue counterpart in the aromatase active site.

One of the key findings in the Ghosh paper responsible for solving the aromatase crystal structure indicated that the active site is very androgen specific, and in contrast to other cytochrome P450s, it is smaller, compact, and not easily flexed by ligand binding (87). Because of these findings, the aromatase active site may only be able to complement steroidal ligands in such a manner that does not allow for adequate flexibility, even among similarly structured compounds. The only physiologically relevant difference in activity that was observed in the compound sets tested were HDDG-046 and HDDG-026, with potencies in the lower nanomolar ranges. Both of these analogs were docked into the aromatase active site in such a way that allowed for the C6-substituted derivatives to protrude outward into the channel entry site, through which the substrate enters. It may be that the additional two carbons provided in HDDG-046 might have van der Waals or other intermolecular attractions with the residues aligning the channel entry site that accounts

for the four-fold increase in activity. A more thorough analysis of both the biological data as well as more *in silico* efforts is necessary to explore this idea.

However, while docking data was unable to rationalize the detected biological activities for these compound sets, computational analyses did reveal a couple of novel findings still relevant in trying to better understand the molecular framework underlying the aromatase active site. For instance, *in silico* data correctly predicted that letrozole, as well as two of our analogs, HDDG-046 and HDDG-058, should be nearly equipotent in inhibiting aromatase (**Fig. 2.5**), which was reflected in our MTT assay in **Fig 2.6**. Moreover, one interesting finding was the observation that letrozole seems to partially mimic the steroidal backbone and this may provide some rationale for letrozole's efficiency in inhibiting aromatase: the nitrogen heterocycle in letrozole binds strongly to the iron heme, whereas the cyanobenzyl moiety essentially acts as a steroidal bioisosphere and retains similar bonding interactions with neighboring active site residues, such as Met374, shown in **Fig. 2.5**. Indeed, this hypothesis has been postulated previously (93); however, in this study, we provide the structural basis supporting these speculations. Finally, we were able to exploit a solved aromatase/HDDG-046 crystallized complex available in the PDB database that revealed how HDDG-046 is binding to the aromatase active site. It was with this actual biological data that we speculated that there was a novel residue, Ser478, well within hydrogen bonding distance of the acetylene group present in the C6-substituent of HDDG-046. Further testing, such as mutagenesis experiments, should be carried out to probe the utility of this residue for enhancing HDDG-046's effects. Further modification within this specific scaffold might also provide another avenue for generating highly specific AIs.

As previously mentioned, the overarching, long-term goal of this study is to design a novel class of AIs that still maintain the potency profile of the current generation of AIs, however with limited toxicities. The most detrimental side-effects that cause for patients to non-adhere to therapy

include aromatase inhibitor associated anthralgias (AIAAs), which account for nearly 20-30% of patient withdrawal from AI therapy. While we seek to mitigate side-effects associated with current AI's, we do not fully anticipate being able to fully alleviate the joint and musculoskeletal side-effects, because these effects are most likely estrogen-dependent (78-80, 94-96). However, we reasoned that if we could even marginally reduce the severity of the reported symptoms, via manipulation of different key pharmacological traits (i.e. mechanism of action, potency), that this could provide the relief that would keep patients adherent to AIs. A thorough combination of optimizing current AIs, along with potential co-administration of other bone-protectant drugs, such as bisphopshonates, might enhance the patient's quality of life while on AIs. Nonetheless, this study highlights the inherent need for better AI therapeutics and provides the molecular and computational framework for the development of improved AIs for postmenopausal, estrogen-dependent breast cancer.

Results from these computational studies highlighted *in silico* docking methodology as one viable option for systematic drug screening. However, as previously mentioned, depending on the information that is known *a priori* about the target and/or existing leads, other screening approaches might be more practical. The next chapter focuses on a second screening approach, virtual high-throughput screening (vHTS), that is also routinely used in the drug discovery process. This vHTS methodology was utilized in the development of novel CXCR4 modulators.

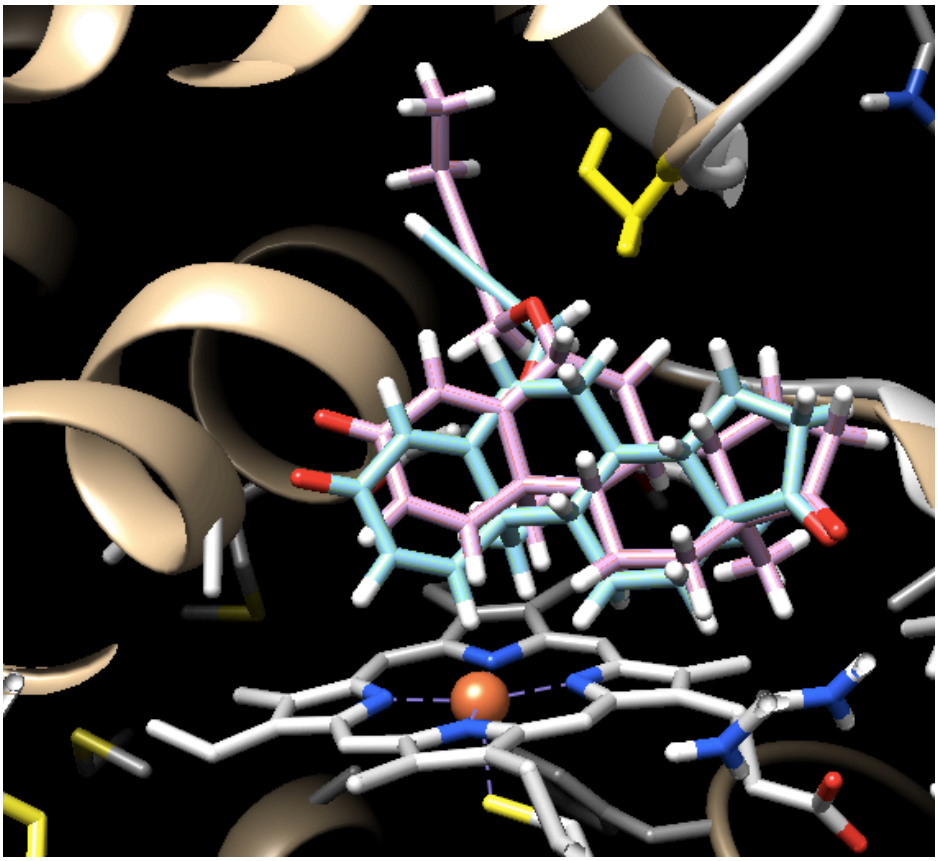

Supplementary Figure 2S1. Superimposition of predicted binding poses for HDDG-046 (purple) and HDDG-026 (blue). Shown above are the predicted binding poses for HDDG-046 (purple) and HDG-026 (blue). The heme iron catalytic site is shown at the bottom of the figure, and residue Ser478, which lines the channel entry site, is highlighted in yellow.

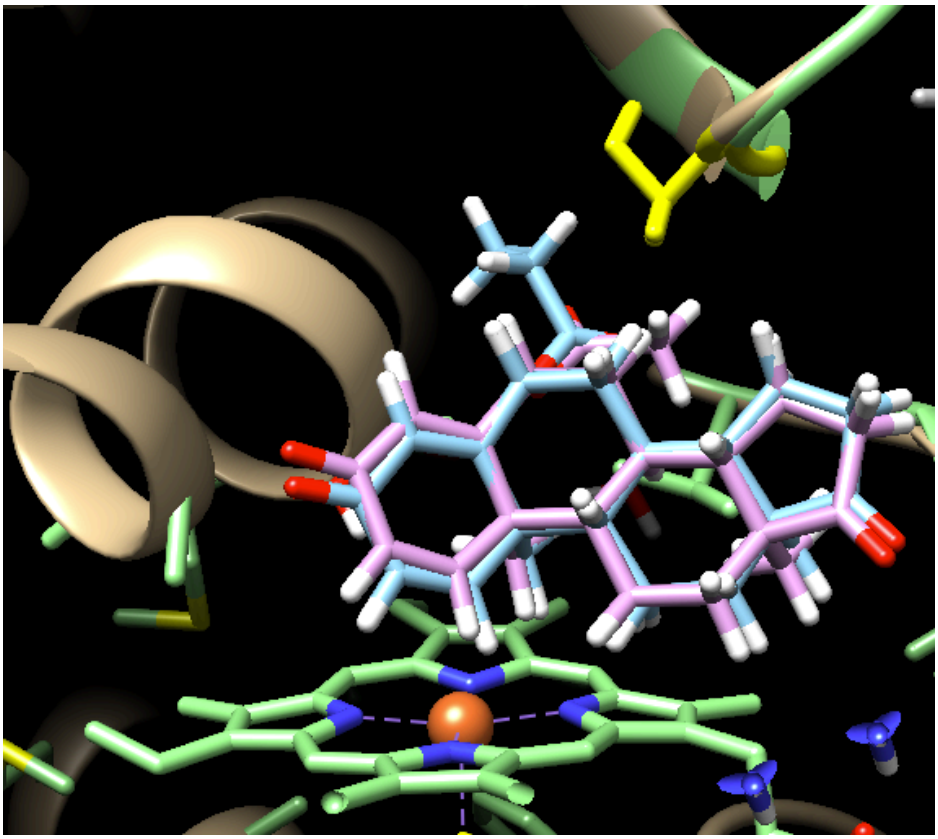

Supplementary Figure 2S2. Superimposition of predicted binding poses for HDDG-050 (purple) and HDDG-043 (blue). Shown above are the predicted binding poses for HDDG-050 (purple) and HDDG-043 (blue). The heme iron catalytic site is shown at the bottom of the figure, and residue Ser478, which lines the channel entry site, is highlighted in yellow.

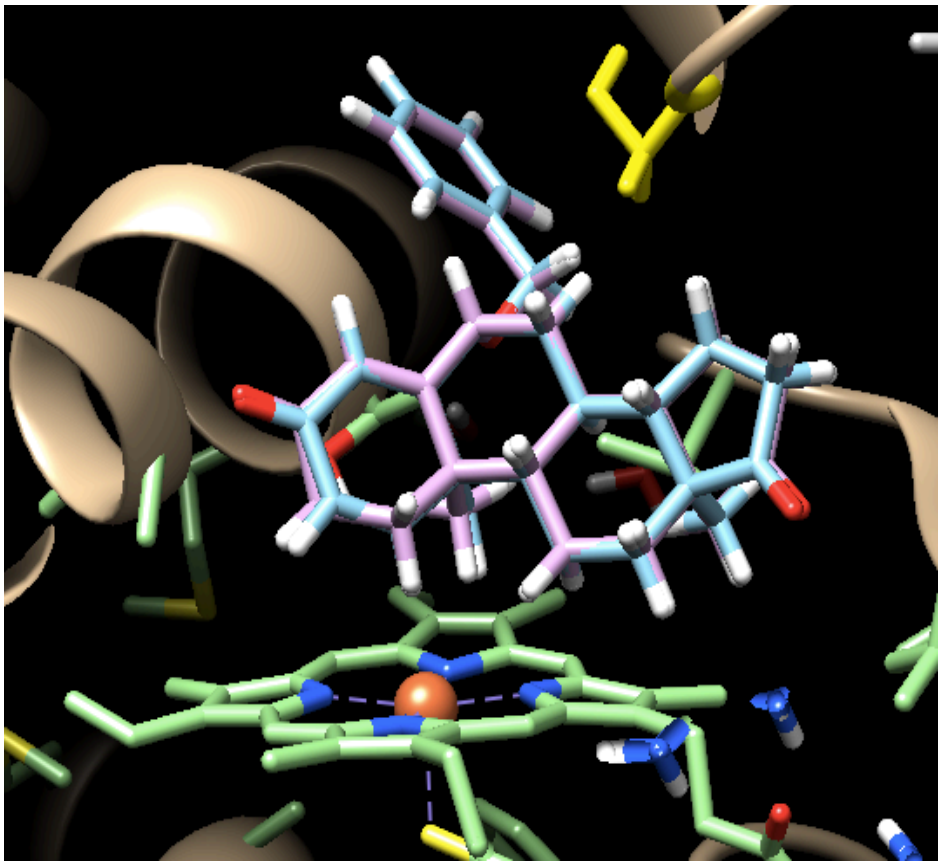

Supplementary Figure 2S3. Superimposition of predicted binding poses for HDDG-016 (blue) and HDDG-041 (purple). Shown above are the predicted binding poses for HDDG-016 (blue) and HDDG-041 (purple). The heme iron catalytic site is shown at the bottom of the figure, and residue Ser478, which lines the channel entry site, is highlighted in yellow.

Chapter 3

Fundamentals of drug design, Part II: virtual high-throughput screening (vHTS) in the development of novel CXCR4 modulators

Adapted with permission from Elsevier B.V. Liang et al. Eur J Med Chem. 2017 Aug; 136:360-371.

3.1 Abstract

While *in* silico drug screening has proven to be a successful route for hit discovery, other screening methods might be more efficient depending on what is known about the target and/or leads. The CXCR4 receptor is a widely studied receptor as it plays a crucial role in the inflammatory disease process, providing an attractive means for drug targeting. The floppy, flexible nature of the receptor, along with previously identified pharmacophores suggested that a virtual high throughput screening approach might work best to identify novel hits. A series of novel amide-sulfamide derivatives were designed, synthesized and comprehensively evaluated. This new scaffold exhibited much more potent CXCR4 inhibitory activity, with more than 70% of the compounds demonstrating notably better binding affinity than the reference drug AMD3100 in the binding assay. Additionally, in the Matrigel invasion screening assay, most of our compounds significantly blocked tumor cell invasion, demonstrating superior efficacy compared to AMD3100. Furthermore, compound **IIj** blocked mice ear inflammation by 75% and attenuated ear edema and damage substantially in an *in vivo* model of inflammation. Western blot analyses revealed that CXCR4 antagonist **IIj** significantly blocked CXCR4/CXCL12-mediated phosphorylation of Akt. Moreover, compound **IIj** had no observable cytotoxicity and displayed a favourable plasma stability in our preliminary pharmacokinetic study. The preliminary structure-activity relationships were also summarized. In short, this novel amide-sulfamide scaffold exhibited potent CXCR4 inhibitory activity both *in vitro* and *in vivo*. These results also confirmed that developing modulators targeting CXCR4 provides an exciting avenue for treatment of inflammation.

3.2 Introduction

Inflammation is a fundamental protective response of the immune system against pathogens or harmful irritants. The classical signs of inflammation are redness, swelling, heat, and pain, which may cause tissue damage and lead to a host of diseases including cancer (97). Nonsteroidal anti-inflammatory drugs (NSAIDs) are some of the most widely prescribed medications around the world (98). However, since 1938, the gastrointestinal (GI) damaging effects of NSAIDs have been very well characterized and recognized as the major limitation for the use of this class of drugs for long term treatment of inflammatory conditions (99). Cyclooxygenase (COX) enzymes are the main target of most NSAIDs and exist in two isoforms, namely COX-1 and COX-2. These side effects are related primarily to suppression of COX-1-derived prostaglandin (PG) synthesis in the stomach by non-selective NSAIDs (100). To overcome the gastrointestinal toxicity, selective COX-2 inhibitors, such as celecoxib and rofecoxib, were introduced for clinical use. However, while selective COX-2 inhibitors reduce gastroduodenal damage, they do not eliminate it. Furthermore, COX-2 inhibitors have also been associated with adverse cardiovascular effects (98). Despite many efforts for the development of NSAIDs, GI bleeding and ulceration remain major clinical concerns. Therefore, the search for safer anti-inflammatory drugs targeting novel pathways remains a feasible and promising strategy.

C-X-C chemokine receptor type 4 (CXCR4) is a 7-transmembrane chemokine receptor in the chemokine family (101). The ligand interacting with CXCR4 is stromal-derived-factor 1 (SDF-1) or C-X-C chemokine ligand 12 (CXCL12) (102). The CXCL12/CXCR4 axis has been shown to be involved in a number of pathological conditions, including cancer and inflammation (103). Although the exact mechanisms are not well understood, it has been proven that CXCR4 plays crucial roles in the pathophysiology of inflammatory diseases, including autoimmune diseases, rheumatoid arthritis, inflammatory bowel disease, ischemic injuries and lung diseases (104).

Taking CXCR4 as a new target, CXCR4 modulators may present a new avenue for the development of novel and safe anti-inflammatory drugs. The first small molecule CXCR4 antagonist to enter clinical trials was AMD3100 (**Fig 3.1**), which was originally used for the treatment of HIV (105). However, AMD3100 was not approved for this purpose due to poor oral bioavailability and serious cardiotoxicity (106-109). In particular, AMD3100, a complete CXCR4 inhibitor, acting as an effective stem cell mobilizer by dissociating CXCR4 from its ligand CXCL12, has been FDA-approved for use in patients with multiple myeloma in order to mobilize and harvest stem cells (110, 111).

Our lab has been developing partial CXCR4 modulators without cell mobilizing capability, which can be safe and effective in long term use (112, 113). We designed a synthesized a series of novel and potent CXCR4 modulators (Class I shown in **Fig. 3.1**) (114, 115). Among the promising candidates, **2** exhibits very low toxicity and excellent activity both *in vitro* and *in vivo*, and has been under Phase II clinical trials. Taking the symmetrical bis-secondary amines (Class I) as lead structures, here we attempted to design and synthesize a novel series of anti-CXCR4 compounds. Based on the principle of bioisosteres, one imine bond (-NH-) in the side chain was substituted with an amide group (-CONH-). In addition, our previous work found that a sulfamide scaffold (-SO_2NH-) is also an effective pharmacophore for CXCR4 inhibitory activity (116). Therefore, the imine bond in the other side chain was then substituted with the sulfamide group, giving rise to the novel amide-sulfamide compounds. Our lab initially employed a virtual high-throughput screening approach (vHTS), where we first queried a series of sulfochlorides and carboxylic acid derivatives which serve as the building blocks for our novel amide-sulfamide scaffold. After filtering for drug-like properties and simultaneously docking into the CXCR4 receptor, the top 30 docking score ranked amide-sulfamide structures were obtained. These compounds were then systemically screened; biological evaluation/validation proved that this amide-sulfamide structure successfully

maintained potent CXCR4 inhibitory activity (117). In this report, the amide side chain was then comprehensively modified and optimized. Nearly forty compounds were prepared and afforded a systematic biological analysis. The preliminary structure-activity relationship (SAR) was also summarized.

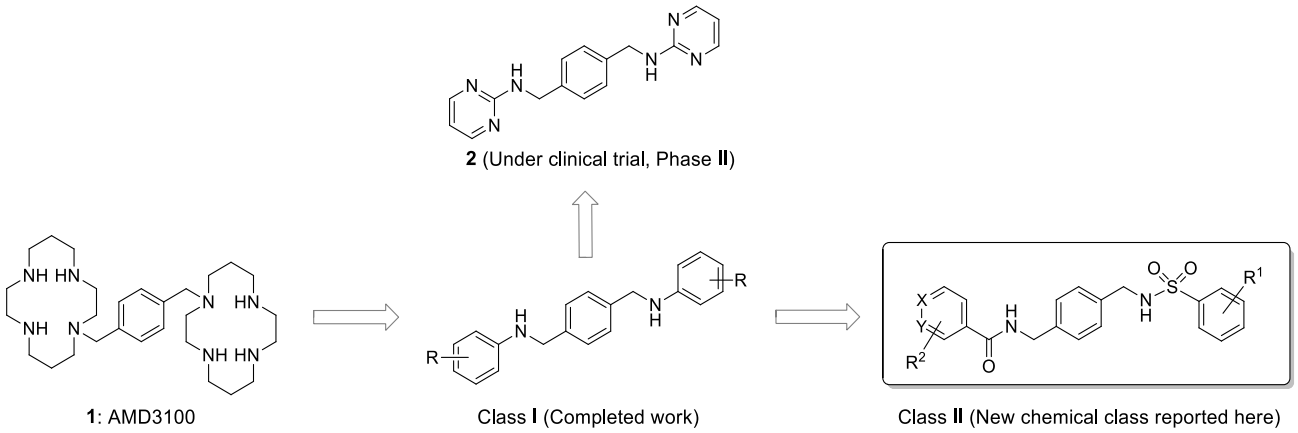

Fig. 3.1. Strategy for the discovery of novel anti-inflammatory agents.

3.3 Materials and Methods

Development of novel CXCR4 inhibitory candidates by vHTS FRESH workflow

A comprehensive background on FRESH methodology can be referenced from our previous publication (117). Briefly, the building block library was queried for two building blocks, sulfochlorides and carboxylic acids. Initially, there were ~100 hits identified as sulfochlorides and ~800 hits as carboxylic acids. These building blocks were then marked as fragments and filtered by several criteria (like no bridge-head or spiral carbon, no silicon, no permanent charges, etc.). The remaining ~50 sulfochlorides and ~360 carboxylic acids were linked to the core structure. About 19000 molecule structures were obtained by combinatorial library enumeration. Then a series of calculations on their physical/ADMET properties were performed based on Lipinski's "Rule of Five", Jorgensen's "Rule of Three", Morelli, Bourgeas, and Roche's "Rule of Four" (118-120). 19000 molecules were reduced to only 364 compounds with drug-like properties. Consequently, after docking with CXCR4 receptor, the preliminary docking scores were obtained. Promising data from this initial study gave rise to the comprehensive evaluation of the amide side chain group present in this novel class of molecules.

Primary binding affinity screening

For binding affinity assay, 2×10^4 MDA-MB-231 cells in 300 µL of cell culture medium were seeded in an 8-well slide chamber 2 days before the experiments were conducted. Various concentrations of different compounds (1, 10, 100, or 1000 nM) were added to the separate wells and incubated for 10 minutes at room temperature, and then the cells were fixed in 4% ice-cold paraformaldehyde. The cells were rehydrated in phosphate-buffered saline (PBS). The slides were subsequently incubated for 30 minutes at room temperature with 0.05 µg/mL biotinylated TN14003, washed three times with PBS, and incubated in streptavidin-rhodamine (1:150 dilution;

Jackson ImmunoResearch Laboratories, West Grove, PA) for 30 minutes at room temperature. Finally, the slides were washed with PBS and mounted in an anti-fade mounting solution (Molecular Probes, Eugene, OR), and the samples were analyzed on a Nikon Eclipse E800 microscope (115, 116, 121).

Matrigel Invasion assay

Matrigel invasion assay was performed by using a Matrigel invasion chamber from Corning Biocoat (Bedford, MA). CXCL12α (200 ng/mL; R & D Systems, Minneapolis, MN) was added to the bottom chamber to induce the invasion of MDA-MB-231 cells through the Matrigel. The selected compounds (100 nM) or AMD3100 were added to the cells before the cells were seeded in the top chamber. The Matrigel invasion chamber was incubated for 22 hours in a humidified cell culture incubator. First, non-invading cells were removed from the top of the Matrigel with a cotton-tipped swab. Invading cells on the filter at the bottom of the Matrigel were fixed in methanol and stained with hematoxylin and eosin (H & E). The percent of invasion was determined by counting the H&E stained cells (116, 121).

Xylene-induced ear inflammation suppression test

Five mice per group were used to determine the effect of the CXCR4 modulators. The inner and outer surfaces of the right ear of each mouse were treated with a total 30 µL of xylene for the induction of ear edema, whereas the left ear was treated with 30 µL of saline, which was used as a non-inflammation control. The selected compounds were dissolved in 10% DMSO and 90% of 45% (2-hydroxypropyl)-β-cyclodextrin (CD) in PBS. 30 minutes after the application of xylene, 14 selected compounds were administered intraperitoneally (i.p.) at 10 mg/kg. Control animals received corresponding i.p. injections of the vehicle. The animals were sacrificed 2 hours later,

and two ear plugs (7 mm in diameter) were removed from both the treated ear and the untreated ears. Weights of treated and untreated ear plugs were measured. The difference in weight of the two ear plugs was taken as a measure of edematous response. The inflammation-suppression percentage was calculated by comparing the drug-treated group to the control group (122).

Western blot analysis

Forty micrograms of protein were separated by SDS-PAGE and transferred to a PVDF membrane (Bio-Rad, Hercules, CA, USA). The membrane was blocked for 30 min in a blocking solution (5 % milk in Trisbuffered saline containing 0.1% Tween-20) and incubated overnight at 4°C using monoclonal rabbit anti-phospho-Akt (Ser473) antibody (Cat No., 9271)/monoclonal rabbit anti-Akt (pan) antibody (cat No., 4691) or monoclonal rabbit anti-phospho-p44/42 MAPK (Thr202/Tyr204) antibody (cat No., 4376)/monoclonal rabbit anti-p44/42 MAPK antibody (cat No., 4695) at 1:500 in blocking solution. All antibodies were purchased from Cell Signaling Technology (Danvers, USA). The membrane was incubated for 1 hour with goat anti-rabbit IgG (H+L)-HRP conjugated secondary antibody at 1:10000 (Cat No. 1706515; Bio-rad, Hercules, USA) after washing. Enzyme-linked chemiluminescence was performed to detect hybridized protein bands.

Preliminary cytotoxicity study of compound IIj (MTT assay)

The antiproliferative activity of the compounds was determined using MTT assay. Human breast cancer MDA-MB-231 or MCF-10A Cells were seeded in 96-well micro culture plates at 3000 cells/well in 100 µl of medium and incubated for 24 h at 37 °C in CO_2 incubator. Following the incubation for 24 h, these cells were treated with Compound IIj for 24 h at 37 °C. Finally, 20

μl of CellTiter 96AQ reagent (Promega, Madison, WI) was added into each well and incubated for an additional 2 h, and the absorbance at 490 nm was measured.

Preliminary pharmacokinetic study of compound IIj

Nude mice with body weight about 20 g were used in the PK study. The mice were anaesthetized with Ketamine hydrochloride (90 mg/kg) and Xylazine (4.5 mg/kg). Compound **IIj** was dissolved in 10% DMSO and 90% of 45% (2-hydroxypropyl)-β-cyclodextrin (CD) in PBS. The mice were warmed by the heat lamp for 2 minutes and then received a single dose (30 mg/kg) of compound **IIj** via intravenous injection (i.v.). Blood samples (100 μL) were collected at 0, 5, 20 and 50 minutes post dose from orbital venous sinus with heparinized capillary tubes (I.D. 1.1–1.2 mm). After collection, the blood sample was centrifuged at 13000 g for 4 min at 4 °C. The supernatant was then filtrated by microcon centrifugal filter (10000 NMWL) at 13000 g for 30 min at 4 °C. The filtrate was frozen at −80°C until HPLC analysis. The HPLC analysis of the blood sample was performed on a C18 column (250*4.6 mm). Acetonitrile (0.1%TFA)-Water (0.1%TFA) (50:50, V/V) was applied as the mobile phase and the detective wavelength was set at 254 nm.

Chemistry

General Information

Proton and carbon NMR spectra were recorded on INOVA-400 (400 MHz), INOVA-600 (600 MHz) or VNMR-400 spectrometers at Emory NMR Research Center. The spectra obtained in $CDCl_3$ and DMSO-d_6 were referenced to the residual solvent peak. Chemical shifts (δ) are reported in parts per million (ppm) relative to residual undeuterated solvent as an internal reference. Mass spectra were recorded on a JEOL spectrometer at Emory University Mass

Spectrometry Center. Analytical thin layer chromatography (TLC) was performed on precoated glass backed plates from Scientific Adsorbents Incorporated (Silica Gel 60 F254; 0.25 mm thickness).

*General procedure for synthesis of intermediate **4***

A solution of 4-(Boc-aminomethyl)benzylamine (**3**) (1.0 mmol) and TEA (3.0 mmol) in anhydrous DCM (8 mL) was cooled with an ice bath, then the corresponding sulfochloride (1.1 mmol, dissolved in 2 mL anhydrous DCM) was added dropwise. The reaction mixture was allowed to stir at 0 °C for 1 h. After removing the cooling bath, the resulting mixture was stirred for 5 h at room temperature, then diluted with saturated aqueous $NaHCO_3$ and extracted with DCM (10 mL) for three times. The combined organic layer was sequentially washed with water and brine, dried with anhydrous Na_2SO_4, and concentrated in vacuo. The crude was purified by column chromatography with DCM/methanol (150:1, v/v) to give the product as a white solid.

*General procedure for synthesis of intermediate **5***

A solution of intermediate **4** (1.0 mmol) in DCM (10 mL) was treated with trifluoroacetic acid (4 mmol) at room temperature. The resulting mixture was stirred for 8 h. The solvent was removed under reduced pressure. The residue was dissolved in saturated aqueous $NaHCO_3$ (2 mL) followed by adding more saturated aqueous $NaHCO_3$ to adjust to pH = 10. Then the mixture was filtered and the intermediate **5** was obtained as the filter cake without further purification.

*General procedure for synthesis of target compounds **Ia-r** and **IIa-r***

A solution of intermediate **5** (1.0 mmol) and TEA (3.0 mmol) in anhydrous DCM (8 mL) was cooled with an ice bath, then the corresponding benzoyl chloride derivatives (1.1 mmol, dissolved in 2 mL anhydrous DCM) was added dropwise. The reaction mixture was allowed to stir

at 0 °C for 1 h. After removing the cooling bath, the resulting mixture was stirred for 5 h at room temperature, then diluted with saturated aqueous $NaHCO_3$and extracted with DCM (10 mL) three times. The combined organic layer was sequentially washed with water and brine, dried with anhydrous Na_2SO_4, and concentrated in vacuo. The crude was purified by column chromatography with DCM/methanol to give the product as a white solid.

*N-(4-(phenylsulfonamidomethyl)benzyl)benzamide (**Ia**)*

White solid, yield 85%, m.p. 139–141 °C. ^{1}H NMR (400 MHz, $CDCl_3$) δ 7.86–7.86 (m, 2H), 7.76–7.79 (m, 2H), 7.56–7.61 (m, 1H), 7.49–7.54 (m, 3H), 7.41–7.46 (m, 2H), 7.25– 7.28 (m, 2H), 7.16–7.20 (m, 2H), 6.42 (s, 1H), 4.72 (s, 1H), 4.59 (d, J = 5.8 Hz, 2H), 4.13 (d, J = 6.2 Hz, 2H). ^{13}C NMR (100 MHz, Methanol-d_4) δ 170.22, 142.31, 139.69, 137.69, 135.77, 133.61, 132.86, 130.25, 129.73, 129.25, 128.77, 128.44, 128.10, 47.79, 44.31. HRMS calcd for $C_{21}H_{21}N_2O_3S$ 381.12674 $[M + H]^+$, found 381.12651.

*2-Methyl-N-(4-(phenylsulfonamidomethyl)benzyl)benzamide (**Ib**)*

White solid, yield 79%, m.p. 129–131 °C. ^{1}H NMR (400 MHz, DMSO-d_6) δ 8.78 (t, J = 6.1 Hz, 1H), 8.15 (t, J = 6.3 Hz, 1H), 7.79 – 7.82 (m, 2H), 7.56 – 7.66 (m, 3H), 7.31 – 7.35 (m, 2H), 7.19 – 7.26 (m, 6H), 4.39 (d, J = 6.1 Hz, 2H), 3.96 (d, J= 6.2 Hz, 2H), 2.32 (s, 3H). ^{13}C NMR (100 MHz, DMSO-d_6) δ 168.97, 140.68, 138.60, 136.98, 136.04, 135.14, 132.29, 130.39, 129.23, 129.15, 127.53, 127.03, 126.96, 126.41, 125.47, 45.87, 42.01, 19.40. HRMS calcd for $C_{22}H_{22}O_3N_2SNa$ 417.12433 $[M + Na]^+$, found 417.12427.

*3-Methyl-N-(4-(phenylsulfonamidomethyl)benzyl)benzamide (**Ic**)*

White solid, yield 81%, m.p. 112–114 °C. ^{1}H NMR (400 MHz, DMSO-d_6) δ 8.97 (t, J = 6.0 Hz, 1H), 8.13 (t, J = 6.2 Hz, 1H), 7.78 – 7.80 (m, 2H), 7.70 (qd, J = 1.3, 0.7 Hz, 1H), 7.65 – 7.68 (m, 1H), 7.55 – 7.63 (m, 3H), 7.34 – 7.35 (m, 2H), 7.16 – 7.23 (m, 4H), 4.41 (d, J = 6.0 Hz, 2H), 3.94 (d, J = 6.2 Hz, 2H), 2.35 (s, 3H). ^{13}C NMR (100 MHz, DMSO-d_6) δ 166.20, 140.66, 138.68, 137.52, 136.01, 134.33, 132.27, 131.72, 129.14, 128.16, 127.75, 127.51, 127.11, 126.41, 124.32, 45.89, 42.28, 20.93. HRMS calcd for $C_{22}H_{23}O_3N_2S$ 395.14239 $[M + H]^+$, found 395.14241.

*4-Methyl-N-(4-(phenylsulfonamidomethyl)benzyl)benzamide (**Id**)*

White solid, yield 87%, m.p. 188–190 °C. ^{1}H NMR (400 MHz, DMSO-d_6) δ 8.94 (t, J = 6.0 Hz, 1H), 8.13 (t, J = 6.3 Hz, 1H), 7.77 – 7.80 (m, 4H), 7.55 – 7.63 (m, 3H), 7.26– 7.28 (m, 2H), 7.15 – 7.20 (m, 4H), 4.41 (d, J = 6.0 Hz, 2H), 3.94 (d, J= 6.2 Hz, 2H), 2.35 (s, 3H). ^{13}C NMR (100 MHz, DMSO-d_6) δ 165.96, 141.02, 140.66, 138.74, 135.98, 132.26, 131.53, 129.13, 128.79, 127.50, 127.20, 127.10, 126.40, 45.88, 42.24, 20.92. HRMS calcd for $C_{22}H_{23}N_2O_3S$ 395.14239 $[M + H]^+$, found 395.14219.

*2-Methoxy-N-(4-(phenylsulfonamidomethyl)benzyl)benzamide (**Ie**)*

White solid, yield 83%, m.p. 123–125 °C. ^{1}H NMR (600 MHz, DMSO-d_6) δ 8.66 (t, J = 6.1 Hz, 1H), 8.12 (t, J = 6.3 Hz, 1H), 7.79 – 7.80 (m, 2H), 7.72 (dd, J = 7.7, 1.9 Hz, 1H), 7.56 – 7.63 (m, 3H), 7.47 (ddd, J = 9.2, 7.3, 1.9 Hz, 1H), 7.23 (d, J= 7.9 Hz, 2H), 7.17 (d, J = 7.9 Hz, 2H), 7.14 (d, J = 8.3 Hz, 1H), 7.03 (t, J = 7.4 Hz, 1H), 4.44 (d, J = 6.1 Hz, 2H), 3.94 (d, J = 6.3 Hz, 2H), 3.88 (s, 3H). ^{13}C NMR (100 MHz, DMSO-d_6) δ 140.66, 138.67, 135.91, 132.28, 132.10, 130.29, 129.14, 127.51, 126.94, 126.41, 123.19, 120.43, 111.96, 55.84, 45.90, 42.24. HRMS calcd for $C_{22}H_{23}N_2O_4S$ 411.13730 $[M + H]^+$, found 411.13739.

*3-Methoxy-N-(4-(phenylsulfonamidomethyl)benzyl)benzamide (**If**)*

White solid, yield 78%, m.p. 120–122 °C. ^{1}H NMR (600 MHz, DMSO-d6) δ 9.01 (t, *J* = 6.1 Hz, 1H), 8.12 (t, *J* = 6.2 Hz, 1H), 7.79 (d, *J* = 7.2 Hz, 2H), 7.56 – 7.63 (m, 3H), 7.37 – 7.47 (m, 3H), 7.22 (d, *J* = 8.0 Hz, 2H), 7.17 (d, *J* = 8.0 Hz, 2H), 7.09 (dd, *J* = 8.1, 2.7 Hz, 1H), 4.42 (d, *J* = 5.9 Hz, 2H), 3.94 (d, *J* = 6.3 Hz, 2H), 3.80 (s, 3H). ^{13}C NMR (100 MHz, DMSO-d_6) δ 165.80, 159.14, 140.65, 138.60, 136.04, 135.72, 132.27, 129.41, 129.14, 127.52, 127.12, 126.40, 119.41, 117.08, 112.33, 55.24, 45.88, 42.33. HRMS calcd for $C_{22}H_{23}N_2O_4S$ 411.13730 $[M + H]^+$, found 411.13721.

*4-Methoxy-N-(4-(phenylsulfonamidomethyl)benzyl)benzamide (**Ig**)*

White solid, yield 85%, m.p. 164–166 °C. ^{1}H NMR (400 MHz, DMSO-d_6) δ 8.88 (t, *J* = 6.0 Hz, 1H), 8.13 (t, *J* = 6.3 Hz, 1H), 7.84 – 7.88 (m, 2H), 7.78 – 7.80 (m, 2H), 7.55 – 7.63 (m, 3H), 7.15 – 7.22 (m, 4H), 6.98 – 7.02 (m, 2H), 4.41 (d, *J* = 6.0 Hz, 2H), 3.94 (d, *J* = 6.3 Hz, 2H),

3.81 (s, 3H). ^{13}C NMR (100 MHz, DMSO-d_6) δ 165.56, 161.52, 138.85, 135.95, 132.27, 129.13, 129.00, 127.49, 127.08, 126.53, 126.40, 113.47, 55.32, 45.89, 42.22. HRMS calcd for $C_{22}H_{23}N_2O_4S$ 411.13730 $[M + H]^+$, found 411.13708.

*2-Fluoro-N-(4-(phenylsulfonamidomethyl)benzyl)benzamide (**Ih**)*

White solid, yield 70%, m.p. 122–124 °C. ^{1}H NMR (400 MHz, $CDCl_3$) δ 8.10–8.14 (m, 1H), 7.86–7.88 (m, 2H), 7.45– 7.60 (m, 4H), 7.09–7.30(m, 6H), 7.03 (s, 1H), 4.78 (t, *J* = 6.2 Hz, 1H), 4.62 (d, *J* = 5.6 Hz, 2H), 4.14 (d, *J* = 6.2 Hz, 2H). ^{13}C NMR (101 MHz, DMSO-d_6) δ 164.26, 160.66, 158.18, 140.83, 138.50, 136.46, 132.94, 132.86, 132.76, 130.36, 130.33, 129.57, 127.91, 127.42, 126.76, 124.95, 124.92, 124.21, 124.07, 116.59, 116.37, 46.18, 42.65. HRMS calcd for $C_{21}H_{19}O_3N_2SFNa$ 421.09926 $[M + Na]^+$, found 421.09950.

*3-Fluoro-N-(4-(phenylsulfonamidomethyl)benzyl)benzamide (**Ii**)*

White solid, yield 74%, m.p. 132–134 °C. ^{1}H NMR (600 MHz, Chloroform-*d*) δ 7.87 (d, *J* = 7.7 Hz, 2H), 7.59 (t, *J* = 7.4 Hz, 1H), 7.49 – 7.53 (m, 4H), 7.40 (td, *J* = 8.0, 5.5 Hz, 1H), 7.17 – 7.22 (m, 5H), 6.45 (s, 1H), 4.76 (t, *J* = 6.2 Hz, 1H), 4.58 (d, *J* = 5.8 Hz, 2H), 4.13 (d, *J* = 6.3 Hz, 2H). ^{13}C NMR (100 MHz, DMSO-d_6) δ 164.74, 163.16, 160.73, 140.66, 138.32, 136.69, 136.63, 136.14, 132.27, 130.52, 130.44, 129.14, 127.54, 127.16, 126.40, 123.37, 118.22, 118.01, 114.12, 113.89, 45.86, 42.41. HRMS calcd for $C_{21}H_{20}O_3N_2SF$ 399.11732 $[M + H]^+$, found 399.11710.

*4-Fluoro-N-(4-(phenylsulfonamidomethyl)benzyl)benzamide (**Ij**)*

White solid, yield 72%, m.p. 162–164 °C. ^{1}H NMR (400 MHz, DMSO-d_6) δ 9.06 (t, *J* = 6.0 Hz, 1H), 8.13 (t, *J* = 6.3 Hz, 1H), 7.93 – 7.98 (m, 2H), 7.78 – 7.81 (m, 2H), 7.55 – 7.63 (m, 3H), 7.28 – 7.34 (m, 2H), 7.16 – 7.23 (m, 4H), 4.42 (d, *J* = 6.0 Hz, 2H), 3.94 (d, *J* = 6.3 Hz, 2H). ^{13}C NMR (100 MHz, DMSO-d_6) δ 165.08, 165.04, 162.60, 140.66, 138.52, 136.08, 132.27, 130.79, 129.88, 129.79, 129.14, 127.53, 127.13, 126.40, 115.31, 115.09, 45.88, 42.36. HRMS calcd for $C_{21}H_{20}O_3N_2SF$ 399.11732 $[M + H]^+$, found 399.11710.

*2-Chloro-N-(4-(phenylsulfonamidomethyl)benzyl)benzamide (**Ik**)*

White solid, yield 76%, m.p. 116–118 °C. ^{1}H NMR (600 MHz, DMSO-d_6) δ 8.96 (t, *J* = 5.6 Hz, 1H), 8.14 (t, *J* = 6.5 Hz, 1H), 7.81 (d, *J* = 7.7 Hz, 2H), 7.63 – 7.65 (m, 3H), 7.38 – 7.51 (m, 4H), 7.27 (d, *J* = 7.6 Hz, 2H), 7.20 (d, *J* = 7.6 Hz, 2H), 4.40 (d, *J* = 6.0 Hz, 2H), 3.96 (d, *J* = 6.2 Hz, 2H). ^{13}C NMR (100 MHz, Chloroform-*d*) δ 166.58, 140.13, 137.83, 135.88, 134.95, 132.96, 131.69, 130.83, 130.53, 130.49, 129.38, 128.49, 128.40, 127.38, 127.32, 47.19, 44.00. HRMS calcd for $C_{21}H_{20}O_3N_2SCl$ 415.08777 $[M + H]^+$, found 415.08759.

*3-Chloro-N-(4-(phenylsulfonamidomethyl)benzyl)benzamide (**Im**)*

White solid, yield 80%, m.p. 114–116 °C. ^{1}H NMR (400 MHz, DMSO-d_6) δ 9.16 (t, J = 6.0 Hz, 1H), 8.13 (t, J = 6.3 Hz, 1H), 7.92 (t, J = 1.9 Hz, 1H), 7.84 (ddd, J = 7.7, 1.7, 1.1 Hz, 1H), 7.78 – 7.80 (m, 2H), 7.50 – 7.63 (m, 5H), 7.22 (d, J = 8.3 Hz, 2H), 7.18 (d, J = 8.3 Hz, 2H), 4.42 (d, J = 5.9 Hz, 2H), 3.94 (d, J = 6.3 Hz, 2H). ^{13}C NMR (101 MHz, DMSO-d_6) δ 164.70, 140.65, 138.33, 136.28, 136.18, 133.21, 132.34, 131.13, 130.40, 129.20, 127.59, 127.22, 127.06, 126.45, 126.04, 45.90, 42.46. HRMS calcd for $C_{21}H_{20}O_3N_2SCl$ 415.08777 $[M + H]^+$, found 415.08771.

*4-Chloro-N-(4-(phenylsulfonamidomethyl)benzyl)benzamide (**In**)*

White solid, yield 78%, m.p. 182–184 °C. ^{1}H NMR (400 MHz, DMSO-d_6) δ 9.12 (t, J = 5.9 Hz, 1H), 8.14 (t, J = 6.3 Hz, 1H), 7.88 – 7.92 (m, 2H), 7.78 – 7.81 (m, 2H), 7.53 – 7.63 (m, 5H), 7.15 – 7.23 (m, 4H), 4.42 (d, J = 4.4 Hz, 2H), 3.94 (d, J= 6.1 Hz, 2H). ^{13}C NMR (100 MHz, DMSO-d_6) δ 164.98, 140.66, 138.40, 136.12, 136.03, 133.00, 132.29, 129.15, 128.38, 127.72, 127.54, 127.15, 126.42, 45.87, 42.27. HRMS calcd for $C_{21}H_{19}O_3N_2SClNa$ 437.06971 $[M + Na]^+$, found 437.07017.

*4-Nitro-N-(4-(phenylsulfonamidomethyl)benzyl)benzamide (**Io**)*

White solid, yield 70%, m.p. 201–203 °C. ^{1}H NMR (400 MHz, DMSO-d_6) δ 9.37 (t, J = 6.0 Hz, 1H), 8.33 (d, J = 8.8 Hz, 2H), 8.10 – 8.15 (m, 3H), 7.79 (d, J = 6.6 Hz, 2H), 7.66 – 7.52 (m, 3H), 7.24 (d, J = 7.9 Hz, 2H), 7.19 (d, J = 7.9 Hz, 2H), 4.45 (d, J = 5.9 Hz, 2H), 3.94 (d, J = 6.2 Hz, 2H). ^{13}C NMR (100 MHz, DMSO-d_6) δ 164.51, 149.01, 140.66, 139.94, 138.07, 136.25, 132.28, 129.14, 128.73, 127.58, 127.23, 126.40, 123.53, 45.85, 42.56. HRMS calcd for $C_{21}H_{20}O_5N_3S$ 426.11182 $[M + H]^+$, found 426.11192.

*2,4,6-Trichloro-N-(4-(phenylsulfonamidomethyl)benzyl)benzamide (**Ip**)*

White solid, yield 79%, m.p. 158–160 °C. ^{1}H NMR (400 MHz, DMSO-d_6) δ 9.19 (t, J = 6.0 Hz, 1H), 8.15 (t, J = 6.3 Hz, 1H), 7.80 – 7.82 (m, 2H), 7.76 (s, 2H), 7.57 – 7.66 (m, 3H), 7.28 (d, J = 8.2 Hz, 2H), 7.20 (d, J = 8.2 Hz, 2H), 4.43 (d, J = 6.0 Hz, 2H), 3.96 (d, J = 6.3 Hz, 2H). ^{13}C NMR (100 MHz, DMSO-d_6) δ 162.88, 140.66, 137.42, 136.34, 135.49, 134.29, 132.31, 132.03, 129.16, 127.93, 127.48, 127.30, 126.42, 45.84, 42.13. HRMS calcd for $C_{21}H_{18}O_3N_2SCl_3$ 483.00982 $[M + H]^+$, found 483.00996.

*N-(4-(phenylsulfonamidomethyl)benzyl)nicotinamide (**Iq**)*

White solid, yield 60%, m.p. 109–111 °C. ^{1}H NMR (400 MHz, $CDCl_3$) δ 8.83 (dd, J = 2.3, 0.9 Hz, 1H), 8.69 (dd, J = 4.9, 1.7 Hz, 1H), 8.11 (ddd, J = 7.9, 2.3, 1.7 Hz, 1H), 7.86–7.90 (m, 2H), 7.57– 7.62 (m, 1H), 7.50–7.54 (m, 2H), 7.36 (ddd, J = 8.0, 4.9, 0.9 Hz, 1H), 7.12–7.25 (m, 4H), 6.79 (t, J = 5.6 Hz, 1H), 5.24 (t, J = 6.1 Hz, 1H), 4.57 (d, J = 5.7 Hz, 2H), 4.11 (d, J = 6.1 Hz, 2H). ^{13}C NMR (101 MHz, $CDCl_3$) δ 165.82, 152.08, 148.20, 140.05, 137.79, 136.05, 135.49, 132.89, 130.11, 129.36, 128.58, 128.30, 127.20, 123.69, 47.09, 43.83. HRMS calcd for $C_{20}H_{20}O_3N_3S$ 382.12199 $[M + H]^+$, found 382.12154.

*N-(4-(phenylsulfonamidomethyl)benzyl)isonicotinamide (**Ir**)*

White solid, yield 63%, m.p. 154–156 °C. ^{1}H NMR (400 MHz, DMSO-d_6) δ 9.33 (t, J = 6.0 Hz, 1H), 8.73 – 8.74 (m, 2H), 8.14 (t, J = 6.3 Hz, 1H), 7.78 – 7.81 (m, 4H), 7.55 – 7.64 (m, 3H), 7.17 – 7.25 (m, 4H), 4.45 (d, J = 6.0 Hz, 2H), 3.95 (d, J = 6.3 Hz, 2H). ^{13}C NMR (100 MHz, DMSO-d_6) δ 164.58, 150.25, 141.21, 140.65, 138.03, 136.25, 132.28, 129.14, 127.57, 127.19, 126.40, 121.21, 45.85, 42.41. HRMS calcd for $C_{20}H_{20}O_3N_3S$ 382.12199 $[M + H]^+$, found 382.12164.

*N-(4-((4-methylphenylsulfonamido)methyl)benzyl)benzamide (**IIa**)*

White solid, yield 89%, m.p. 162–164 °C. ^{1}H NMR (400 MHz, $CDCl_3$) δ 7.75–7.79 (m, 4H), 7.49–7.53 (m, 1H), 7.41–7.46 (m, 2H), 7.27–7.33 (m, 4H), 7.18–7.20 (m, 2H), 6.41 (s, 1H), 4.62 (s, 1H), 4.60 (d, *J* = 5.7 Hz, 2H), 4.11 (d, *J* = 6.2 Hz, 2H), 2.44 (s, 3H). ^{13}C NMR (100 MHz, Methanol-d_4) δ 170.22, 144.69, 139.66, 139.25, 137.76, 135.75, 132.84, 130.78, 129.72, 129.24, 128.74, 128.45, 128.19, 47.77, 44.32, 21.57. HRMS calcd for $C_{22}H_{22}O_3N_2SNa$ 417.12433 $[M + Na]^+$, found 417.12417.

*2-Methyl-N-(4-((4-methylphenylsulfonamido)methyl)benzyl)benzamide (**IIb**)*

White solid, yield 87%, m.p. 147–149 °C. ^{1}H NMR (400 MHz, DMSO-d_6) δ 8.79 (t, *J* = 6.1 Hz, 1H), 8.05 (t, *J* = 6.3 Hz, 1H), 7.68 – 7.71 (m, 2H), 7.38 – 7.40 (m, 2H), 7.30 – 7.36 (m, 2H), 7.19 – 7.26 (m, 6H), 4.39 (d, *J* = 6.1 Hz, 2H), 3.92 (d, *J* = 6.3 Hz, 2H), 2.38 (s, 3H), 2.32 (s, 3H). ^{13}C NMR (100 MHz, DMSO-d_6) δ 168.98, 142.54, 138.59, 137.78, 136.99, 136.10, 135.15, 130.40, 129.57, 129.24, 127.53, 127.02, 126.97, 126.51, 125.47, 45.87, 42.03, 20.94, 19.39. HRMS calcd for $C_{23}H_{25}O_3N_2S$ 409.15804 $[M + H]^+$, found 409.15808.

*3-Methyl-N-(4-((4-methylphenylsulfonamido)methyl)benzyl)benzamide (**IIc**)*

White solid, yield 82%, m.p. 123–125 °C. ^{1}H NMR (400 MHz, DMSO-d_6) δ 8.98 (t, *J* = 6.0 Hz, 1H), 8.03 (t, *J* = 6.3 Hz, 1H), 7.65 – 7.71 (m, 4H), 7.34 – 7.39 (m, 4H), 7.17 – 7.24 (m, 4H), 4.42 (d, *J* = 6.0 Hz, 2H), 3.90 (d, *J* = 6.3 Hz, 2H), 2.37 (s, 3H), 2.35 (s, 3H). ^{13}C NMR (100 MHz, DMSO-d_6) δ 166.21, 142.52, 138.66, 137.76, 137.52, 136.07, 134.34, 131.72, 129.56, 128.16, 127.75, 127.51, 127.10, 126.50, 124.33, 45.88, 42.28, 20.92. HRMS calcd for $C_{23}H_{25}O_3N_2S$ 409.15804 $[M + H]^+$, found 409.15771.

*4-Methyl-N-(4-((4-methylphenylsulfonamido)methyl)benzyl)benzamide (**IId**)*

White solid, yield 80%, m.p. 180–182 °C. ^{1}H NMR (400 MHz, DMSO-d_6) δ 8.95 (t, J = 6.0 Hz, 1H), 8.03 (t, J = 6.3 Hz, 1H), 7.79 (d, J = 8.2 Hz, 2H), 7.68 (d, J = 8.3 Hz, 2H), 7.37 (d, J = 7.6 Hz, 2H), 7.27 (d, J = 7.6 Hz, 2H), 7.22 (d, J = 8.2 Hz, 2H), 7.17 (d, J = 8.3 Hz, 2H), 4.42 (d, J = 6.0 Hz, 2H), 3.90 (d, J = 6.3 Hz, 2H), 2.37 (s, 3H), 2.35 (s, 3H). ^{13}C NMR (100 MHz, DMSO-d_6) δ 165.98, 142.53, 141.03, 138.73, 136.05, 131.55, 129.56, 128.79, 127.51, 127.21, 127.09, 126.50, 45.88, 42.25, 20.92. HRMS calcd for $C_{23}H_{25}N_2O_3S$ 409.15804 $[M + H]^+$, found 409.15776.

*2-Methoxy-N-(4-((4-methylphenylsulfonamido)methyl)benzyl)benzamide (**IIe**)*

White solid, yield 79%, m.p. 154–156 °C. ^{1}H NMR (600 MHz, DMSO-d_6) δ 8.66 (t, J = 5.9 Hz, 1H), 8.03 (t, J = 6.3 Hz, 1H), 7.71–7.74 (m, 1H), 7.68 (dd, J = 8.1, 1.9 Hz, 2H), 7.47 (ddd, J = 8.2, 7.2, 1.8 Hz, 1H), 7.38 (dd, J = 8.6, 1.0 Hz, 2H), 7.24 (d, J = 8.4 Hz, 2H), 7.18 (d, J = 6.7 Hz, 2H), 7.14 (d, J = 8.4 Hz, 1H), 7.03 (td, J = 7.4, 1.1 Hz, 1H), 4.45 (d, J = 6.1 Hz, 2H),3.91 (d, J = 6.3 Hz, 2H), 3.88 (s, 3H), 2.37 (s, 3H). ^{13}C NMR (101 MHz, DMSO-d_6) δ 165.10, 156.93, 142.60, 138.70, 137.74, 135.99, 132.16, 130.33, 129.62, 127.56, 126.97, 126.56, 123.21, 120.46, 111.97, 55.85, 45.93, 42.28, 20.98. HRMS calcd for $C_{23}H_{25}N_2O_4S$ 425.15295 $[M + H]^+$, found 425.15280.

*3-Methoxy-N-(4-((4-methylphenylsulfonamido)methyl)benzyl)benzamide (**IIf**)*

White solid, yield 82%, m.p. 130–132 °C. ^{1}H NMR (600 MHz, DMSO-d_6) δ 9.02 (t, J = 6.1 Hz, 1H), 8.02 (t, J = 6.3 Hz, 1H), 7.68 (d, J = 8.3 Hz, 2H), 7.36 – 7.47 (m, 5H), 7.22 (d, J = 8.2 Hz, 2H), 7.18 (d, J = 8.2 Hz, 2H), 7.09 (dd, J = 8.0, 3.0 Hz, 1H), 4.43 (d, J = 6.1 Hz, 2H), 3.90 (d, J = 6.4 Hz, 2H), 3.80 (s, 3H), 2.37 (s, 3H). ^{13}C NMR (100 MHz, DMSO-d_6) δ165.81, 159.15, 142.53, 138.58, 137.75, 136.11, 135.73, 129.56, 129.40, 127.52, 127.11, 126.50, 119.42, 117.08, 112.34, 55.24, 45.87, 42.33, 20.92. HRMS calcd for $C_{23}H_{25}N_2O_4S$ 425.15295 $[M + H]^+$, found 425.15283.

*4-Methoxy-N-(4-((4-methylphenylsulfonamido)methyl)benzyl)benzamide (**IIg**)*

White solid, yield 75%, m.p. 147–149 °C. ^{1}H NMR (600 MHz, DMSO-d_6) δ 8.87 (t, J = 6.0 Hz, 1H), 8.02 (t, J = 6.3 Hz, 1H), 7.86 (d, J = 8.8 Hz, 2H), 7.68 (d, J = 8.3 Hz, 2H), 7.37 (d, J = 8.0 Hz, 2H), 7.21 (d, J = 8.0 Hz, 2H), 7.17 (d, J = 8.0 Hz, 2H), 6.99 (d, J = 8.8 Hz, 2H), 4.41 (d, J = 6.0 Hz, 2H), 3.90 (d, J = 6.2 Hz, 2H), 3.80 (s, 3H), 2.37 (s, 3H). ^{13}C NMR (100 MHz, DMSO-d_6) δ 165.57, 161.53, 142.52, 138.83, 137.74, 136.02, 129.55, 129.01, 127.49, 127.07, 126.53, 126.49, 113.46, 55.32, 45.88, 42.23, 20.92. HRMS calcd for $C_{23}H_{25}O_4N_2S$ 425.15295 $[M + H]^+$, found 425.15334.

*2-Fluoro-N-(4-((4-methylphenylsulfonamido)methyl)benzyl)benzamide (**IIh**)*

White solid, yield 70%, m.p. 138–140 °C. ^{1}H NMR (400 MHz, DMSO-d_6) δ 8.04 (t, J = 6.3 Hz, 1H), 7.67 – 7.69 (m, 2H), 7.62 (td, J = 7.4, 1.7 Hz, 1H), 7.50 – 7.56 (m, 1H), 7.37 – 7.39 (m, 2H), 7.18 – 7.32 (m, 7H), 4.41 (s, 2H), 3.91 (d, J= 6.3 Hz, 2H), 2.38 (s, 3H). ^{13}C NMR (100 MHz, DMSO-d_6) δ 163.56, 160.32, 142.53, 138.18, 136.15, 132.40, 132.31, 130.03, 130.00, 129.56, 127.71, 127.54, 127.27, 127.01, 126.52, 126.50, 124.48, 124.44, 116.18, 115.96, 45.86, 42.18, 20.93. HRMS calcd for $C_{22}H_{22}O_3N_2SF$ 413.13297 $[M + H]^+$, found 413.13295.

*3-Fluoro-N-(4-((4-methylphenylsulfonamido)methyl)benzyl)benzamide (**IIi**)*

White solid, yield 72%, m.p. 137–139 °C. ^{1}H NMR (600 MHz, Chloroform-*d*) δ 7.75 (d, *J* = 8.4 Hz, 2H), 7.49 – 7.53 (m, 2H), 7.37 – 7.41 (m, 1H), 7.31 (d, *J* = 7.8 Hz, 2H), 7.25 – 7.26 (m, 2H), 7.17 – 7.21 (m, 3H), 6.51 (t, *J* = 5.5 Hz, 1H), 4.75 (t, *J* = 6.2 Hz, 1H), 4.57 (d, *J* = 5.7 Hz, 2H), 4.09 (d, *J* = 6.4 Hz, 2H), 2.44 (s, 3H). ^{13}C NMR (100 MHz, DMSO-d_6) δ 164.77, 163.16, 160.73, 142.53, 138.31, 137.75, 136.69, 136.63, 136.20, 130.52, 130.44, 129.56, 127.55, 127.14, 126.50, 123.38, 118.22, 118.01, 114.12, 113.90, 45.86, 42.42, 20.92. HRMS calcd for $C_{22}H_{22}O_3N_2SF$ 413.13297 $[M + H]^+$, found 413.13274.

*4-Fluoro-N-(4-((4-methylphenylsulfonamido)methyl)benzyl)benzamide (**IIj**)*

White solid, yield 67%, m.p. 187–189 °C. ^{1}H NMR (400 MHz, DMSO-d_6) δ 9.06 (t, *J* = 6.0 Hz, 1H), 8.03 (t, *J* = 6.3 Hz, 1H), 7.93 – 8.00 (m, 2H), 7.66 – 7.69 (m, 2H), 7.36 – 7.37 (m, 2H), 7.28 – 7.34 (m, 2H), 7.17 – 7.24 (m, 4H), 4.43 (d, *J* = 6.0 Hz, 2H), 3.90 (d, *J* = 6.3 Hz, 2H), 2.37 (s, 3H). ^{13}C NMR (100 MHz, DMSO-d_6) δ 165.04, 162.61, 142.53, 138.51, 137.76, 136.14, 132.01, 130.79, 129.88, 129.79, 129.56, 127.53, 127.11, 126.50, 115.30, 115.09, 109.54, 45.87, 42.36, 20.92. HRMS calcd for $C_{22}H_{22}O_3N_2SF$ 413.13297 $[M + H]^+$, found 413.13303.

*2-Chloro-N-(4-((4-methylphenylsulfonamido)methyl)benzyl)benzamide (**IIk**)*

White solid, yield 80%, m.p. 140–142 °C. ^{1}H NMR (600 MHz, DMSO-d_6) δ 8.97 (t, *J* = 6.1 Hz, 1H), 8.05 (t, *J* = 6.3 Hz, 1H), 7.70 (d, *J* = 8.0 Hz, 2H), 7.50 – 7.51 (m, 1H), 7.38 – 7.46 (m, 5H), 7.27 (d, *J* = 7.8 Hz, 2H), 7.20 (d, *J* = 8.1 Hz, 2H), 4.41 (d, *J* = 6.0 Hz, 2H), 3.92 (d, *J* = 6.3 Hz, 2H), 2.39 (s, 3H). ^{13}C NMR (100 MHz, DMSO-d_6) δ 166.30, 142.55, 138.06, 137.78, 136.88, 136.20, 130.72, 129.82, 129.58, 128.82, 127.52, 127.09, 127.05, 126.51, 109.53, 45.85, 42.11, 20.95. HRMS calcd for $C_{22}H_{22}O_3N_2SCl$ 429.10342 $[M + H]^+$, found 429.10349.

*3-Chloro-N-(4-((4-methylphenylsulfonamido)methyl)benzyl)benzamide (**IIm**)*

White solid, yield 71%, m.p. 110–112 °C. ^{1}H NMR (400 MHz, DMSO-d_6) δ 9.16 (t, J = 6.0 Hz, 1H), 8.03 (t, J = 6.3 Hz, 1H), 7.92 (td, J = 1.7, 0.9 Hz, 1H), 7.84 (ddd, J = 7.7, 1.7, 1.1 Hz, 1H), 7.66 – 7.69 (m, 2H), 7.61 (ddd, J = 8.0, 2.2, 1.1 Hz, 1H), 7.49 – 7.53 (m, 1H), 7.36 – 7.39 (m, 2H), 7.17 – 7.24 (m, 4H), 4.43 (d, J = 5.9 Hz, 2H), 3.90 (d, J = 6.3 Hz, 2H), 2.37 (s, 3H). ^{13}C NMR (100 MHz, DMSO-d_6) δ 164.66, 142.52, 138.26, 137.79, 136.26, 136.20, 133.16, 131.05, 130.32, 129.55, 127.54, 127.16, 127.01, 126.49, 125.98, 45.86, 42.44, 20.92. HRMS calcd for $C_{22}H_{22}O_4N_3S$ 429.10342 $[M + H]^+$, found 429.10327.

*4-Chloro-N-(4-((4-methylphenylsulfonamido)methyl)benzyl)benzamide (**IIn**)*

White solid, yield 71%, m.p. 201–203 °C. ^{1}H NMR (400 MHz, $CDCl_3$) δ 7.71–7.77 (m, 4H), 7.19–7.41 (m, 8H), 6.38 (s, 1H), 4.62 (s, 1H), 4.59 (d, J = 5.8 Hz, 2H), 4.10 (d, J = 6.2 Hz, 2H), 2.44 (s, 3H). ^{13}C NMR (101 MHz, DMSO-d_6) δ 165.75, 143.08, 138.67, 137.90, 136.52, 133.27, 131.49, 129.98, 129.48, 128.81, 127.91, 127.53, 126.84, 46.16, 42.73, 21.26. HRMS calcd for $C_{22}H_{21}O_3N_2SClNa$ 451.08536 $[M + Na]^+$, found 451.08588.

*N-(4-((4-methylphenylsulfonamido)methyl)benzyl)-4-nitrobenzamide (**IIo**)*

White solid, yield 66%, m.p. 207–209 °C. ^{1}H NMR (400 MHz, DMSO-d_6) δ 9.37 (t, J = 6.0 Hz, 1H), 8.31 – 8.34 (m, 2H), 8.02 – 8.12 (m, 2H), 8.04 (t, J = 6.3 Hz, 1H), 7.68 (d, J = 8.2 Hz, 2H), 7.38 (d, J = 8.0 Hz, 2H), 7.25 (d, J = 8.0 Hz, 2H), 7.19 (d, J = 8.0 Hz, 2H), 4.46 (d, J = 5.9 Hz, 2H), 3.91 (d, J = 6.3 Hz, 2H), 2.37 (s, 3H). ^{13}C NMR (100 MHz, DMSO-d_6) δ 164.51, 149.00, 142.53, 139.94, 138.05, 137.73, 136.31, 129.56, 128.73, 127.58, 127.21, 126.49, 123.53, 45.84, 42.57, 20.93. HRMS calcd for $C_{22}H_{22}N_3O_5S$ 440.12747 $[M + H]^+$, found 440.12768.

*2,4,6-Trichloro-N-(4-((4-methylphenylsulfonamido)methyl)benzyl)benzamide (**IIp**)*

White solid, yield 77%, m.p. 188–190 °C. ^{1}H NMR (400 MHz, DMSO-d_6) δ 9.19 (t, J = 6.0 Hz, 1H), 8.05 (t, J = 6.3 Hz, 1H), 7.76 (s, 2H), 7.68 – 7.70 (m, 2H), 7.38 – 7.40 (m, 2H), 7.29 (d, J = 8.2 Hz, 2H), 7.20 (d, J = 8.2 Hz, 2H), 4.43 (d, J = 6.0 Hz, 2H), 3.92 (d, J = 6.3 Hz, 2H), 2.39 (s, 3H). ^{13}C NMR (100 MHz, DMSO-d_6) δ 162.88, 142.56, 137.76, 137.40, 136.39, 135.49, 134.29, 132.03, 129.58, 127.93, 127.48, 127.28, 126.51, 45.84, 42.12, 20.95. HRMS calcd for $C_{22}H_{20}N_2O_3SCl_3$ 497.02547 $[M + H]^+$, found 497.02593.

*N-(4-((4-methylphenylsulfonamido)methyl)benzyl)nicotinamide (**IIq**)*

White solid, yield 65%, m.p. 120–122 °C. ^{1}H NMR (400 MHz, Chloroform-d) δ 8.86 (d, J = 1.8 Hz, 1H), 8.70 (dd, J = 4.9, 1.8 Hz, 1H), 8.11 (dt, J = 7.9, 2.0 Hz, 1H), 7.75–7.78 (m, 2H), 7.35–7.38 (m, 1H), 7.27–7.33 (m, 3H), 7.18–7.25 (m, 3H), 6.75 (t, J = 5.9 Hz, 1H), 5.07 (t, J = 6.1 Hz, 1H), 4.59 (d, J = 5.7 Hz, 2H), 4.09 (d, J = 6.1 Hz, 2H), 2.44 (s, 3H). ^{13}C NMR (100 MHz, $CDCl_3$) δ 165.86, 152.19, 148.30, 143.70, 137.82, 137.10, 136.16, 135.35, 130.08, 129.96, 128.56, 128.30, 128.27, 123.62, 47.07, 43.84, 21.72. HRMS calcd for $C_{21}H_{22}O_3N_6S$ 396. 13764 $[M + H]^+$, found 396.13734.

*N-(4-((4-methylphenylsulfonamido)methyl)benzyl)isonicotinamide (**IIr**)*

White solid, yield 63%, m.p. 163–165 °C. ^{1}H NMR (400 MHz, DMSO-d_6) δ 9.33 (t, J = 6.0 Hz, 1H), 8.72 – 8.74 (m, 2H), 8.04 (t, J = 6.3 Hz, 1H), 7.78 – 7.79 (m, 2H), 7.67– 7.70 (m, 2H), 7.37 – 7.39 (m, 2H), 7.16 – 7.25 (m, 4H), 4.45 (d, J= 6.0 Hz, 2H), 3.91 (d, J = 6.3 Hz, 2H), 2.37 (s, 3H). ^{13}C NMR (100 MHz, DMSO-d_6) δ 164.58, 150.24, 142.53, 141.21, 138.01, 137.75, 136.31, 129.56, 127.58, 127.18, 126.50, 121.22, 45.84, 42.42, 20.92. HRMS calcd for $C_{21}H_{22}O_3N_3S$ 396.13764 $[M + H]^+$, found 396.13739.

3.4 Results

Chemistry

The synthetic route chosen to synthesize the targeted compounds was outlined in **Fig 3.2** on the following page. The target compounds were prepared from 4-(Boc-aminomethyl)benzylamine (**3**). Compound **4** was synthesized by sulfonylation of the starting material **3** with the corresponding sulfonylchlorides in dichloromethane (DCM). The protective group Boc was subsequently removed in the presence of trifluoroacetic acid (TFA) producing the benzylamine intermediate **5**. The final compounds **Ia-r** and **IIa-r** were synthesized by the acylation of intermediate **5** with corresponding benzoyl chloride derivatives.

Primary binding affinity screening

All of the prepared compounds were first screened with a binding affinity assay as described in our previous publications (115, 116, 121). This is a competitive binding assay between a potent CXCR4 peptidic inhibitor, biotinylated TN14003, and the target compounds **Ia-r** and **IIa-r** at concentrations of 1, 10, 100, and 1000 nM, for binding to the CXCR4 receptors. The effective concentration (EC) is defined as the lowest concentration at which a significant reduction in the rhodamine fluorescent color is observed as compared to control (**Fig. 3.3**, without CXCR4 modulators). Thus, this initial screening is a semi-quantitative, primary screening of the level of activity, which is different from IC_{50}.

When the two -NH- groups were substituted with -CONH- and -SO_2NH-, respectively, the obtained amide-sulfamide parent structure successfully maintained significant CXCR4 binding affinity and showed even greater activity. Surprisingly, among the 34 synthesized compounds, only three compounds (**If, IIa** and **IIq**) displayed weaker binding affinity compared to the

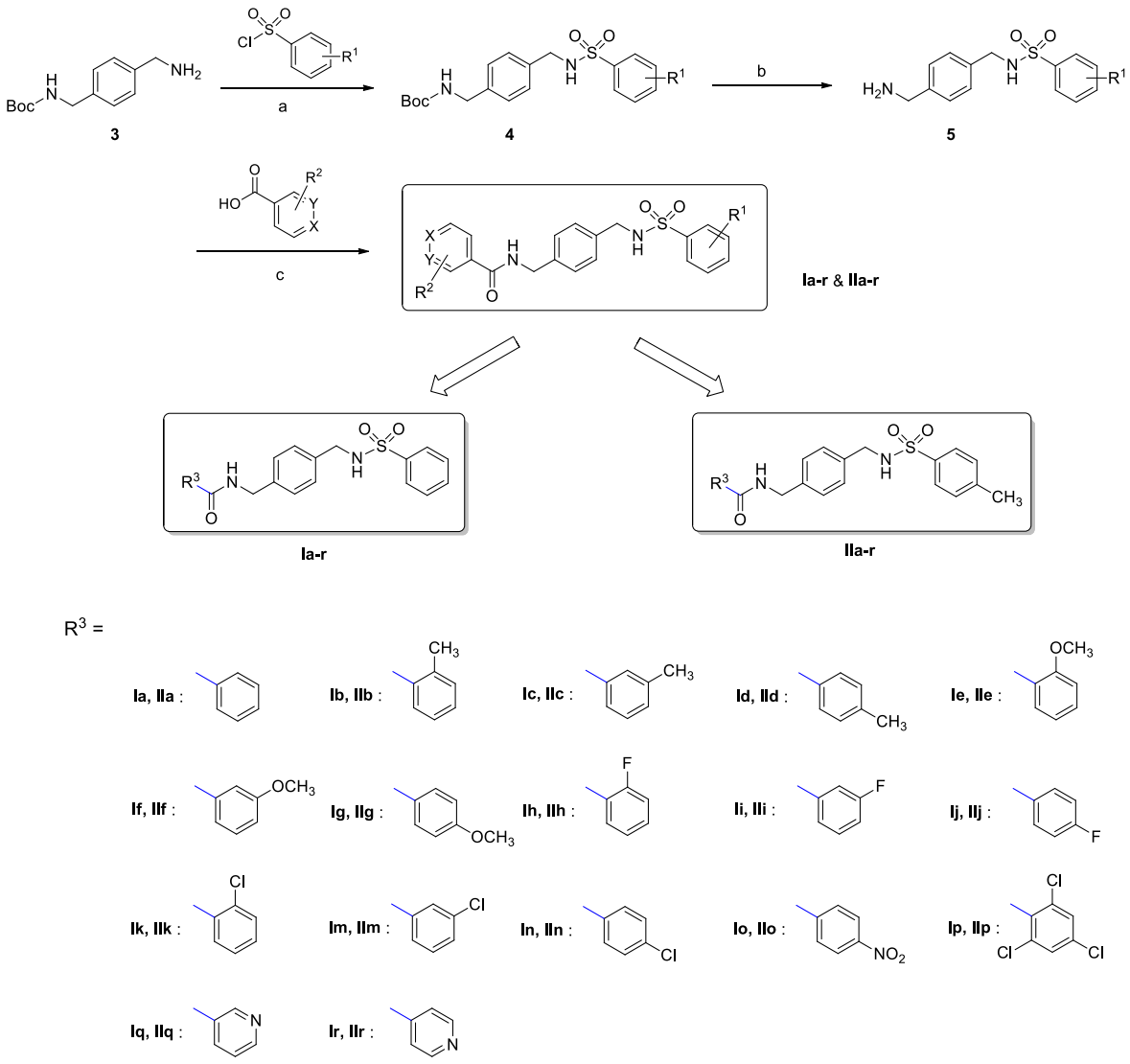

Figure 3.2. Reaction scheme for synthesis of novel amide-sulfamide analogs. (a) DCM, triethylamine (TEA), ice bath to r.t., 6 h, 75-90%; (b) i. DCM, TFA, r.t., 8 h; ii. $NaHCO_3$, 88-95%; (c) DCM, TEA, benzoyl chloride derivatives, ice bath to r.t., 6 h, 60-89%.

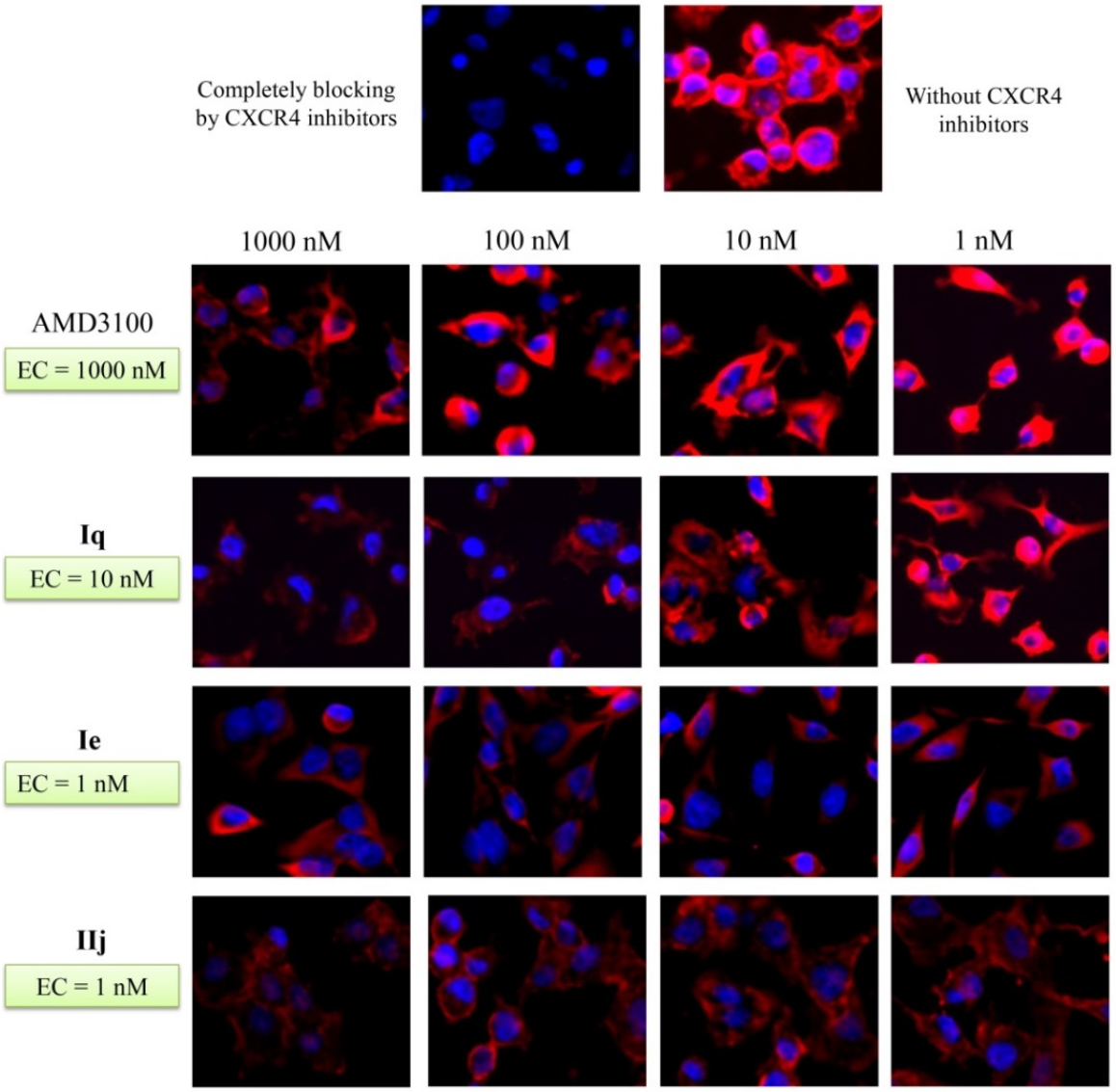

Figure 3.3. **Representative immunofluorescence images of competition-binding affinity assay of three selected compounds compared to AMD3100.** CXCR4 receptors on the cell surface are shown in red fluorescent color in this binding affinity assay using biotinylated TN14003 that binds to CXCR4. When our test compounds are preincubated with the cells and block the binding of biotinylated TN14003, the red fluorescent color gets reduced. The effective concentration (EC) of AMD3100 was 1000 nM, while compounds Ie, IIj, and Iq showed much better EC of only 1, 1, and 10 nM, respectively.

Compd	EC (nM)	Compd	EC (nM)	Compd	EC (nM)	Compd	EC (nM)
Ia	1	**Ij**	100	**IIa**	>1000	**IIj**	1
Ib	1	**Ik**	10	**IIb**	100	**IIk**	10
Ic	1000	**Im**	1000	**IIc**	1000	**IIm**	100
Id	100	**In**	100	**IId**	1000	**IIn**	10
Ie	1	**Io**	100	**IIe**	100	**IIo**	10
If	>1000	**Ip**	10	**IIf**	10	**IIp**	10
Ig	1000	**Iq**	10	**IIg**	100	**IIq**	>1000
Ih	1000	**Ir**	10	**IIh**	1000	**IIr**	10
Ii	100			**IIi**	1		
AMD3100	**1000**						

Table 3.1. Preliminary effective concentration (EC) of anti-CXCR4 compounds.

reference drug AMD3100. More than 70% of the compounds showed significantly better binding effects (**Fig. 3.3**, **Table 3.1**). Compounds **Ia, Ib, Ie, Iii** and **IIj** exhibited 1000-fold stronger potency than AMD3100, with an EC of only 1 nM. Generally, most of the derivatives substituted at the 2'-position of the benzamide group showed more potent activity. Incorporating a methyl group to the benzene sulfonamide side chain significantly enhanced the binding affinity. Further modification of the benzenesulfonamide group was needed to summarize and explain the structure-activity relationships (SARs).

Matrigel Invasion Assay

Activation of CXCR4 through its ligand CXCL12 mediates migration and invasion. Thus, we used the Matrigel invasion assay to probe whether the selected compounds from our primary binding affinity assay can block CXCR4/CXCL12 mediated chemotaxis and invasion (116, 121). The target compounds (100 nM) and cells were added to in the upper chamber of a vessel and CXCL12 was added in the lower chamber as a chemoattractant in serum-free medium. The binding of CXCR4 in cell surface with the selected compounds would block CXCL12 chemotaxis to the cells. Therefore, the MDA-MB-231 human breast cancer cells in the top chamber treated with the compounds would be inhibited to migrate from the top chamber through the Matrigel-coated filter pores to the bottom of the filter. The inhibition of cell invasion with each tested compound was calculated by comparing to the cell invasion without treatment. The results of Matrigel invasion were summarized in **Fig. 3.4** and **Fig. 3.5** on the following pages.

24 compounds showing greater binding affinity than AMD3100 were selected for the Matrigel invasion assay. Most of the corresponding compounds displayed exceptional inhibition of CXCR4, except **Id**, **In**, and **IIb**, with less than 50% inhibition. Compounds **Io, IIg, Iii, IIo, IIp,**

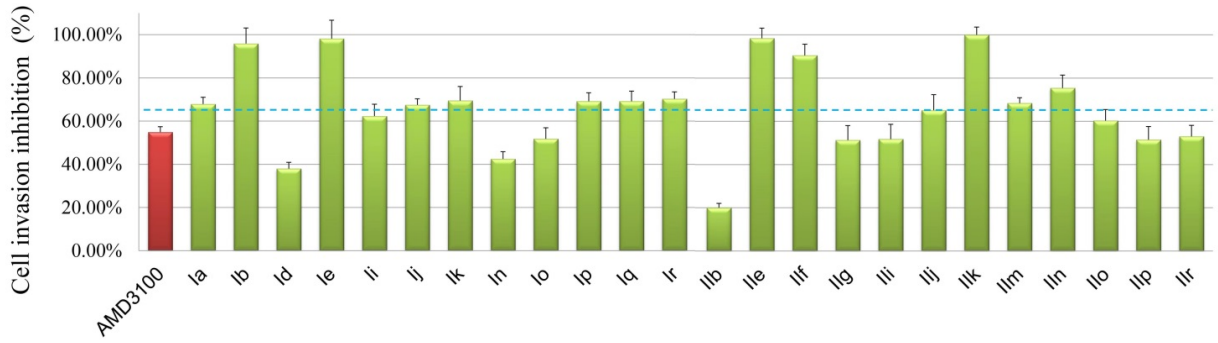

Figure 3.4. Summary of Matrigel invasion assay results induced by CXCR4/CXCL12-mediated interaction using MDA-MB-231 cells in the presence of CXCR4 modulators.

CXCL12α was added to the bottom chamber, and the compounds were added to the top chamber. After incubating for 22 hours, the invading cells were fixed in methanol and stained with hematoxylin and eosin. The percent of invasion was determined by counting the stained cells. 0% inhibition was determined with CXCL12α added to the bottom chamber, but without any CXCR4 inhibitor. 100% was defined by counting the stained cells without adding neither CXCL12α nor compound. Compounds achieving greater than 65% inhibition (over blue line) were evaluated in the ear edema test.

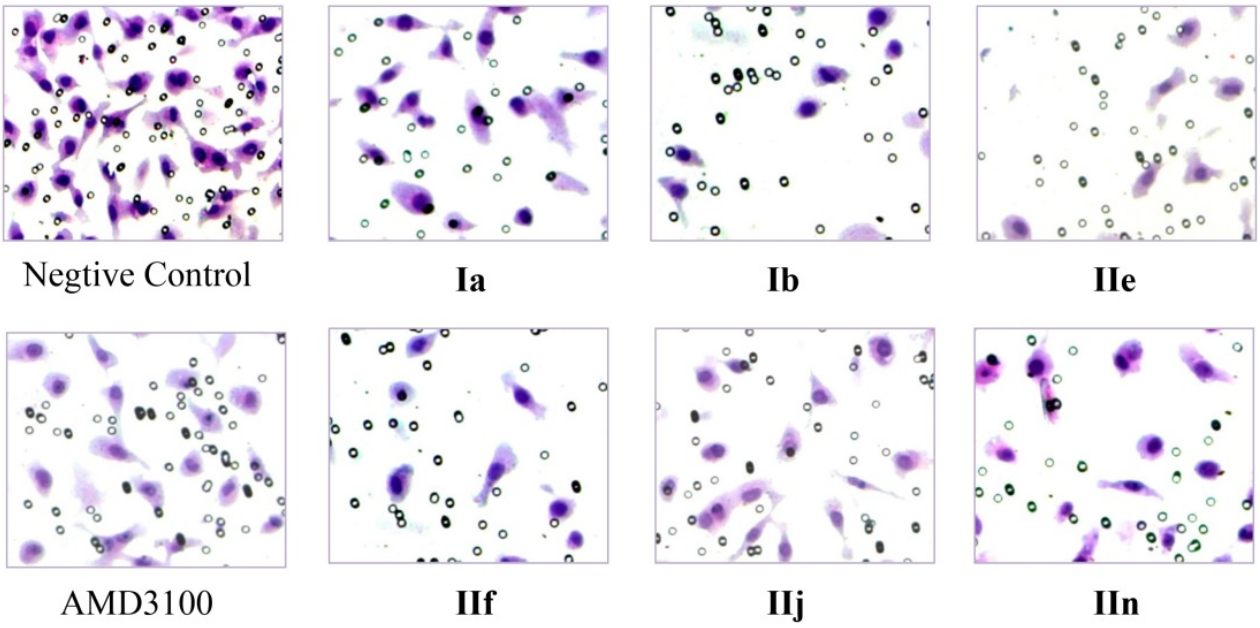

Figure 3.5. Micrographs of Matrigel invasion assay induced by CXCR4/CXCL12-mediated interaction using MDA-MB-231 cells in the presence of CXCR4 modulators. The number of invading cells to the bottom chamber decreased when cells were incubated with our compounds in the top chamber.

and **IIr** showed favorable blocking effect comparable to AMD3100 (55%), while **Ia, Ii, Ij, Ik, Ip, Iq, Ir, IIj, IIm** and **IIn** performed quite well in the Matrigel assay with more than 60% inhibition. Compounds **Ib, Ie, IIe, IIf**and **IIk** exhibited the most potent anti-invasion effect, preventing more than 90% cells from invading through the Matrigel gel. These invasion results give eloquent proof that the designed amide-sulfamide scaffold is a novel structure to block CXCR4 function.

In vivo suppression against xylene-induced ear edema

To evaluate the *in vivo* anti-inflammatory activity of the amide-sulfamide compounds, we performed a xylene-induced ear edema experiment (122). This xylene-induced ear edema model is widely used in the evaluation of inflammatory activity. The application of xylene induces neurogenous edema, which is partially associated with substance P. In the periphery, release of substance P from sensory neurons leads to vasodilatation and plasma extravasations, which causes ear swelling in mice (123). Compounds achieving greater than 65% inhibition in the Matrigel assay were evaluated in the ear edema test. Although AMD3100 is the best investigated small molecule CXCR4 antagonist, its bicyclam structure leads to serious toxicity in this animal model. Therefore, AMD3100 was not selected as the reference drug in this test (112).

Most of the selected compounds displayed moderate to significant anti-inflammatory activity. Interestingly, compounds **Ib, Ie, Ik, Ip,** and **IIe** demonstrated excellent anti-CXCR4 activity in the Matrigel invasion assay, but were ineffective in suppressing the mice ear inflammation (**Fig. 3.6**). Compounds **IIf** and **IIk** also exhibited weak activity (28% and 26% inhibition). Substances **Ij** and **Ir** had moderate anti-inflammatory effect with ~40% inhibition. Meanwhile, compounds **Iq, Iim,** and **IIn** suppressed inflammation by 53%, 57%, and 50%, respectively. Suprisingly, compounds **Ia** and **IIj** showed excellent suppressive activity with 62%

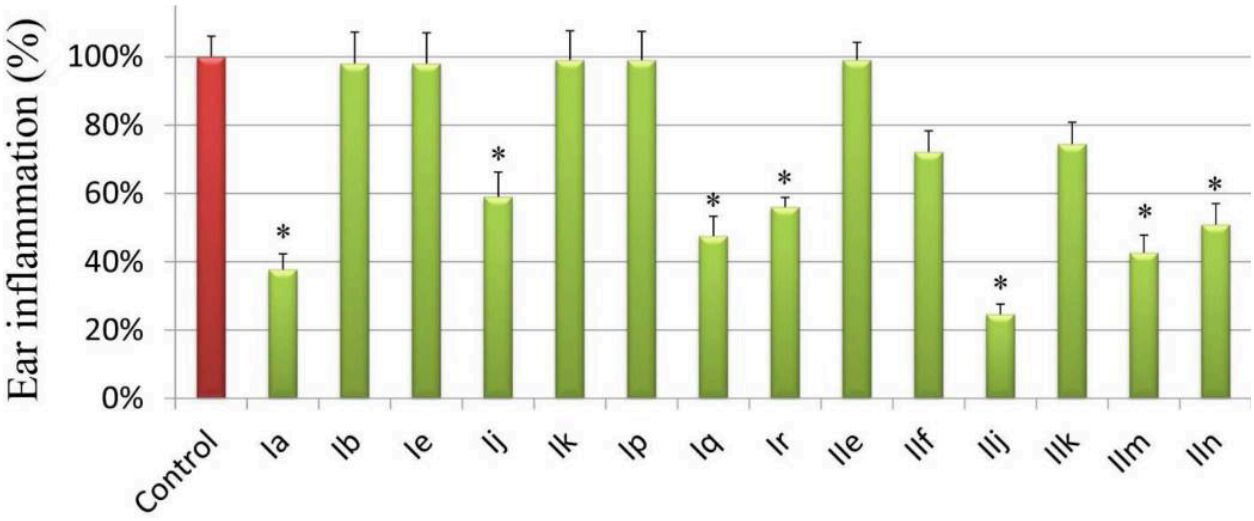

Figure 3.6. *in vivo* anti-inflammatory activity of 14 selected compounds (n=5, * P < 0.05).

The right ear of each mouse was treated with 30 uL of xylene. The selected compounds were administered intraperitoneally (i.p.) at 10 mg/kg, 30 minutes later. Two hours later, one ear plug was removed from both ears and weighted to calculate the inflammation-suppression percentage.

and 75% inhibition, respectively. Histological analysis was then performed to further investigate the significant anti-inflammatory activity of compound **IIj**. As shown in **Fig. 3.7**, a histological assay of compound **IIj** showed remarkable attenuation of ear inflammation and damage with decreases in ear thickness, edema volume, and the number of inflammatory cells (C1–2). These results confirm that the amide-sulfamide compound **IIj** targeting CXCR4 can inhibit inflammation as anticipated. In addition, developing anti-CXCR4 agents for inflammation provides an exciting avenue to target different pathways from COX.

Evaluation of anti-CXCR4 activity of compound IIj at the molecular level

Phosphoinositide 3-kinase (PI3K) activates Akt, a serine threonine kinase which plays a key role in tumor cell survival and possibly proliferation. PI3K/Akt pathways are independently involved in the proliferative signal caused by CXCL12 (124). Our previous results demonstrated that CXCR4/CXCL12 induced Akt phosphorylation, which resulted in tumor angiogenesis and progression of tumors by increasing expression of vascular endothelial growth factor (VEGF) through the activation of the PI3K/Akt pathway (125). The activity of **IIj** in blocking the PI3K/Akt pathway was investigated yb Western blot analysis. As shown in **Fig 3.8**, CXCR4 modulator **IIj** blocked the CXCR4/CXCL12-mediated phosphorylation of Akt in a dose-dependent manner, and significantly inhibited phosphorylation at concentrations of 10 and 100 nM.

Preliminary cytotoxicity evaluation of compound IIj

In addition to their therapeutic effects, cytotoxic agents have the potential of causing serious destruction to healthy and normal cells. To preliminarily evaluate the safety of compound **IIj**, its cytotoxicity was evaluated on two representative human breast cancer cell lines,

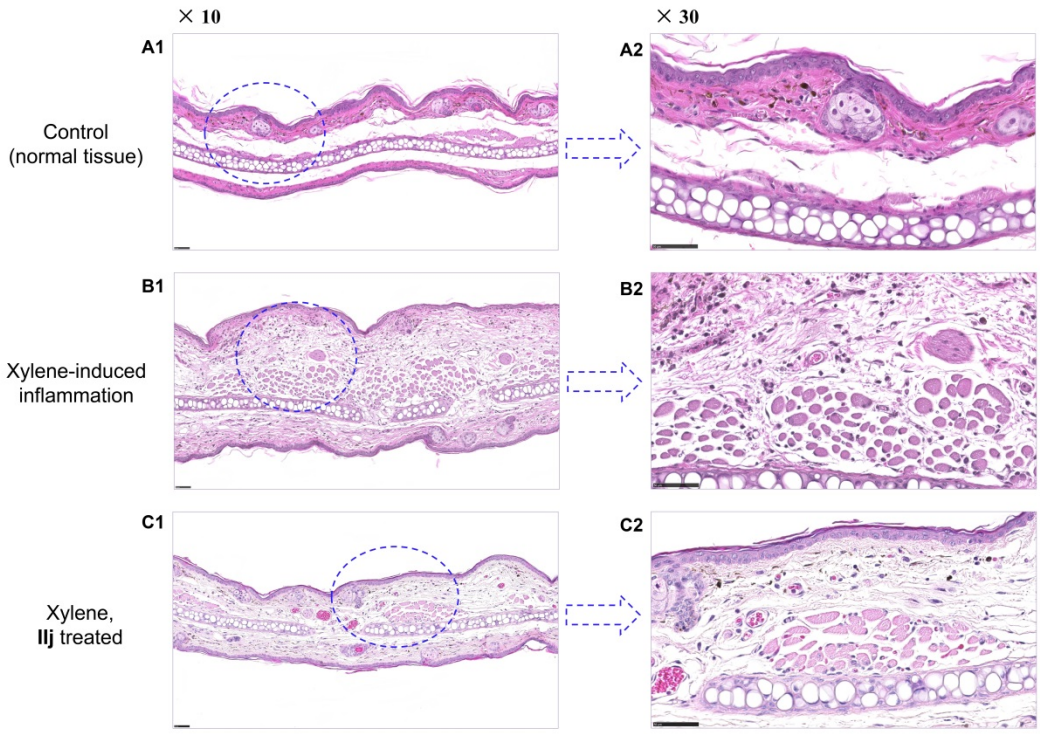

Figure 3.7. Histological analysis of the anti-inflammatory activity of compound IIj. Whole tissue slices were scanned/digitized by NanoZoomer 2.0 HT. Software NDP.view 2 was used to zoom in.

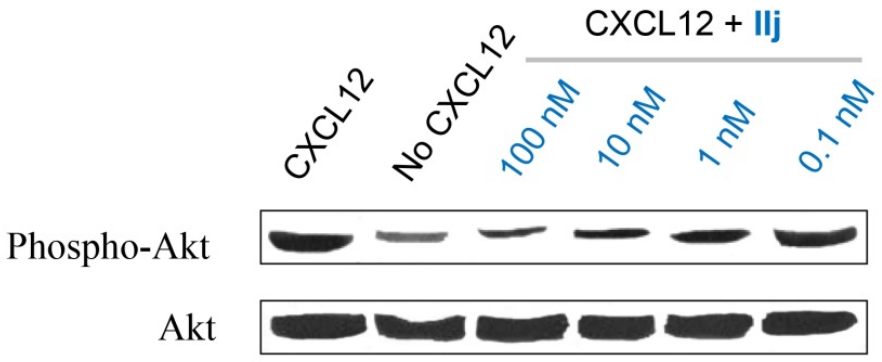

Figure 3.8. Compound IIj blocked the phosphorylation of Aky mediated by the CXCR4/CXCL12 axis. MDA-MD-231 cells were incubated with different concentrations of IIj, and phosphorylated-Akt levels, as well as total Akt levels, were quantified as shown.

MDA-MB-231 (CXCR4-positive) and MCF-10A (CXCR4-negative) by a cell viability (MTT) assay. Of note, blocking CXCR4 does not impact adherent cell proliferation (126). Compound **IIj** displayed potent CXCR4 binding affinity at only 1 nM, however it did not inhibit the proliferation of MDA-MB-231 and MCF-10A cells even at concentrations as high as 10 uM (**Fig. 3.9**), a 1000-fold increase to the working concentrations. Generally, **IIj** had no observable cytotoxicity.

Preliminary pharmacokinetic study of compound IIj

The plasma stability of a drug has a significant influence on the concentration of drug available in circulation. To determine the preliminary pharmacokinetics of these amide-sulfamide compounds, the concentration and stability of compound **IIj** in plasma were evaluated in a mouse model. The peak area of **IIj** in plasma was detected by high-performance liquid chromatography (HPLC) at three time points: 5, 20 and 50 minutes. Generally, compound **IIj** demonstrated a satisfying plasma stability. When normalizing the concentration of compound **IIj** to the peak area at 5 minutes (100%), the concentration remained 65% and 45% at 20 and 50 minutes, respectively (**Fig. 3.10**). The approximate half-life ($t_{1/2}$) was calculated to be ~40 minutes. However, the basal metabolic rate per gram of body weight (the mass-specific rate) is seven times greater in mice than in humans (127). Therefore, we inferred that $t_{1/2}$ of **IIj** in humans would be reasonable. Compared to a previously reported candidate belonging to Class I (115), which was nearly undetectable by HPLC within 1 hour, **IIj** exhibited favorable plasma stability. The amide-sulfamide structure is not only effective both *in vitro* and *in vivo*, but is also a metabolically tolerated pharmacophore.

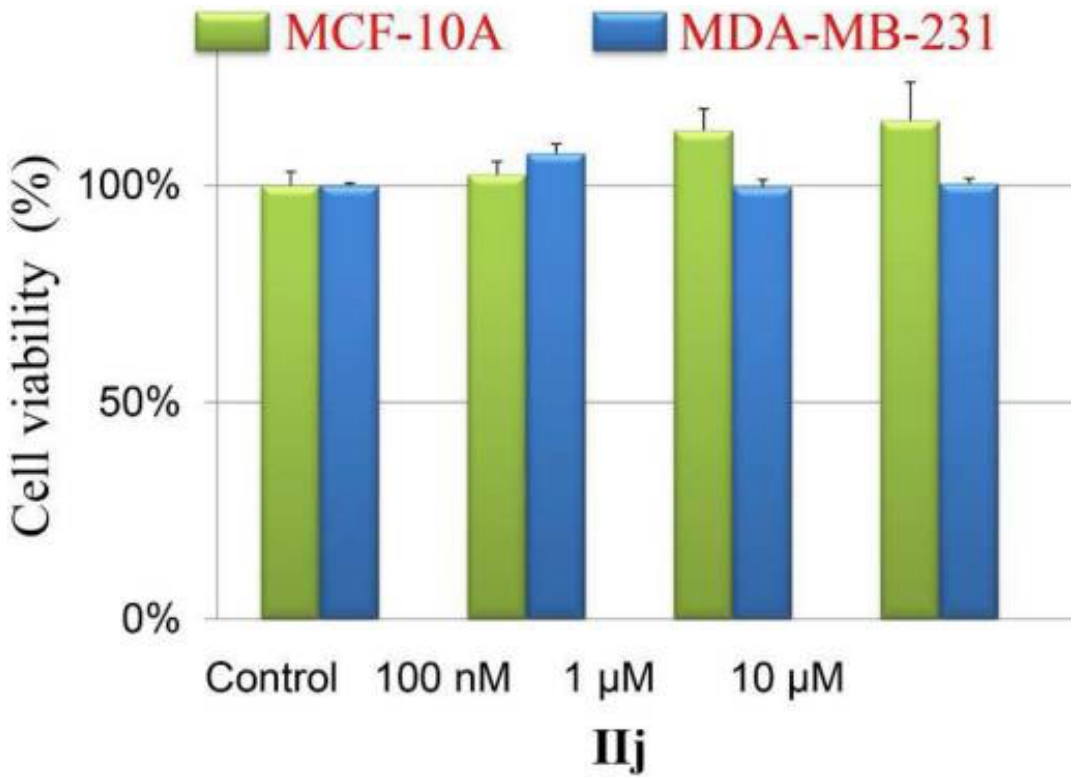

Figure 3.9. Cytotoxicity evaluation of compound IIj in MDA-MB-231 and MCF-10A cell lines. The antiproliferative activity of the compounds was determined using MTT assay. CXCR4-positive MDA-MB-231 or CXCR4-negative MCF-10A cells were treated with compound **IIj** or vehicle control for 72 h. The results showed no statistically significant difference, which suggests that **IIj** does not have antiproliferative activity.

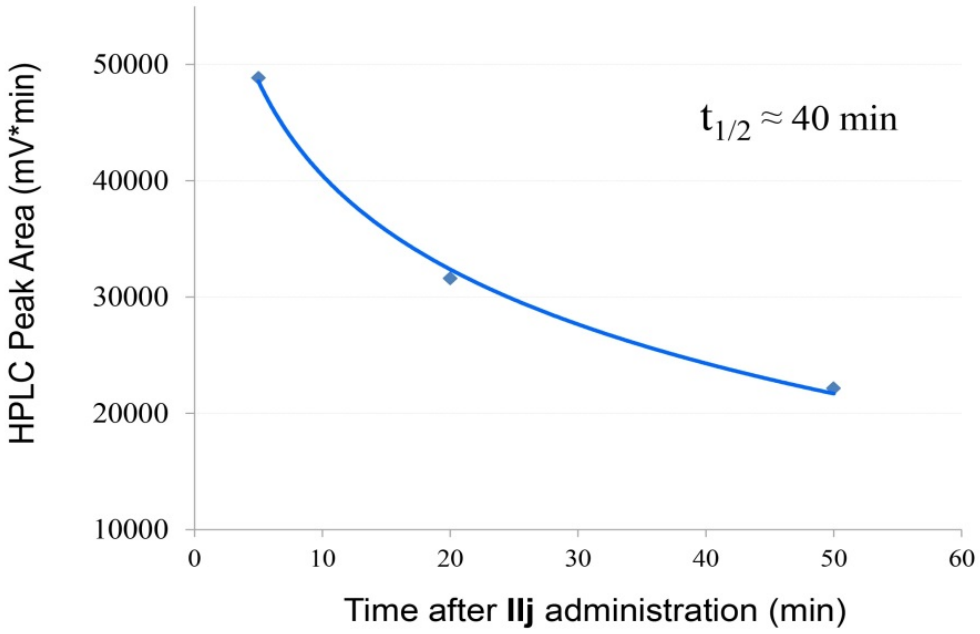

Figure 3.10. Peak area of compound IIj versus time in mice plasma following a single dose intravenous injection administration at 30 mg/kg. Nude mice received a single dose (30 mg/kg) of compound **IIj** via intravenous injection (i.v.). Blood samples (100uL) were collected at 0, 5, 20, and 50 minutes. The blood sample was centrifuged and filtrated and analyzed by HPLC to estimate the amount of compound in serum.

3.5 Discussion

Based on the results of binding affinity screening, Matrigel invasion test and *in vivo* anti-inflammatory evaluation, the preliminary SARs were then characterized on the following page (**Fig 3.11**). In terms of binding affinity, the benzamide side chain showed favorable tolerance. The influence of electron-withdrawing and electron-donating groups on the binding activity did not demonstrate a notable difference; both could maintain or improve the binding affinity. When the 2'-position of the benzamide side chain was substituted, most of the derivatives exhibited better affinity, which was basically stronger than the 3' or 4'-position substituted compounds. A direct comparison between the 3' and 4'-position substituted derivatives showed no obvious difference in binding affinity. Moreover, when an electron-donating substituent, such as a methyl group, was introduced to the 4'-position of the benzene sulfonamide side chain, binding affinity increased significantly. Further modification on the benzene sulfonamide structure is needed.

In terms of the Matrigel invasion test, the benzamide scaffold was still tolerated. Both electron-withdrawing and electron-donating groups enhanced the inhibitory potency. When the 2'-position was substituted with methyl, methoxyl or chlorine groups, these corresponding compounds displayed the most potent activity, better than 3' or 4'-position modified compounds. In contrast, when substituted with fluorine, the 3' and 4'-position substituted compounds demonstrated a greater effect. In the *in vivo* anti-inflammatory evaluation, when the 4'-position of benzamide side chain was substituted, the melting point increased significantly, especially with strong electron-withdrawing groups. These changes decreased the solubility of the target compounds, and may also impact the bioavailability. Although compound **IIj** (4'-position substituted with fluorine) showed the strongest anti-inflammatory activity, its solubility was not favourable. Taking **IIj** as the lead compound, introducing groups containing nitrogen atoms to the

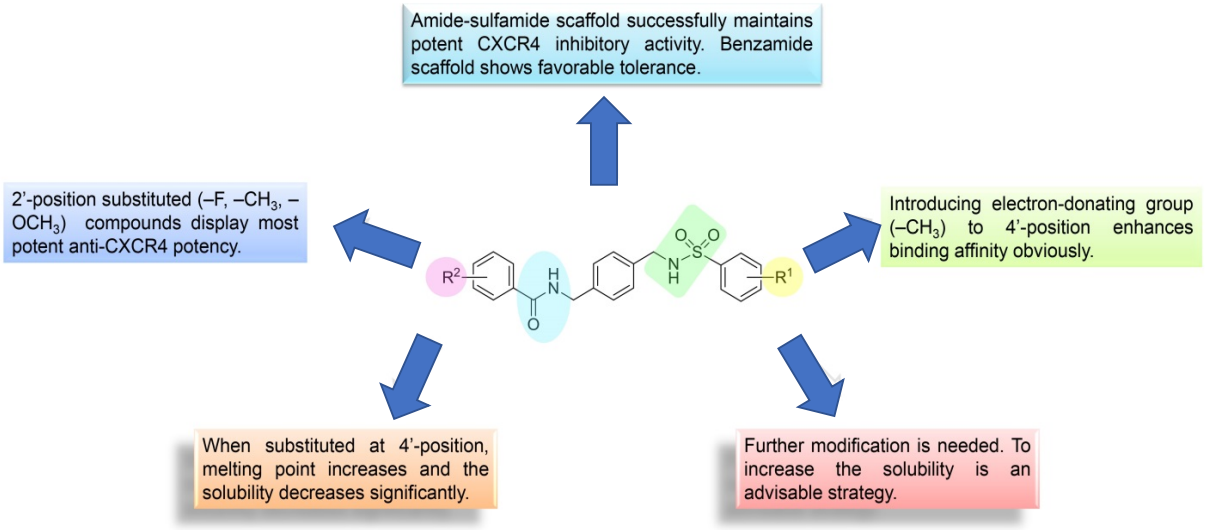

Figure 3.11. Structure-activity relationships of amide-sulfamide compounds.

benzene sulfonamide structure will be an advisable strategy in the future optimization. The obtained compounds can be converted into salts to address the solubility issues. All in all, compared to the bis-secondary amine lead structure, this novel amide-sulfamide scaffold successfully maintained the potent CXCR4 blocking effect, and showed even stronger activity both *in vitro* and *in vivo*. Based on the summarized SARs, further modification and optimization will be performed, especially to the benzene sulfonamide side chain.

Taking the symmetrical bis-secondary amines (Class I) as lead structures, a series of novel amide-sulfamide derivatives were designed, synthesized and comprehensively evaluated. This novel amide-sulfamide scaffold not only maintained significant CXCR4 modulating effect, but also exhibited more potent anti-CXCR4 activity. In the *in vitro* assays, more than 70% of compounds showed notably better binding affinity than the reference drug AMD3100. Compounds **Ia, Ib, Ie, Iii** and **IIj** exhibited 1000-fold stronger potency than AMD3100, with an EC of only 1 nM. In the Matrigel invasion assay, most of the compounds significantly blocked tumor cell invasion, demonstrating superior inhibition compared to AMD3100. For the *in vivo* evaluation, compounds **Ia** and **IIj** showed excellent mice ear inflammation suppressive activity (62% and 75%, respectively). Histological analysis proved that compound **IIj**attenuated ear edema and damage substantially, with ear thickness, edema volume, and the number of inflammatory cells all decreasing by a wide margin. Western blot analyses revealed that CXCR4 modulator **IIj** blocked the CXCR4/CXCL12-mediated phosphorylation of Akt in a dose-dependent manner. Compound **IIj** also significantly attenuated the amount of TNF-α by 59% in bacterial-infected J774A.1 macrophages. In the preliminary pharmacokinetic study, compound **IIj** also displayed a favourable plasma stability. In the cytotoxicity screening, **IIj** did not inhibit the proliferation of MDA-MB-231and MCF-10A cells even at 10 μM, and showed no observable cytotoxicity.

Based on the results of binding affinity screening, Matrigel invasion test, *in vivo* anti-inflammatory evaluation and preliminary pharmacokinetic study, the preliminary SARs were summarized. Future directions for this work will include further optimization and modification of the benzene sulfonamide scaffold, especially the introduction of hydrophilic structures or groups containing nitrogen atom(s) to improve the solubility and bioavailability. In summary, the novel amide-sulfamide scaffold exhibited potent CXCR4 inhibitory activity both *in vitro* and *in vivo*, and showed reasonable metabolic stability. These results also confirmed that compound **IIj** targeting CXCR4 can inhibit inflammation as anticipated. Developing inhibitors targeting CXCR4 provides an exciting strategy for treatment of inflammation.

In summary, results from chapters 2 and 3 provide two widely accepted methods for hit discovery: *in silico* drug design (chapter 2) as well as virtual high throughput screening (chapter 3). At this stage in the drug discovery project, hits have been identified and only preliminarily characterized. In order to progress into human clinical trials, hits must first be systematically evaluated for their mechanisms of action in both an *in vitro* and *in vivo* preclinical setting. This will provide the rationale for how the candidate drug is acting in its respective biological system. Thus, the following chapter summarizes a preclinical mechanistic study elucidating the mechanism of action of a new class of drugs, histone deacetylase inhibitors (HDACi's). In contrast to the first two targets that have been discussed in previous chapters, very little is known with respect to how HDACi's work, making it a clear candidate to develop expertise in this part of the drug discovery endeavor.

Chapter 4

Post-drug screening preclinical mechanistic studies unraveling histone deacetylase inhibitor mode of action

Adapted with permission from Elseiver B.V. Biochem Biophys Res Commun. 2018 Sep 5; 503(2):1087-1091.

4.1. Abstract

Following successful hit discovery, the candidate drug must then be comprehensively studied and its mechanism of action must be characterized which rationalizes its utility for potential use in the clinic. While HDAC inhibitors (HDACi's) are emerging as promising anticancer agents, such as in the triple negative breast cancer (TNBC) setting, little is known with respect to how they function. Thus, studying this drug class in a mechanistic setting is ideal for providing the skillset required to properly characterize lead compounds. Triple negative breast cancer (TNBC) is among the most aggressive breast cancer subtypes with poor prognosis. The purpose of this study is to better understand the molecular basis of TNBC as well as develop new therapeutic strategies. Our results demonstrate that HDAC9 is overexpressed in TNBC compared to non-TNBC cell lines and tissues and is inversely proportional with miR-206 expression levels. We show that HDAC9 selective inhibition blocked the invasion of TNBC cells *in vitro* and repressed the angiogenesis shown via *in vivo* Matrigel plug assays. Subsequent HDAC9 siRNA knockdown was then shown to restore miR-206 while also decreasing VEGF and MAPK3 levels. Furthermore, the inhibition of miR-206 neutralized the action of HDAC9 siRNA on decreasing VEGF and MAPK3 levels. This study highlights HDAC9 as a mediator of cell invasion and angiogenesis in TNBC cells through VEGF and MAPK3 by modulating miR-206 expression and suggests that selective inhibition of HDAC9 may be an efficient route for TNBC therapy. It also demonstrates that HDAC inhibitors partly exert their function in the TNBC setting via HDAC9 inhibition.

4.2 Introduction

Two classes of enzymes impact the acetylation state of histone proteins – histone acetyltransferases (HATs) and histone deacetylases (HDACs) (128, 129). The HDAC family of enzymes is involved in various biological processes including transcriptional control, growth arrest, and cell death, particularly in tumor development and proliferation (130-134). Emerging studies on a number of HDAC inhibitors have demonstrated that not only are they generally nontoxic, they are also potent anti-proliferative agents in both *in vitro* and *in vivo* studies (135-138). The results from these studies and their proposed mechanisms indicate that HDACs are excellent targets for cancer treatment. However, clinical benefits of selective versus broad HDAC inhibitors are unknown and the appropriateness of inhibitor may depend on tumor HDAC enzyme expression, enzyme selectivity of the inhibitor, and the desired effects. Although there are several published studies (139, 140) and numerous ongoing clinical trials involving HDAC inhibitors (141), very little is known about the roles of individual HDAC enzymes, and a formal assessment of HDAC enzyme expression is not routinely done.

Emerging data suggests that the currently used HDAC inhibitors may differ significantly with regard to target selectivity. In addition, the expression of HDAC enzymes may vary considerably between normal and tumor tissues and likely between different phenotypes of tumor tissues. HDAC9 is thought to regulate gene expression through epigenetic modulation of the chromatin structure by catalyzing the deacetylation of histone proteins (142). HDAC9 is also known to target non-histone proteins, such as forkhead box protein 3, ataxia telangiectasia group D-complementing protein (ATDC), and glioblastoma 1 protein, which are members of pathways implicated in carcinogenesis (143, 144). More recently, aberrant HDAC9 expression has been observed in several types of cancers, including medulloblastoma (144), acute lymphoblastic

leukemia (145), glioblastoma (146), and osteosarcoma (147). HDAC9 has been shown to promote the growth of these tumors.

Triple negative breast cancer (TNBC) continues to be one of the most clinically aggressive subtypes of breast cancer with overall poor prognosis (148, 149). TNBC lacks expression of the estrogen receptor (ER), progesterone receptor (PR) or human epidermal growth factor receptor 2 (her2/neu) (150); as a result, conventional therapies targeting each of these receptors prove to be unsuccessful in TNBC. Therefore, there is a major unmet need to better understand the molecular basis of this type of breast cancer as well as develop new therapeutic strategies. Emerging studies have highlighted microRNAs (miRNAs) as critical mediators of tumorigenesis, as their involvement have been well-established across several types of cancers, including breast, prostate, ovarian, and head and neck cancers (151-153). A large-scale profile study in 2013 demonstrated that there were over 100 deregulated miRNAs in primary TNBC, some of which were upregulated and others which were downregulated (154). Previous work from our group identified miR-206 as a critical tumor suppressor in TNBC and showed that downregulation of miR-206 lead to an upregulation of VEGF, MAPK3, and SOX9, crucial drivers of invasion and tumorigenesis (155). In this study, we demonstrate that overexpression of HDAC9 promotes the invasion and angiogenesis in TNBC by directly modulating miR-206 and provides a selective basis for TNBC treatment.

4.3 Materials and Methods

Breast cancer cell lines and culture

Human breast cancer cell lines MDA-MB-231, HCC1143, HCC1395, MDA-MB-361, and SKBR3, were grown in RPMI1640 medium supplemented with 10% FBS, 100 U/ml of penicillin sodium, and 100ug/ml of streptomycin sulfate at 37°C in a 5% CO_2-humidified atmosphere. The ER-positive breast cancer cell line MCF-7 was cultured in DMEM medium containing 10% FBS plus 10ug/ml of insulin. SKBR3 is a Her2/neu-expressing human breast cancer cell line, and MDA-MB-361 is positive for ER, PR, and Her2/neu. MDA-MB-231, HCC1143, and HCC1395 are all triple negative cell lines.

Tissue samples and immunohistochemical staining

A formalin-fixed and paraffin-embedded breast cancer tissue array was obtained from US Biomax (Derwood, Maryland, USA). This is a breast cancer and matched metastatic carcinoma tissue array, including TNM and pathology grade, with ER, PR and Her-2 (neu) IHC results, 50 cases/100 cores. The sources and characteristics of archived breast tumor samples are summarized in Table 4.1 on the following page. HDAC9 antibody (Abcam, Cat No. ab70954) was applied on slides at 1:1000 and incubated for 1 h at room temperature after deparaffinized, antigen-retreieved (DAKO, Cat No., S1699), and endogenous peroxidase block with 3% hydrogen peroxide (DAKO, Cat No., S2003). Visualization and detection were established using DAKO EnVision + Dual (mouse and rabbit) Link System-HRP (Cat No., K4061) with an incubation time of 30 min. The detailed staining procedure and semi-quantitative method of immunohistochemical staining of these tissue sections for HDAC9 are described in our previous paper (156) (DAKO, Cat No., K4061).

	Total	T stage		Sex		Age	
		T1&T2	T3T4	Male	Female	<50	≥50
Triple Negative	41	25	16	0	41	22	19
Non-triple negative	59	48	11	0	59	28	31
Total	100	73	27	0	100	50	50

Table 4.1. Characteristics and HDAC9 expression of tissue specimens of breast tumors.

Quantitative real-time RT-PCR

Regular and quantitative RT-PCR were performed following our previous protocol (125). Primer sequences of *miR-206*, and *U6 snRNA* have been described in our previous report (155). Primer sequences of HDAC9 are as follows: (GeneBank accession number BC152405), 5'-CAGCAACGAAAGACACTCCA-3' and 5'-CAGAGGCAGTTTTTCGAAGG-3'. SYBR Green quantitative PCR reaction was carried out in a 15ul reaction volume containing 2xPCR Master Mix (Applied Biosystems) per our previous reports (157, 158).

Construction of HDAC9 siRNAs and transfection

We designed and purchased the small interfering RNA (siRNA) duplexes against HDAC9 (Genbank accession no., BC152405) from ThermoFisher Scientific (Grand Island, NY, USA). The target sequence of HDAC9 siRNA1 is 5'-UAAAAUCUUCCUGCCCACCdTdT-3'. The target sequence of HDAC9 siRNA2 is 5'-GCCAGUAGUCCUAGGUUAUUGUGUAdTdT-3'. The nonspecific control siRNA duplexes were purchased from ThermoFisher Scientific with the same GC content as HDAC9 siRNAs. The siRNA or control oligonucleotides were transfected into TNBC cells at a final concentration of 100nM with lipofectamine 2000 per the instructions.

Matrigel invasion assay

The invasion assay was performed via a Matrigel invasion chamber from Corning Biocoat (Tewksbury, MA) as previously described (159). $5x10^4$ HDAC9 inhibitor-transfected or control oligonucleotide-transfected TNBC MDA-MB-231 and HCC143 cells were added to the top chambers. The Matrigel invasion chambers were then incubated for 20h in a humidified tissue culture incubator. After the 20-h time point, H&E staining was performed on invading cells and were counted at the bottom of the chamber.

Matrigel plug assay and hemoglobin assay

For the *in vivo* angiogenesis assay (Matrigel plug assay), $2x10^5$ MDA-MB-231 TNBC cells or HDAC9 siRNA-transfected MDA-MB-231 cells were mixed with 0.5ml of growth factor-reduced Matrigel (Corning, Tewksbury, MA) and implanted into the flanks of nude mice via subcutaneous injection. For TMP269 treated group and its control groups, five mice in each group received 15 mg/kg TMP269 every other day by intraperitoneal injection between the two plugs on the back of the mice. Following animal sacrifice, the Matrigel plugs were then excised 10 days after Matrigel injection. The excised plugs were homogenized and hemoglobin content was then measured with 100uL of Drabkin's solution (Sigma, St. Louis, MO) following manufactural instruction and our previous description (115).

Western blot analysis

Protein was loaded and separated on 12% SDS-PAGE, and then transferred onto PVDF membranes (Bio-Rad, Hercules, CA, USA). The membranes were incubated overnight at 4°C with antibodies against HDAC9, VEGF, MAPKs (Abcam, Cambridge, MA, USA), and β-Actin (Sigma-Aldrich, St. Louis, MO, USA) with 5% non-fat dried milk. After washing with TBST, the membranes were incubated for 1h with peroxidase-conjugated anti-mouse IgG (Bio-Rad, Hercules, CA, USA).

Statistical Analysis

Real-time RT-PCR reaction was run in triplicate for each sample and repeated at least twice, and the data were statistically analyzed via a Student T-test.

4.4 Results

HDAC9 is overexpressed in TNBC and is inversely consistent with miR-206

HDAC1-11 expression levels in three TNBC cell lines, MDA-MB-231, HCC1143, and HCC1395 compared to those in three non-TNBC cell lines, MCF-7, MDA-MB-361, and SKBR3 were profiled with qRT-PCR analysis. Compared to non-TNBC cells, TNBC cells expressed much higher HDAC9 (**Fig. 4.1a**). Quantitative RT-PCR results reveal that expression levels of miR-206 are notably lower while HDAC9 levels are inversely higher in TNBC cell lines than those in non-TNBC cell lines (**Fig. 4.1b**). Furthermore, we analyzed HDAC9 protein expression levels via immunohistochemical staining in breast cancer tissue samples. TNBC tissues express higher levels of HDAC9 compared to non-TNBC tissues samples (**Fig. 4.1c**). These results demonstrate that HDAC9 expression is upregulated in TNBC tissues compared to non-TNBC tissue samples and are inversely consistent with miR-206 expression levels.

Inhibition of HDAC9 blocks the invasion of TNBC cells in vitro

To investigate the effect of HDAC9 inhibition on blocking TNBC invasiveness, TNBC MDA-MB-231 and HCC1143 cells were treated with TMP269, a selective class IIa HDAC inhibitor, or HDAC9 siRNAs prior to Matrigel invasion assay. The invasive cells from treated groups were determined and compared to their controls by Matrigel invasion assay. **Fig. 4.2a** depicts representative cell photographs of MDA-MB-231 and HCC1143 invasive cells from their respective groups. Results from the Matrigel Invasion assay demonstrate that the invasion of MDA-MB-231 and HCC1143 TNBC cells treated with selective class IIa HDAC inhibitor TMP269 was inhibited compared to control cells (**Fig. 4.2a** and **b**). Similarly, HDAC9 siRNA1 and siRNA2 both significantly blocked MDA-MB-231 and HCC1143 TNBC cell invasion

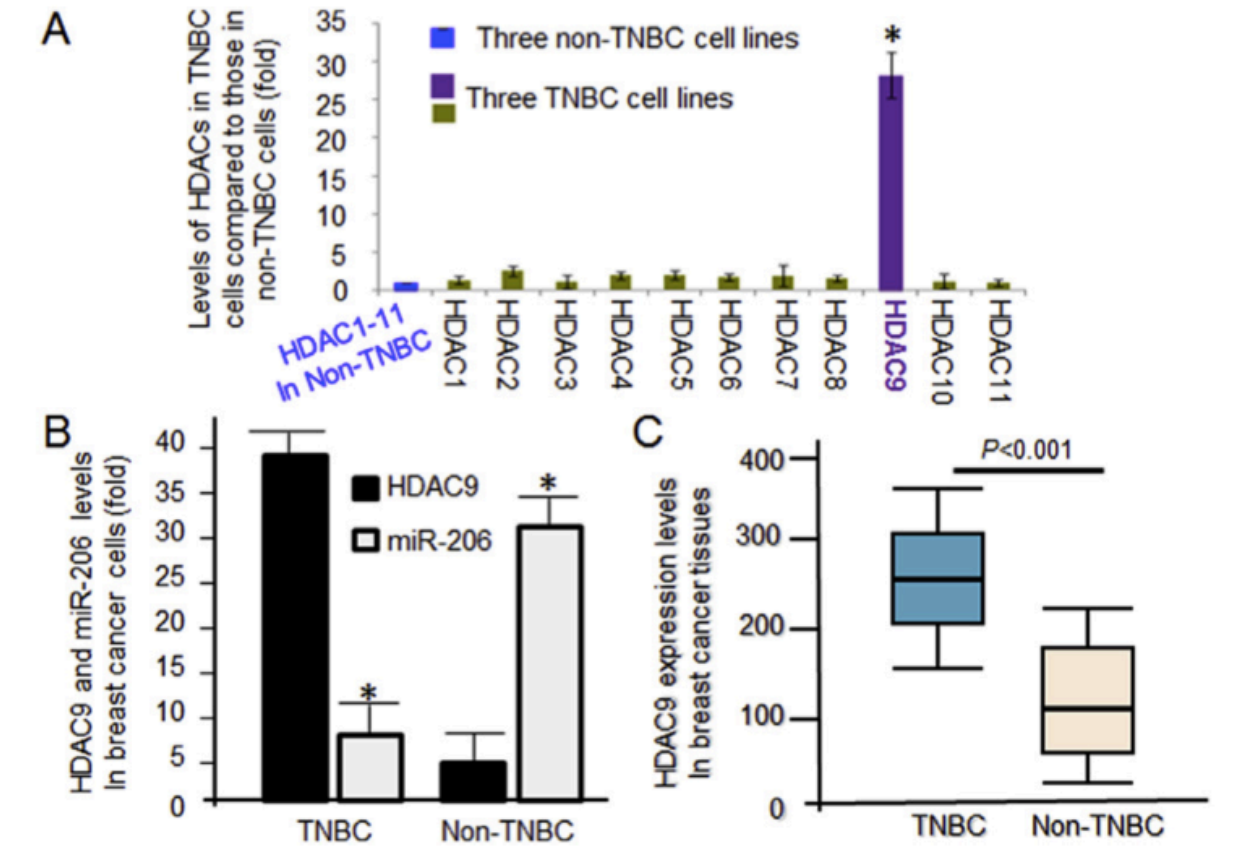

Figure 4.1. HDAC9 is overexpressed in TNBC cells and tissues. (A) Expression levels of HDAC1-9 mRNAs in three TNBC cell lines, MDA-MB-231, HCC1143, and HCC1395 compared to those in three non-TNBC cell lines, MCF-7, MDA-MB-361, and SKBR3 determined by quantitative RT-PCR analysis. (B) HDAC9 expression levels in triple negative breast cancer cell lines are inversely consistent with those of miR-206. (C) A box and whisker plot diagram showing the comparison of HDAC9 levels in triple negative breast cancer tissues (n = 41), and non-TNBC breast cancer tissues (n = 59) determined with HDAC9 IHC staining. Horizontal lines in the boxes represent the median HDAC9 value of each group. Top and bottom edges of the boxes indicate the score values of the 25th and the 75th percentile, respectively. Whiskers represent the highest and lowest values. The range is shown as a vertical line.

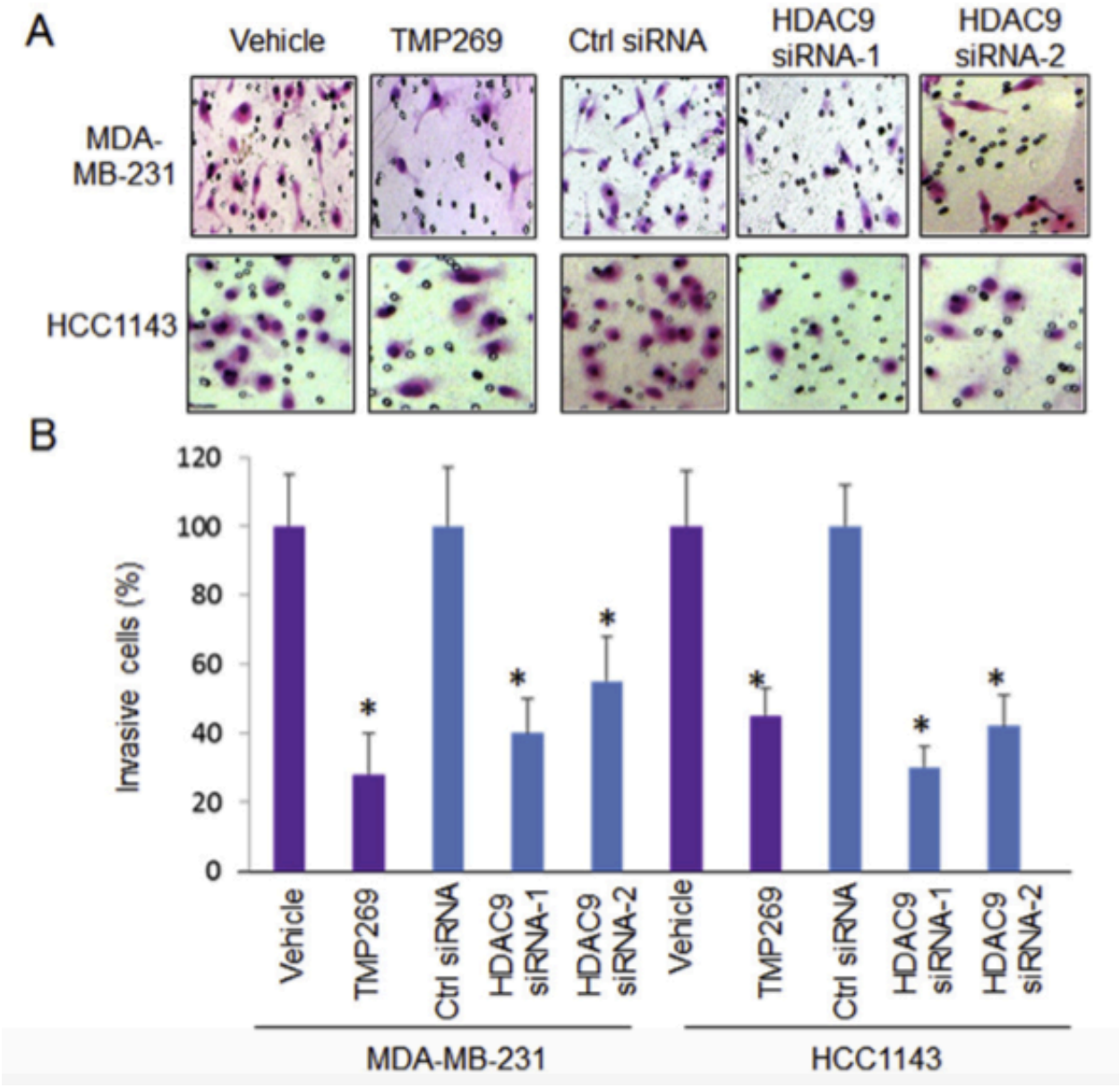

Figure 4.2. Selective HDAC9 inhibition blocks invasion of human breast cancer MDA-MB-231 and HCC1143 TNBC cells. (a) Representative photograph for TNBC invasion cells from either HDAC9 siRNA-treated, TMP269-treated or control groups. (b) Quantitative comparison of invasive MDA-MB-231 and HCC1143 TNBC cells of selective HDAC9 inhibition and their controls by Matrigel Invasion assay. *$P < 0.01$ compared to their controls.

(**Fig. 4.2a** and **b**). These results suggest that selective HDAC9 inhibition efficiently blocks the invasion of TNBC cells.

Knockout of HDAC9 inhibits the angiogenesis of TNBC tumors

A Matrigel plug assay was performed in nude mice to assess the effect of selective HDAC9 inhibition on angiogenesis *in vivo*. Briefly, a mixture of $2x10^5$ TNBC MDA-MB-231 cells or HDAC9 siRNA-transfected MDA-MB-231 cells in 0.5 ml of growth factor reduced Matrigel was implanted at two subcutaneous sites. For TMP269 treated group and its control groups, five mice from each group received 15 mg/kg TMP269 every other day by intraperitoneal injection between the two plugs on the back of the mice. Ten days after the Matrigel implant, the mice were sacrificed. The Matrigel plugs were excised, photographed, and processed to measure hemoglobin content by using Drabkin's solution following manufacturer instructions. When MDA-MB-231 cells successfully promote neovasculature formation within the Matrigel plug, these neovasculatures allow tumor cells to proliferate much better than those without neovasculatures. Therefore, the two groups with better angiogenesis in the Matrigel plug showed more red cells than the treated groups (**Fig. 4.3a**). **Fig. 4.3b** summarizes the quantification of percentage of antiangiogenic efficacy based on hemoglobin content in 10 Matrigel plugs per group. In comparison to their controls, TMP269 treatment or HDAC9 siRNA transfection shows an obvious angiogenic effect with 76% and 72% inhibition of angiogenesis, respectively. These results suggest that selective inhibition of HDAC9 effectively inhibits TNBC angiogenesis.

HDAC9 regulates expression of VEGF and MAPK3 through modulating miR-206 miRNA

To determine whether HDAC9 regulates miR-206 expression, HDAC9 levels were

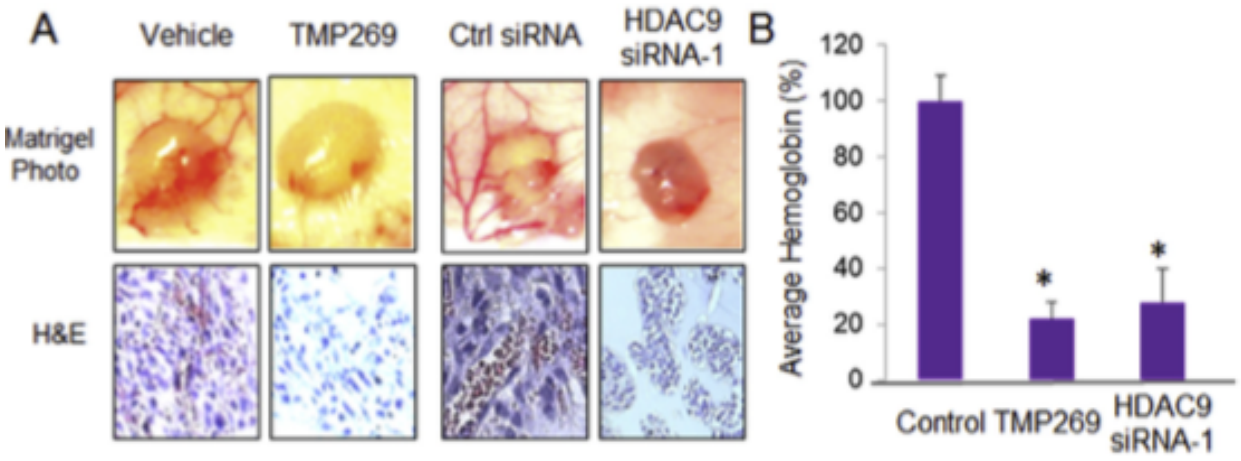

Figure 4.3. Efficacies of HDAC9 inhibition on Matrigel plug angiogenesis *in vivo*. (A) Microphotograph of Matrigel plug representatives from the control and the treated groups, and representative pictures of H&E staining for Matrigel plug sections. (B) The column graph shows the comparison of average hemoglobin in plugs from the control and HDAC9-inhibited groups. *P < 0.001 compared to their controls.

downregulated with HDAC9 siRNA and then miR-206 levels were measured by quantitative RT-PCR analysis. The results show that selective HDAC9 inhibition significantly downregulated miR-206 expression (**Fig. 4.4a**). To investigate whether miR-206 affects regulation of HDAC9 on VEGF and MAPKs, TNBC MDA-MB-231 cells were treated with HDAC9 siRNA, miR-206 mimics of a combination of HDAC9 siRNA and miR-206 inhibitor. The protein levels of VEGF and MAPK3 were measured by Western blot analysis. The results demonstrated that selective inhibition of HDAC9 and forced miR-206 expression both decreased the expression levels of VEGF and MAPK3 compared to their controls (**Fig. 4.4b**). Inversely, miR-206 inhibitor neutralized the action of HDAC9 siRNA on decreasing the expression of VEGF and MAPK3 (**Fig. 4.4b**). Furthermore, the results of a Targetscan predicted target search revealed that VEGF and MAPK3 are predicted targets of miR-206 (**Fig. 4.4c**).

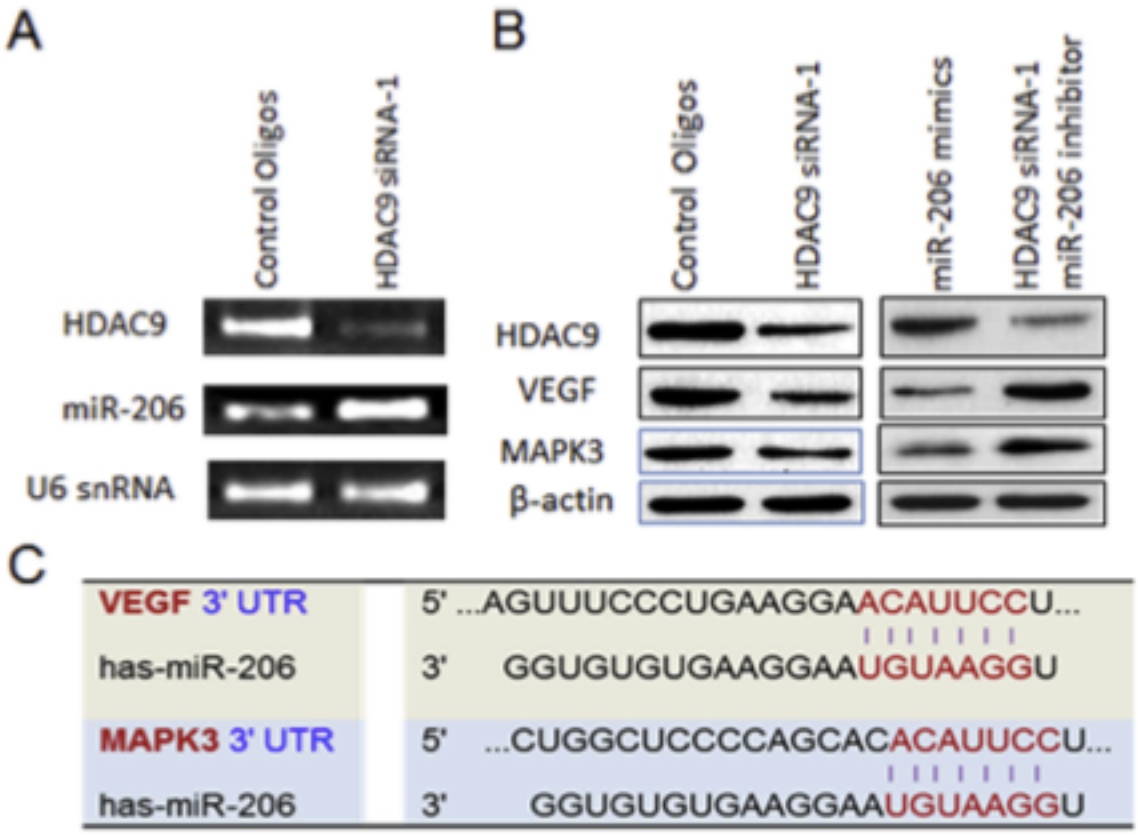

Figure 4.4. HDAC9 decreased expression levels of VEGF and MAPK3 via modulating miR-206 levels in TNBC cells. (A) miR-206 expression levels in TNBC MDA-MB-231 cells treated by HDAC9 siRNA. (B) HDAC9 inhibition decreased expression levels of VEGF and MAPK3 via modulating miR-206 determined by Western blot analysis. (C) Targeting sequences of miR-206 on 3'UTRs of VEGF and MAPK3.

4.5. Discussion

It is now widely accepted that aberrant expression or activity of HDAC enzymes may lead to carcinogenesis and that specific HDAC enzymes are associated with particular malignancies; in turn, the inhibition of HDAC enzymes can result in therapeutic benefits in certain cancer types (160). However, clinical benefits of selective versus broad HDAC inhibitors are unknown and the appropriateness of inhibitor may depend on tumor HDAC enzyme expression, enzyme selectivity of the inhibitor, and the desired effects. Although there are several published studies (139) and numerous ongoing clinical trials involving HDAC inhibitors (141), very little is known about the roles of individual HDAC enzymes, and a formal assessment of HDAC enzyme expression is not routinely done. Emerging data suggests that the currently used HDAC inhibitors may differ significantly with regard to target selectivity. In addition, the expression of HDAC enzymes may vary considerably between normal and tumor tissues and likely between different phenotypes of tumor tissues. HDAC9 is thought to regulate gene expression through epigenetic modulation of the chromatin structure by catalyzing the deacetylation of histone proteins (142). More recently, aberrant HDAC9 expression has been observed in several types of cancers, including medulloblastoma (144), acute lymphoblastic leukemia (145), glioblastoma (146), and osteosarcoma (147). HDAC9 has been shown to promote the growth of these tumors.

Our previous studies have revealed that miR-206 is an anti-invasive and anti-angiogenic agent in TNBC via modulation of VEGF and MAPK3 (155). VEGF has continuously been shown to actively promote angiogenesis, metastasis, and chemoresistance (161, 162). Mitogen-activated protein kinase (MAPK) overexpression has been shown to be associated with advanced stages and short survival in patients with some cancers (163). However, miR-206 has not been characterized as targets of HDAC9 regulation. Our findings demonstrated that the selective inhibition of HDAC9 in siRNA-transfected TNBC MDA-MB-231 cells not only increased expression of miR-206, but

also repressed the expression of VEGF and MAPK proteins and further inhibited TNBC cell invasion and angiogenesis. Furthermore, miR-206 inhibitor neutralized the action of HDAC9 siRNA on decreasing the expression of VEGF and MAPK3. Herein, we report for the first time the involvement of HDAC9 as a mediator of VEGF-mediated invasion and angiogenesis of TNBC tumor cells via modulating miR-206 expression. The results further confirmed that miR-206 actively regulates the expression of VEGF and MAPK3 in TNBC cells.

In conclusion, higher expression levels of HDAC9 are inversely correlated with miR-206 expression in TNBC cells. Furthermore, the selective inhibition of HDAC9 not only modulated the expression of miR-206, VEGF, and MAPK3, but also particularly inhibited TNBC invasion and angiogenesis. Our findings suggest that HDAC9 overexpression in TNBC cells promotes the invasion and angiogenesis through VEGF and MAPK3 via modulating miR-206. These findings may be beneficial for better understanding TNBC regulation and designing personalized therapies for breast cancer patients. Moreover, results from this study revealed a distinct mechanism of action through which HDACi's exert their function. Preclinical mechanistic studies are instrumental in providing a molecular basis for how a candidate drug is eliciting its therapeutic, and sometimes toxic, effects. It is only after rigorous testing has been done in both cells and animals that the candidate drug may proceed into human clinical trials. The following chapter highlights an ongoing multisite clinical trial exploring the effects of an HDACi, belinostat, in improving patient outcome and quality-of-life. Highly controlled and carefully executed clinical trials ensure that the drug is not only safe, but also efficacious and feasible for patient administration.

Chapter 5

From cells to humans: Phase I & ongoing Phase II Clinical Trial studies assessing the effects of the HDAC inhibitor belinostat in combination with standard of care on glioblastoma patients

Adapted from unpublished work that is currently being submitted to Tomography.

5.1 Abstract

It is only after stringent preclinical testing and subsequent IND filing has been done that studies may progress from cells and animals to humans. Clinical trials must always prioritize the safety of the enrolled subjects, and thus, careful planning and research design is crucial for providing balance between scientific advancement and patient quality-of-life. This clinical trial study continues to focus on HDACi's and their role as potent anticacncer agents. As previous mentioned, histone deacetylase inhibitors (HDACi's) have emerged as promising anticancer agents exhibiting pleiotropic effects among a variety of different cancer types, including glioblastoma. Glioblastoma (GBM) is the most common adult primary brain tumor in the United States and despite advancements in its standard of care, the median survival for GBM patients remains low. Proton spectroscopic MRI (sMRI) is rapidly demonstrating promise as a novel, noninvasive imaging algorithm which is able to quantify endogenous tumor metabolism without the need for ionizing radiation or injection of exogenous contrast agents. Herein, we report the first ever clinical trial which assesses the efficacy of belinostat, an HDACi, in combination with standard of care on GBM progression and quality of life. sMRI technology was used to visualize GBM-positive cells and monitor GBM progression. Belinostat was first tested *in vitro* and restored mRNA expression of key enzymes implicated in mood and neuronal integrity: myo-inositol and N-acetylaspartate, respectively. Moreover, belinostat displayed a potent antitumor effect in an *in vivo* orthotopic rat glioma model as well as an antidepressant effect in a mouse model of depression. A Phase I dose escalation study was conducted to establish a belinostat dosing regimen – after two patients experienced thrombocytopenia at a dose of 750mg/m^2, the dose was de-escalated down to 500mg/m^2 and this was the administered dose moving forward in Phase II clinical trials. Phase II clinical trials then monitored patient progression receiving either placebo or 500mg/m^2 belinostat in combination with standard of care; patient surveys were administered

in conjunction with sMRI scans throughout the course of treatment to correlate changes in tumor activity with patient neurocognition and quality-of-life (i.e. depression). Preliminary data from this ongoing study suggest that belinostat in combination with chemoradiation may delate initial recurrence of disease and improve depressive symptoms. This study highlights the potential of belinostat to be a synergistic therapeutic agent for the treatment of gliomas.

5.2. Introduction

Glioblastoma multiforme (GBM) is one of the most common malignant types of brain cancer, with an incidence of about 2-3 new cases per 100,000 people per year worldwide (164). Currently, the standard of care for GBM consists of maximal safe surgical resection followed by radiation therapy (RT) with concurrent adjuvant temozolomide chemotherapy. Unfortunately, even with such aggressive, chemotoxic treatment, recurrence rates remain high: about 70% recurrence is observed within 6 months of RT, and with a median overall survival (OS) of 13-15 months (165). Therefore, novel interventions with improved toxicity profiles are desperately needed to improve patient outcome. Histone deacetylases (HDACs), or key regulators of gene expression, have garnered considerable interest as promising targets for several types of cancers, including glioblastoma (144-147). HDACs act as gene repressors as they deacetylate lysine residues of both histone and nonhistone proteins. This results in the modification of the chromatin structure towards a heterochromatic, wound state in which the DNA is tightly wrapped around the histone core (166). In the GBM setting, it is believed that by introducing a histone deacetylase inhibitor (HDACi), not only will this inhibit tumor proliferation, but this will also promote the unwinding of the tight DNA-histone complexes and thus, the DNA would be more susceptible to both radiation and DNA damage caused by the DNA intercalating agent temozolomide (167).

Unsurprisingly, increasing evidence has suggested that HDACi's exhibit various pleiotropic effects in addition to inhibiting tumor proliferation; research has shown that HDACi's also exert anti-inflammatory properties (168). These findings are significant in that GBM is frequently associated with neuroinflammation, which is thought to have pro-tumorigenic effects. Inflammatory cell infiltrates such as macrophages are recruited to hypoxic and necrotic regions of GBM and promote tumorigenesis through the expression of genes with mitogenic, angiogenic, and migration/invasion stimulating properties (169, 170). Furthermore, HDACi's have demonstrated mood-altering properties as an anti-depressant; in a mouse model of chronic social defeat stress, altered patterns of histone acetylation were observed with similar findings in depressed humans in a post-mortem exam. Interestingly, infusion of an HDACi was shown to exert potent anti-depressant effects in this *in vivo* model (171). These findings are highly relevant to the GBM population given the high frequency of depression (15-39%) in brain tumor patients. In this population, depression is consistently associated with cognitive impairment, reduced physical function and poor quality-of-life (172). Taken together, these results strongly suggest that GBM patients may benefit from concomitant HDACi and standard of care therapy not only as a chemo- and radiosensitizer, but also as a mood and neurocognitive enhancing agent via its anti-inflammatory properties.

Suberanilohydroxamic acid (SAHA), an HDAC inhibitor which targets both class I and class II HDACs, became the first FDA-approved HDACi in 2006 for use as an adjuvant chemotherapy for patients with cutaneous T-cell lymphoma (173). The applicability of HDACi's for use in other cancer types, including glioblastoma, are currently under investigation across several groups; not only was SAHA shown to exhibit anti-glioma properties *in vivo* (174), another HDACi, valproic acid, is currently being tested in combination with chemoradiation as a novel therapy for GBM patients (175). While SAHA is readily orally bioavailable, other potent HDACis

with improved blood-brain barrier penetrability might improve GBM patient outcome as more of the drug would reach the site of action. Recently, another pan-HDACi, belinostat, whose structure is closely similar to that of SAHA, has been shown to improve upon its blood-brain barrier uptake abilities and thus, rationalizes its use as a therapy for CNS tumors (176). In, addition, belinostat has recently shown promise for patients with peripheral T-cell lymphoma in 2014 as it received FDA approval for use (177). However, belinostat's direct applicability in the GBM setting, and whether it may also have radio- and chemosensitizing capabilities, in addition to mood and neurocognitive enhancing properties, remains unknown.

Molecular imaging techniques such as MR spectroscopy and fluorescence spectroscopy have become the standard imaging tools used to visualize and guide tumor resection for GBM patients; however, caveats with these technologies include low spatial resolution, limited field of view, and insufficient tools for spectral display and analysis (178). Current modalities depend on gadolinium-based contrast agents to accumulate in leaky vasculature regions where the blood-brain barrier has been comprised by GBM tumors. Unfortunately, these contrast agents are ineffective at reaching dense, infiltrating tumor regions with limited perfusion (179, 180). Thus, there likely remains a significantly unnoticed portion of tumor-positive tissue after MR visualization and resection. Proton spectroscopy and 3D MR spectroscopic imaging are emerging as novel, complementary imaging tools for tumor visualization that takes advantage of endogenous tumor metabolism to identify regions of significant tumor infiltration beyond that of contrast diffusion (181, 182). Indeed, proton spectroscopic MRI (sMRI) has been validated as a promising tool to guide and improve tumor control in GBM patients (178).

Our research group is currently part of a multisite, interdisciplinary clinical trial (ClinicalTrials.gov ID NCT02137759) which includes Emory University (our home site), University of Miami, and Johns Hopkins University. This is the first clinical trial which assesses

the impact of the HDACi belinostat, in combination with standard RT and temozolomide therapy, in improving patient outcome and quality of life. We plan to use sMRI-guided imaging to not only monitor patient progression through this novel combination treatment, but also to correlate changes in tumor response to changes in quality-of-life metrics, namely neurocognition and depression. Here, we present results from *in vitro* and *in vivo* preclinical studies, as well as results from our ongoing clinical trial studies which not only have identified a tolerable dose for patients moving forward in the trial (Phase I), but also have monitored patient progression throughout the course of treatment in a small (n=26) cohort of patients (Phase II). Firstly, we show that belinostat was able to restore mRNA levels of bottleneck enzymes for the production of N-acetylaspartate (NAA) and myo-inositol (MI); namely, NAT8L and myo-inositol phosphatase, two sMRI-detectable metabolites known to be downregulated in GBM (183). Moreover, we demonstrate the anti-tumor effect of belinostat in an orthotopic rat glioma model. In the clinical setting, we demonstrate that after experiencing severe thrombocytopenia in two patients at a belinostat dose of 750 mg/m^2, the dose was de-escalated down to 500 mg/m^2, and this was the established dose for progression onto Phase II trials. Phase II clinical trials involved a single-blinded design in which patients received either placebo or 500 mg/m^2 belinostat, with both arms receiving concurrent standard of care treatment. sMRI scans as well as depression and neurocognitive assessments were conducted at distinct time points and were analyzed to observe any correlations between patient progression with quality-of-life. Results from this study support the validity of belinostat as an adjuvant therapy for GBM and sMRI as a quantitative imaging technique that can non-invasively monitor therapy response potentially distinguishing true responses from pseudoprogression.

5.3 Materials and Methods

Cell culture and in vitro HDACi treatment

Belinostat and other HDACis were dissolved in dimethyl sulfoxide (DMSO) to obtain a 100 mM stock solution. The rat glioma cell line 9L was maintained in Dulbecco's modified eagle medium (DMEM) (Mediatech, Manassas, MA) supplemented with 10% fetal bovine serum (FBS) and antibiotics at 37°C in 5% CO2. 9L cells were plated in 100 mm cell culture petri-dishes. Cells were then treated two days following seeding with fresh medium containing various HDACis at concentrations of 1 μM for 12 hours and were collected to prepare total RNA.

RNA isolation, RT-PCR, and real-time RT-PCR

Cells were collected 12 hours post-incubation and underwent RNA isolation and RT-PCR to assess the total mRNA expression levels of the key enzymes in the synthesis of NAA (aspartate N-acetyltransferase, NAT8L) and MI (myo-inositol phosphate synthase, MIP) (183). Total RNA was extracted from cultured cells following the manufacturer's instructions described in our previous publication (158). Primer sequences of MIP-1 and NAT8L are as follows: MIP-1 (GeneBank accession number NM_016368), 5'- AGCTGCATCGAGAACATCCT -3' and 5'- GGGTACCGGTCCTTTCTTGT -3'; NAT8L (GeneBank accession number NM_001191681), 5'- GCCAAGAAGGACGCGCTGCT -3' and 5'- GATGCCGTCGTAGAAGATGC -3'. SYBR Green quantitative PCR reaction was carried out in a 15 μl reaction volume containing 2× PCR Master Mix (Applied Biosystems) following our previous reports (158).

Anti-tumor effect in an in vivo rat glioma model

Using a previously described orthotopic rat glioma model (183), the tumoricidal and psychological effects of belinostat were tested. 9L rat glioma cells were stereotactically injected into the frontal lobes of male Fischer 344 rats (n=9). At post-injection day 9, rats were treated with a daily intraperitoneal injection of either vehicle (10% DMSO, n=1) or tiered doses of belinostat (n=2 each of 25mg/kg, 50mg/kg, 75mg/kg, and 100mg/kg) for four days. Throughout the experiment, rats were monitored for mood behavior and activity levels using the volume of droppings as a surrogate measurement. Animals were sacrificed on post-injection day 12 and tumors were excised. This protocol was approved by the Institutional Animal Care and Use Committee (IACUC) at Emory University.

Antidepressant effect in an in vivo model of depression

We used the forced swim test to evaluate the antidepressant potential of belinostat, an established model for measuring antidepressant efficacy (184). Briefly, two 4-liter beakers were filled approximately 75% with water at a temperature of 25 +/- 0.5 degrees Celsius. Two camcorders were placed, respectively, directly across from each beaker and every trial was recorded in this manner. The beakers were encapsulated by cardboard boxes to prevent the mice from any visual distractions that might perturb the results. Mice were treated by 75 mg/kg belinostat via I.P. injection 6 hours prior to conducting the forced swim test. Control/treated mice pairs were then placed into the beaker and recorded for 10 minutes prior to being placed into a housing chamber. This was done for all 5 control-treated pairs.

Phase I clinical trial studies

Patients with newly diagnosed GBM were enrolled in the treatment arm of an Institutional Review Board (IRB)-approved clinical trial at Emory University (ClinicalTrials.gov ID NCT02137759), where they received intravenous belinostat (Spectrum Pharmaceuticals, Irvine, CA) as an investigational therapeutic. Inclusion criteria includes: (i) histologically confirmed GBM diagnosis; (ii) ≥ 18 years old; (iii) can undergo MRI; (iv) have measurable contrast-enhancing residual tumor (> 5 mm in shortest diameter); (v) life expectancy of ≥ 3 months. All patients underwent maximal safe tumor resection prior to enrolling in the study, and tissue samples were collected from the excised tumor. Tissue samples underwent immunohistochemistry (IHC) analysis and were stained with anti-acetylated histone H4 antibody (Acetyl H4, #Ab15823, Abcam, Cambridge, UK). The amount of nuclei staining for acetylated H4 corresponds to how active the HDACs are in those cells.

Patients received standard-of-care therapy consisting of daily 75mg/m^2 of temozolomide and a 60Gy fractionated dose of radiation to residual contrast-enhancing tissue (per T1-weighted MRI post-resection). To test tolerability of combining belinostat with standard RT/TMZ in newly-diagnosed GBM patients, the 3+3 dose escalation design was used (53). Briefly, up to six patients will receive a belinostat dose of 750 mg/m^2 for five days every 21 days starting at week zero (one week prior to start of RT/TMZ), week three (third week of RT/TMZ), and week 6 (sixth week of RT/TMZ) (three total cycles) with final toxicity assessment for determining tolerability at 28 days after completion of RT/TMZ (**Figure 5.1**). If the first three patients tolerate 750 mg/m^2 well, the dose will be escalated to 1000 mg/m^2 at the same schedule for up to six additional patients. If the 750 mg/m^2 dose is not tolerated, we will de-escalate the dose down to 500 mg/m^2 at the same schedule for up to six patients as well. We will continue this process until a maximum tolerate dose is obtained for progression into Phase II studies.

Phase II clinical trial studies

After having established the maximal tolerated dose from Phase I studies, progression onto Phase II clinical trials aims to assess the tolerability and efficacy of dual belinostat/RT/TMZ treatment on improving patient outcome and quality-of-life. 28 patients were randomly assigned to the control arm receiving placebo or the belinostat treatment arm. Prior to receiving chemoradiation, all patients received a baseline sMRI scan conducted in a 3T MR scanner (Siemens TimTrio, 32 channel head coil) using the echo planar MR spectroscopy sequence and MIDAS processing software developed at the University of Miami (185, 186). The sMRI volumes were co-registered to a T1-weighted (T1w) MRI taken during the same scanning session with the patient in the same orientation. A second sMRI scan was obtained one month after completing radiation therapy to determine therapeutic response. Patients are continued to be followed up with standard of care imaging for 12 months post-treatment (**Figure 5.2**).

Imaging parameters, including a short echo time (TE=17.6ms) were used to enhance the signal of choline (a metabolite involved in the synthesis of the phospholipid cell membrane and increased in tumors) and NAA (a healthy neuronal marker decreased as neoplasia invades into and destroys neuronal tissue). The ratio of these two metabolites (Cho/NAA) was computed, and the value of this ratio within regions of tumor was normalized to the value of the ratio in the contralateral normal appearing white matter (NAWM). This Cho/NAA ratio has previously been shown to be sensitive to tumor density in GBM and has been correlated with histological markers of glioma, such as SOX-2 (178, 187).

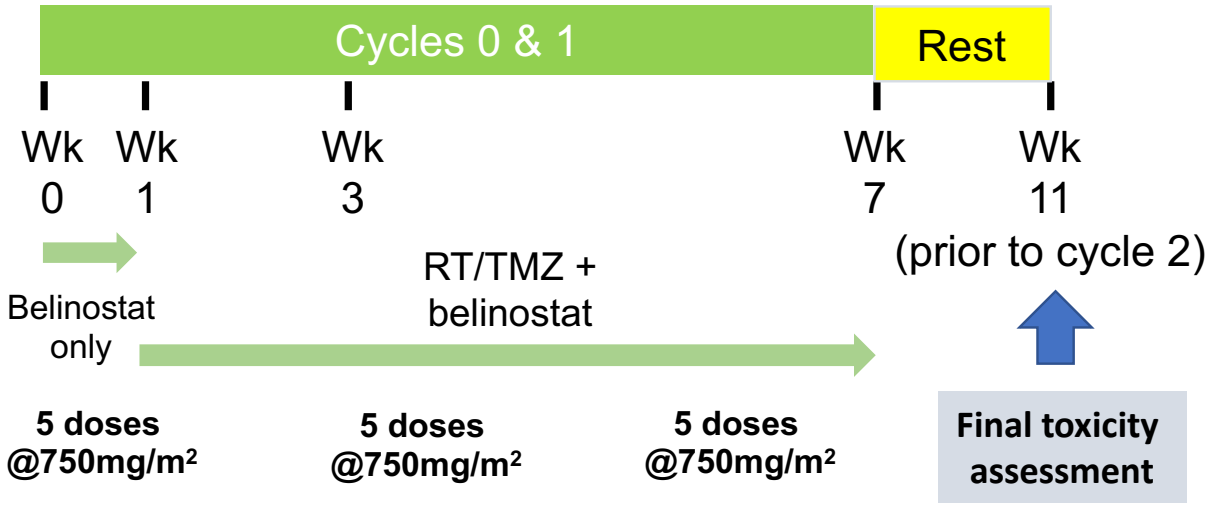

Figure 5.1. 3+3 design for Phase I clinical trial study. In this design, up to six patients will first receive 750 mg/m^2 belinostat as a series of five doses throughout week zero (Wk 0). Patients will then receive concurrent RT/TMZ therapy in addition to 750 mg/m^2 belinostat a week later, and will continue to receive belinostat every three weeks, as shown. After a four week rest period, final toxicity assessments will be measured.

Finally, throughout the course of treatment, various questionnaires were administered that measured patient depression (i.e. IDS-SR surveys), as well as neurocognition and quality-of-life (i.e. HVLT-R, QLQ-C30, QLQ-BN20). The exact timeline for survey administration can be seen in **Figure 5.2** on the following page.

IDS-SR survey for depression

Symptoms of depression were measured during each MRSI session using the Inventory of Depressive Symptoms-Self Report (IDS-SR), a 30-item instrument with excellent psychometric properties that was designed to measure symptom constructs consistent with current diagnostic nosology regarding depression. This instrument is widely used as a self-report outcome measure in treatment trials and has been approved for use by the FDA (188, 189). The instrument provides severity assessments of disturbances in mood, sleep, appetite, energy, cognitive function, level of interest, and self-esteem. IDS-SR were administered before imaging sessions and at the time intervals indicated in **Figure 5.2**. IDS-SR results were analyzed and correlated with MRS--detectable MI, Cho and NAA levels within the surrounding "normal" brain. In addition, depression scores will be compared before and during treatment in belinostat-treated versus untreated patients.

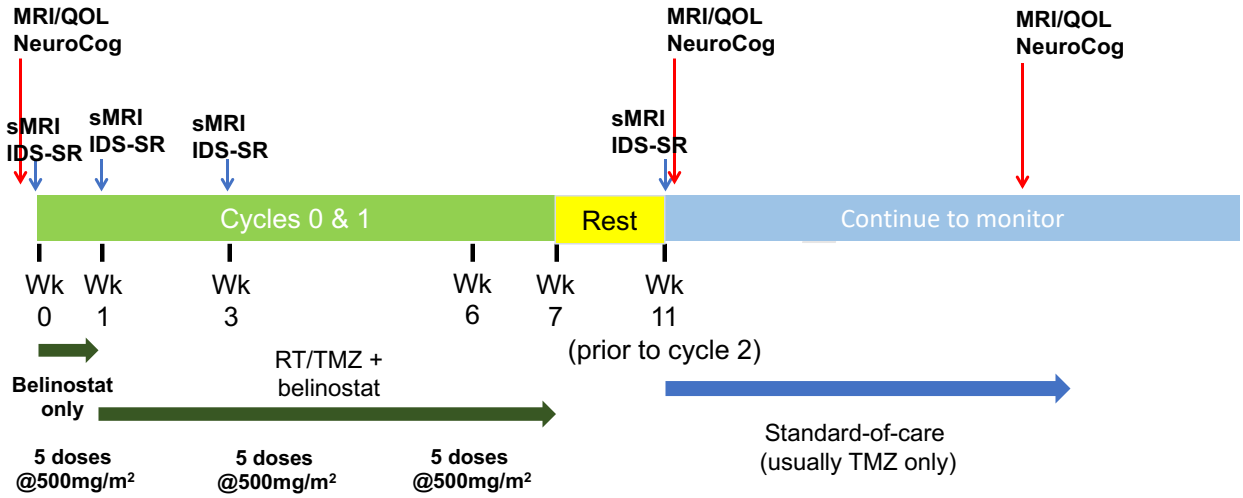

Figure 5.2. Timeline for treatment for Phase II clinical trial studies. The dosing regimen in this clinical trial phase is identical to the dose escalation Phase I study. In addition to receiving concurrent belinostat and standard of care treatment, various depression surveys (i.e. IDS-SR) as well as neurocognition and quality of life (i.e. QOL) surveys were administered at the timepoints indicated above.

Neurocognition and quality-of-life (QOL) surveys

Because depression may potentially influence neurocognition in GBM patients and GBM has been associated with neurocognitive impairment (172), quantitative measurements of neurocognitive function will be a useful adjunct in the evaluation of these patients to determine impact of belinostat on brain metabolism and behavior. As noted above, depression can also significantly impair QOL. Standard instruments to assess neurocognitive function and QOL were incorporated in the recently completed phase III trial (RTOG 0825) for newly diagnosed GBM, and these results can serve as historical controls. These instruments include the HVLT-R, Trail Making A/B, and COWAT for neurocognition and the EORTCQLQ30/BCM20 for QOL. MI, Cho and NAA levels as well as depression scores will be correlated with cognitive function and QOL scores. In addition, cognitive performance and QOL will be compared before and during treatment in belinostat and control patients.

5.4. Results

In vitro study of mRNA expression

mRNA expression levels of MIP and NAT8L (bottleneck enzymes that are key to the production of MI and NAA, respectively) from HDACi-treated cells are shown in **Fig. 5.3** as fold-increases in log scale compared to those of the untreated cells (DMSO vehicle control). Belinostat showed greater increases in restoration of mRNA levels at the same concentration as other HDACi, including SAHA. The only other HDACi which achieved greater efficacy is quisinostat (JNJ-26481585), a second-generation pan-HDACi which was being tested in Phase II clinical trials for multiple myeloma (190). However, currently there are no active trials for quisinostat on ClinicalTrials.gov.

In vivo orthotopic rat model

Photographs of the 9 rats evaluated in this experiment are shown in their cage at pre-treatment with belinostat and at day 12 four days after treatment when the rats were sacrificed in **Fig. 5.4**. The volume of animal droppings can be seen in the cage, a measure of activity and normal physiology. Rats showed decreased movement and grooming, measures of mood, prior to treatment with belinostat. The restoration of activity and improved moved was observed in a dose-dependent manner, with normal levels observed in rats treated with the highest two doses (75 mg/kg and 100 mg/kg). Photographs of the tumor *in situ* and excised are also shown in **Fig. 5.4**, showing a similar dose dependent decrease in tumor volume from untreated mice through the increasing doses of belinostat.

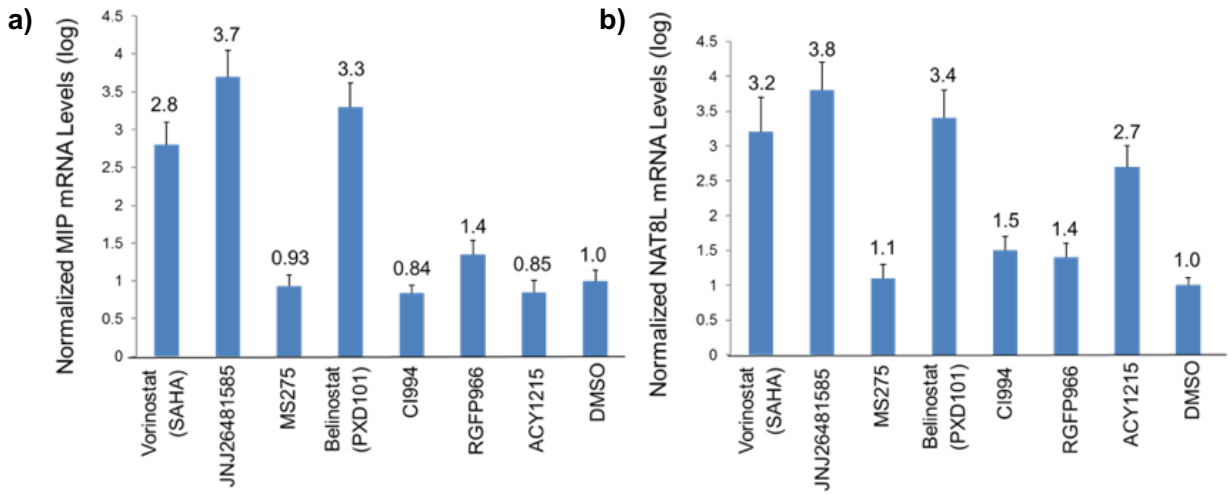

Figure 5.3. Belinostat (PXD101) restores MIP and NAT8L expression in rat glioma 9L cells. 9L rat glioma cells were treated with 1uM of various HDACi's for 12 hours and were then lysed and total RNA was extracted to perform RT-PCR analysis. Shown above are the results for fold-changes in (a) MIP and (b) NAT8L levels.

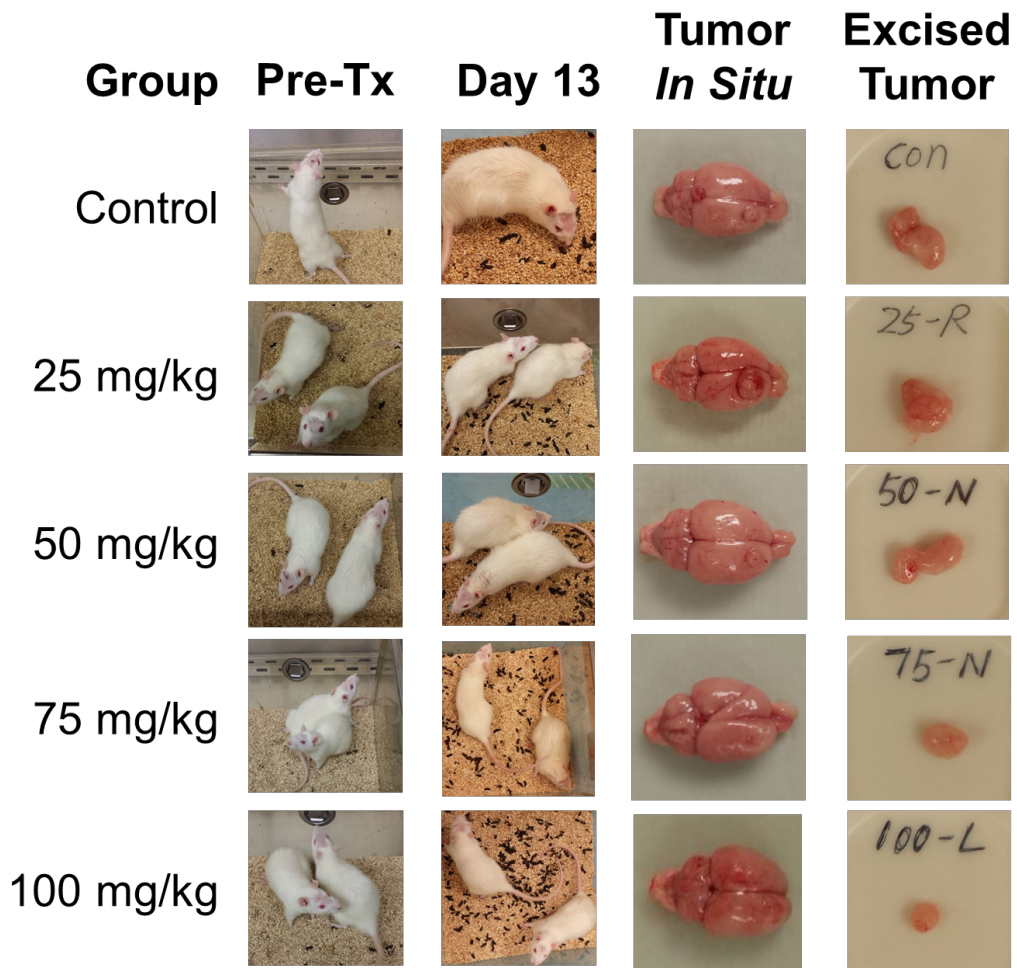

Figure 5.4. Belinostat exhibits dose-dependent anti-tumor and mood-enhancing effects in orthotopic rat model. Shown above are representative photographs of rats injected with 9L glioma cells and treated with 25, 50, 75, and 100 mg/kg belinostat, respectively, compared to control. The number of droppings, as well as increased movement with increasing belinostat doses suggests improved mood. Excised tumor volumes also decreased with increasing belinostat doses.

Forced swim test of depression

Five groups of control/belinostat treated pairs were subject to the forced swim test to measure belinostat's antidepressant potential in an *in vivo* model. Results are shown in **Fig. 5.5**; the belinostat treated group displayed a trend to be more actively swimming in the beaker which is reflected by a decrease in the time spent immobile. This decrease in immobility is correlated to an antidepressed state, whereas mice that are immobile in the beaker are thought to be socially defeated and translates to a depressed state. While this did not reach significance, this can likely be attributed to the low sample count (n = 5) per mouse group. Furthermore, there was one mouse in the belinostat treated group that deviated significantly from the other mice in their group, which contributed to the large error bars. Nonetheless, results from the forced swim test clearly demonstrate the potential of belinostat to be a viable antidepressant in the clinic.

Phase I studies

In this Phase I study, we aimed to determine the maximal safe tolerable dose of belinostat for use in Phase II and subsequent clinical trial studies. We employed the 3+3 dose escalation design in which 3 patients received a belinostat dose of 750 mg/m^2 and assessed for any toxicity associated with belinostat administration. We found that two out of the three patients experienced severe thrombocytopenia with the 750mg/m^2 dose; thus, the dose was de-escalated down to 500mg/m^2 and this was the established dose moving forward in Phase II studies.

Phase II studies

21 patients who met inclusion criteria for analysis were assessed to determine differences in PFS between the two arms (Supplementary Figure 5S1). A table summarizing basic demographics of the two arms of the clinical study is shown in **Fig. 5.6a**. Both arms showed similar

distributions of known genetic targets that improve response to radiation – mutation of isocitrate dehydrogenase 1 (IDH1) and promoter methylation of the gene for O[6]-methylguanine-DNA methyltransferase (MGMT) (165). **Figure 5.6b** shows Kaplan-Meier curves for PFS from date of surgery (tick marks indicate time of censoring). Six-month PFS was 73% for the control arm and 100% for the belinostat arm. A log-rank test assessing PFS data up to 6 months trended towards statistical significance (p=0.09). No statistically significant difference was observed on a log-rank test assessing PFS data up to 12 months (p=0.45). Of these 21 patients, 17 completed an IDS-SR survey at both baseline (week 0 for belinostat arm, week 1 for control arm) and at week 11 (Sipplemental Figure 5S1). While no significant difference in the scores was observed at either time point, the belinostat cohort had a statistically significant improvement in scores over the course of treatment using a two-tailed unpaired T-test (p=0.04, **Table 5.1**).

Next, we sought to assess the feasibility and reliability of sMRI imaging compared to that of standard MRI scans. **Figure 5.7** depicts sMRI and clinical CE-T1w MRI scans for two representative patients, one from each of the study arms. At baseline, both patients showed elevated choline metabolism (red arrows) around the resection cavities, indicating the presence of increased cellular turnover associated with neoplasia. One month post-RT (week 11), both patients showed decreased levels of choline compared to baseline, and low NAA levels due to subsequent radiation damage to in-field neurons (data not shown). The control patient (**Fig. 5.7a**) was deemed to have potential progression of her disease because of the thickened contrast enhancement around the resection cavity on CE-T1w imaging; a month later, however, the thickened contrast rim was gone, and the patient was deemed to not yet have disease progression. The patient in the belinostat

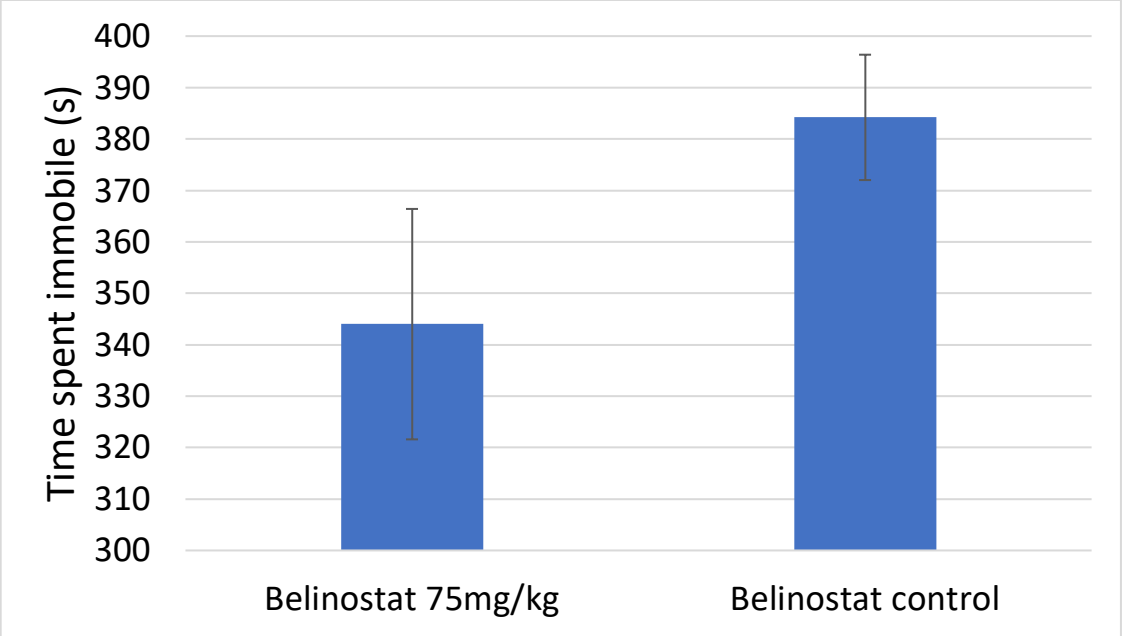

Figure 5.5. Belinostat-treated mice show a trend (p = 0.1) for antidepressant behavior via the forced swim test. The forced swim test was used to measure belinostat's antidepressant potential. Five control/belinostat mice pairs were individually placed into 4-liter beakers containing 3 liters of water at a temperature of 25 +/- 0.5 degrees Celsius and recorded for 10 minutes. Each mouse was then analyzed and the collective amount of time spent immobile (sec) was determined for minutes 2-10. Data was averaged for each mouse pair and plotted; error bars represent standard deviation.

a)

	Control	Belinostat
Number of patients	11	10
Age	57.5 ± 12.3	50.3 ± 13.6
IDH1 mutation	1 (9%)	1 (10%)
MGMT methylated	3 (27%)	3 (30%)
6 Month PFS	8 (73%)	10 (100%)

b)

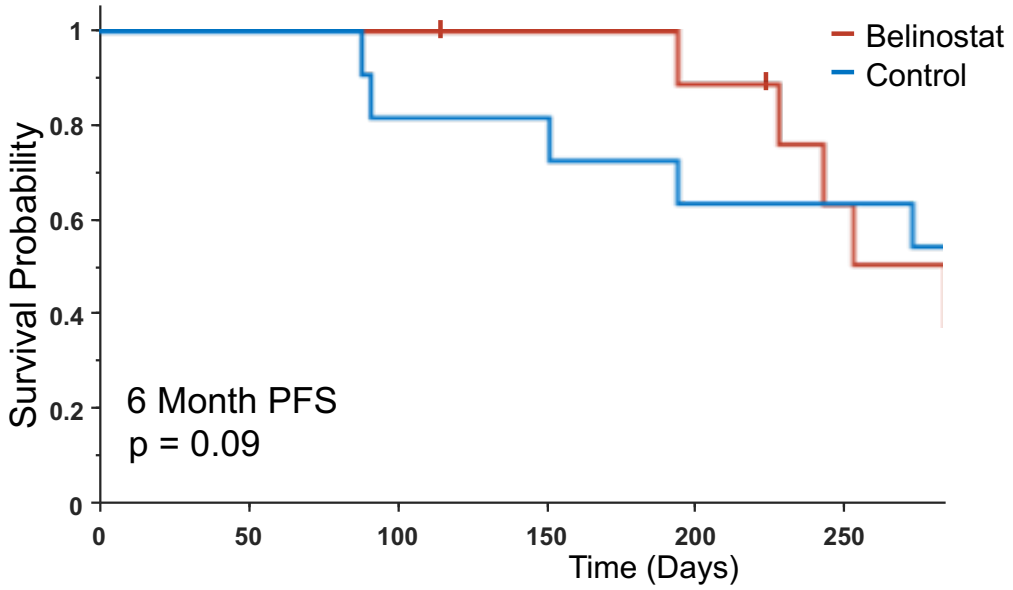

Figure 5.6. Basic demographics of patients and Kaplan-Meier survival data in both control and belinostat arms. (a) 21 total patients were assigned to either the control (11 patients) or belinostat (10 patients) arm. Data highlights similar distributions of known genetic targets that improve response to radiation. (b) Kaplan-Meier survival curves show a trend for improved PFS for the belinostat arm at 6 months (p=0.09).

arm (**Fig. 5.7b**) had a similar course, only the increase in enhancement occurred 3 months after radiation was completed.

	Control	Belinostat	*P value*
Number of Patients	10	7	
Baseline Score	18.2 ± 9.1	22.0 ± 9.8	0.43
Week 11 Score	22.3 ± 10.9	16.1 ± 15.5	0.39
Change in Score	4.1 ± 9.7	-5.9 ± 8.7	**0.04**

Table 5.1. GBM patients receiving belinostat exhibit a statistically significant improvement in depressive symptoms throughout course of treatment. IDS-SR assessment of patients in both study arms between baseline and 1 month post-RT shows a statistically significant improvement in assessment scores for patients who received belinostat. P values indicate results of a two-tailed unpaired T-test.

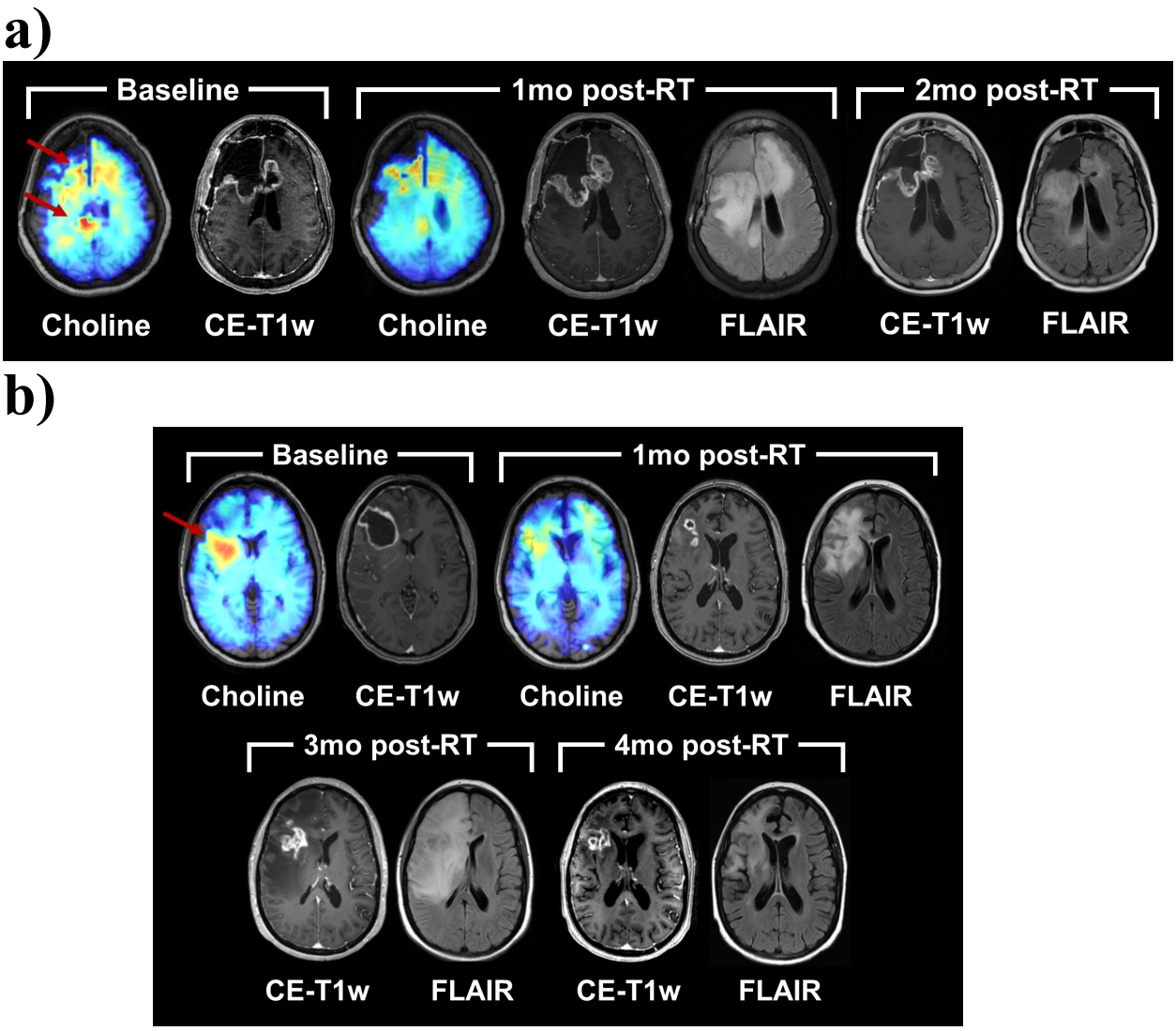

Figure 5.7. Representative sMRI vs CE-T1w MRI images show a discrepancy for disease progression versus pseudoprogression. Longitudinal imaging of a patient in the (a) control arm and (b) belinostat arm. (a) An sMRI map of choline indicates a response to chemoradiation between baseline and the first follow-up; however, standard clinical imaging indicates potential progression of disease. Further follow-up indicates that the imaging finding at 1 month were attributable to pseudo-progression. (b) An sMRI map of choline indicates a response to chemoradiation as assessed at 1 month post-RT. Clinical imaging correlates at that time-frame, and pseudoprogression was considered at later time points.

5.5. Discussion

The *in vitro* cell study showed that belinostat had restorative activity for both key enzymes that are involved in the production of NAA and MI which are downregulated in gliomas due to the destruction of healthy neuronal and supportive tissue. The restored mRNA levels were similar to those of SAHA, which was the first FDA-approved HDACi for cancer treatment. A HDACi tested that had higher restoration than belinostat was quisinostat (JNJ26481585); however, there is no clinical trial currently enrolling patients testing quisinostat. As such, belinostat shows promise as a targeted HDACi for glioblastoma because of its increased uptake into the brain and its efficacy in restoring key metabolic activity. Efficacy of belinostat in reducing tumor volume was assessed in an orthotopic rat glioma model. Here, a dose dependent reduction in tumor size was observed, suggesting the anti-tumor properties of the drug are effective *in vivo*. Additionally, it was observed that the activity levels of rats, as measured by grooming activities and droppings, were higher in those treated with increased doses of belinostat. These improvements are consistent with previously reported by Covington et al (171) that HDAC inhibitors possess antidepressant actions in addition to their tumoricidal effect. Additional testing of this drug in human subjects can help with separating this improved mood/activity effect due to a primary property of HDACi's from improvement as a secondary effect to reduced tumor burden.

Our belinostat clinical trial completed new enrollment of patients as of August 2018, and patients are continuing to be followed to assess outcomes including progression-free and overall survival. While statistical claims cannot yet be made regarding long-term survival and efficacy, a comparison of six-month PFS and initial changes in mood are shown in this work. The cohort receiving belinostat showed a trend of improved 6-month PFS compared to the control cohort ($p=0.09$), although this did not appear to hold up when assessing 12-month PFS ($p=0.45$). Despite a limited sample size for this study, these results suggest that belinostat may improve response to

chemoradiation therapy as hypothesized. A speculated reason for the improved PFS at 6 months but not at 12 months is that belinostat was only given to subjects for a short-term during RT. While 6-month PFS outcomes approached statistical significance, the belinostat cohort did achieve a statistically significant improvement in depression as measured by the IDS-SR. These preliminary data support the antidepressant effect induced by belinostat and suggest a larger cohort of patients to be evaluated in the future for improved statistical power.

Furthermore, this study showed the potential of sMRI as a non-invasive monitoring tool for investigational therapeutics. As shown in **Figure 5.7**, both patients appeared to have a metabolically normalized tumor when assessing choline metabolism at week 1, one month after the completion of RT. Standard imaging, however, differed between the two patients and suggested that the control patient may have been experiencing disease progression, when eventually it turned out to be stable disease at that time. This is a phenomenon known as pseudo-progression, the ambiguity of CE-T1w findings in differentiating true progression of disease from normal tissue response to high dose radiation. sMRI, however, is robust to the pseudoprogression phenomenon since the modality is measuring endogenous intracellular metabolism rather than vasculature damages/changes or tissue phenomena such as edema. Both patients showed similar metabolic signatures, which turned out to be more accurate of the underlying pathology compared to clinical imaging.

In summary, our pilot clinical study described the therapeutic and anti-tumor effects of belinostat, a potent pan-HDACi with blood-brain barrier permeability, in patients with glioblastoma. The results from this work suggest belinostat may be an effective HDACi at delaying disease progression and improving depression as measured by the IDS-SR survey. Furthermore, it shows that the treatment response can be monitored non-invasively using spectroscopic MRI during pseudoprogression period. Further studies and analysis of the ongoing clinical trial may

yield a better understanding of the role that HDACi's play in the metabolic profiles of GBM and motivate the development of better, targeted therapies for patients with this debilitating disease.

Ideally, following successful Phase II studies, Phase III studies will then be conducted and a much larger cohort of patients will be enrolled and assessed for long-term efficacy and toxicity. These steps are the final steps of the drug development process; following Phase III studies, an NDA may then be submitted which the FDA will review and assess the results obtained from the previous three clinical trial Phase studies. Following FDA approval, the drug may then be legally marketed to the public and may then be used for its intended therapeutic purpose. The framework illustrated in this chapter provides the essential training required to carefully implement and design human clinical trial studies. Collectively, the results presented in the previous chapters offer a broad range of training which provide the foundation for a career in the drug development industry.

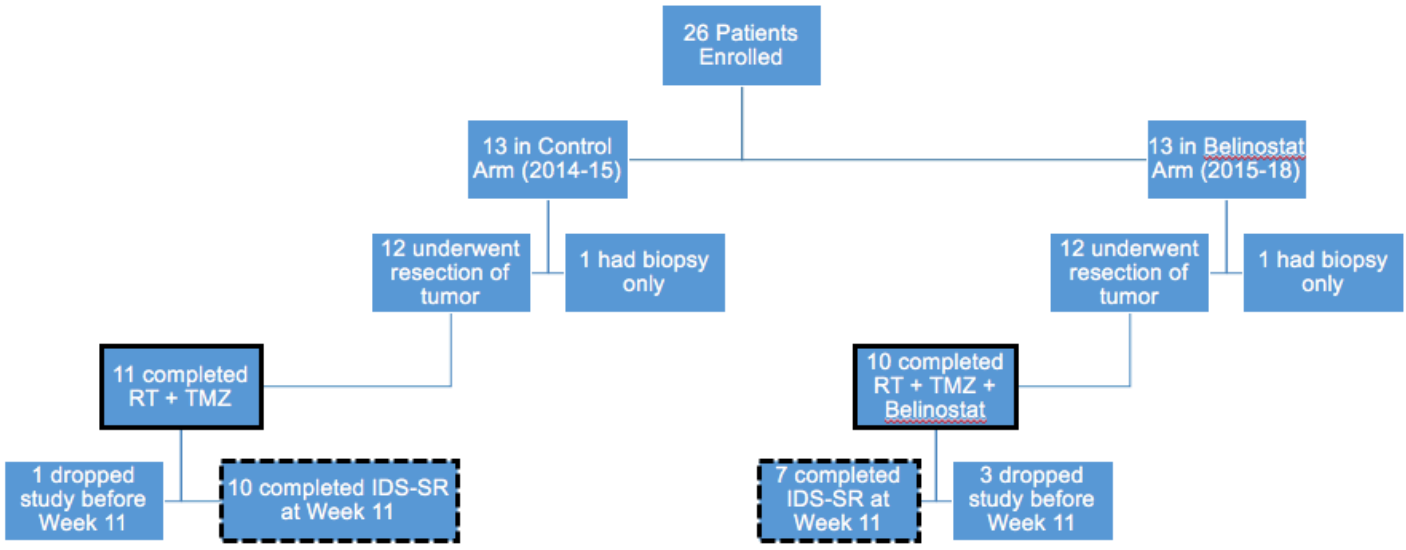

Supplemental Figure 5S1. Summary of patient enrollment and the final number of patients who completed IDS-SR surveys through week 11. Flow diagram of patients enrolled in NCT02137759. Bold solid outlines indicate subjects used in PFS analysis; bold dotted outlines indicate subjects used in depression analysis.

Chapter 6

General Discussion

6.1 General Discussion

The results presented in this work provide a comprehensive understanding of the methodology and processes required to successfully maneuver a candidate compound from bench to bedside. One of the most important realizations of drug discovery research is that it is no easy feat; only 1 compound in about 5000 which demonstrates preliminary promise actually translates into a novel therapeutic (5). Remarkable progress has been made throughout the past couple of centuries due to the birth of various fields integral fields required for drug discovery research, such as molecular biology, medicinal chemistry and biochemistry. Prior to the discovery of these fields, humans primarily relied on natural products as the major source of therapeutic relief. Peoples from various civilizations and countries throughout the world have long documented plants and herbs which harbor medicinal properties despite an unclear understanding of the exact mechanisms of action. Unsurprisingly, naturally derived medicines still have a profound impact on drug discovery research in the modern era; once the active compounds become extracted from its primary source, researchers may then build upon its properties to develop a semi-synthetic compound or can learn information about the compound's target to develop a purely synthetic compound.

Drug discovery research is seldom a unidirectional process and is oftentimes instead an iterative process where compounds are screened, assessed for efficacy, and depending on the results, may be further optimized or may be discarded for another round of screening. Where a research group might begin on a drug discovery effort largely depends on what is known *a priori* about the disease or condition, any known targets, or already established compounds known to impact disease outcome. The three major targets that are discussed throughout this work include aromatase (chapter 2), the CXCR4 receptor (chapter 3), and histone deacetylases (HDACs) (chapters 4 and 5). All three of these targets are already well-established within their respective fields and thus, appropriate target selection was not a consideration for any of these drug discovery

efforts: aromatase is the key enzyme responsible for the biosynthesis of estrogen from their androgenic precursors, and thus, is clearly one of the most attractive targets for this type of hormone receptor positive (i.e. ER-positive), postmenopausal breast cancer (71). The CXCR4 receptor has well-established roles in HIV entry, metastasis, and particular to this work, inflammation (103, 104). While other anti-inflammatory drugs (i.e. NSAIDs) are currently known to target inflammation, they have long term toxicity profiles which cannot be ignored, and thus, CXCR4 becomes the next logical target for inflammation. Finally, histone deacetylases, given their crucial role in chromatin regulation and gene expression, are emerging as an attractive target for cancer treatment, given the inherent genetic instability that is instrumental for oncogenic development (191). While HDAC inhibitors still remain poorly understood, their preliminary promise should not be ignored and is worth further exploration.

After having a solid basis for target selection, then identification and selection of hit compounds becomes the next major challenge. There are a variety of methods that a research team might use to achieve hit compounds, with *in silico* virtual design and virtual high-throughput screening, a corollary to traditional high-throughput screening, being the two techniques used in this work. As previously mentioned, what is already known *a priori* about the target and/or current hit compounds will have a significant influence on the method to pursue. The aromatase drug discovery project was unique in that it has been a well-established target for several decades; thus, there have already been three generations of aromatase inhibitors (AIs) that are out on the market. The current third generation inhibitors (i.e. letrozole, exemestane, and anastrozole) show remarkable, potent, nanomolar potencies towards aromatase. However, while they work well at inhibiting aromatase, they do so at the expense of the quality-of-life of the patient receiving treatment. Aromatase-inhibitor associated anthralgia (AIAA), or joint pain, presents in about 20-30% of AI patients which causes for a good majority of patients to fail to adhere to AI therapy (77-

79). Thus, toxicity, and not potency, was the primary endpoint for the development of a potential novel generation of AIs. Our ultimate goal was to retain potency yet limit toxicity in AI patients.

One of the most recent breakthroughs in aromatase research came in 2009 when the Ghosh group successfully crystallized and characterized the aromatase protein for the first time. A couple of noteworthy observations was that the active was small, compact, and not easily flexed by ligand binding. Furthermore, the channel entry site through which the substrate enters is oriented in a way that directly faces the C4- and C6- positions, respectively, of the androgen scaffold (87). Thus, we believed that an *in silico* approach would be a logical approach for drug discovery given the specificities of the binding pocket. We chose to use the current steroidal AI exemestane as the parent compound due its resemblance to the endogenous substrate androstenedione and took advantage of a series of previously synthesized androstenedione-like analogues, some of which were only crudely characterized. Interestingly, in the clinic, the steroidal, irreversible AI exemestane and the nonsteroidal, reversible AI's letrozole and anastrozole show distinct patient profiles; whereas nonsteroidal, reversible letrozole inhibits global estrogen production by a larger margin than steroidal, irreversible exemestane, patients have reported AIAA symptoms to be less severe in exemestane than in letrozole (82-86). Again, since toxicity was our primary endpoint, exemestane was the clear choice as the parental structure against which further analogues were synthesized and studied and docked into the aromatase active site. We sought to investigate if the pharmacological properties of the class of drugs (i.e. potency, specificity, mechanism of action) might have an impact on their clinical toxicity profile.

We then took preliminary data on a subset of the compounds which had crude aromatase inhibition data and generated a first pass structure activity relationship (SAR) report which would reveal so-called activity cliffs: compounds with very similar structures possessing significantly different potencies. From this analysis, we identified three particular activity cliffs that had key

differences in their structure relevant to the understanding of the aromatase active site: (i) compounds HDDG-046 and HDDG-026 (HDDG-046 has two carbons proceeding the terminal C6-alknyloxy group); (ii) HDDG-050 and HDDG-043 (key differences in A-ring stereochemistry which might dictate mechanism of action); (iii) HDDG-016 and HDDG-041 (hypothesized mechanical switch in A-ring stereochemistry that would render a compound as reversible vs irreversible). This preliminary analysis gave us a focused compound set to then revalidate in our own aromatase inhibition model. Upon rescreening, we showed that the trends held true for two out of the three activity cliff pairs, with one dataset showing no difference in activity. Overall, the potencies for all compounds were still near or below the targeted range, and when docking studies were conducted to correlate potencies with predicted binding poses, there was no apparent distinction that could be observed. For nearly all three datasets, the molecular docking software generated nearly indistinguishable poses that suggested that the compounds should elicit similar activities *in vitro*.

All in all, while docking data was unable to rationalize the detected biological activities for these compound sets, computational analyses did reveal a couple of novel findings still relevant in trying to better understand the molecular framework underlying the aromatase active site. For instance, *in silico* data correctly predicted that letrozole, as well as two of our analogs, HDDG-046 and HDDG-058, should be nearly equipotent in inhibiting aromatase, which was reflected in a MTT assay. Moreover, one interesting finding was the observation that letrozole seems to partially mimic the steroidal backbone and this may provide some rationale for letrozole's efficiency in inhibiting aromatase. Indeed, this hypothesis has been postulated previously (93); however, in this study, we provide the structural basis supporting these speculations. Finally, we were able to exploit a solved aromatase/HDDG-046 crystallized complex available in the PDB database that revealed how HDDG-046 is binding to the aromatase active site. It was with this actual biological

data that we speculated that there was a novel residue, Ser478, well within hydrogen bonding distance of the acetylene group present in the C6-substituent of HDDG-046. Further testing, such as mutagenesis experiments, should be carried out to probe the utility of this residue for enhancing HDDG-046's effects.

While we sought to mitigate side-effects associated with current AI's, we do not fully anticipate being able to fully alleviate the joint and musculoskeletal side-effects, because these effects are most likely estrogen-dependent (78-80, 94-96). However, we reasoned that if we could even marginally reduce the severity of the reported symptoms, via manipulation of different key pharmacological traits (i.e. mechanism of action, potency), that this could provide the relief that would keep patients adherent to AIs. A thorough combination of optimizing current AIs, along with potential co-administration of other bone-protectant drugs, such as bisphopshonates, might enhance the patient's quality of life while on AIs. Nonetheless, this study highlights the inherent need for better AI therapeutics and provides the molecular and computational framework for the development of improved AIs for postmenopausal, estrogen-dependent breast cancer.

As previously mentioned, while *in silico* drug design offers the advantage that the researcher is able to directly manipulate a compound via its solved protein structure for optimal potency, there are other methods that one can use in the discovery of novel hit compounds. The second approach used in this work involved using a virtual high-throughput screening approach in the development of novel anti-inflammatory CXCR4 modulators. Previous research on the CXCR4 receptor has shown that, unlike the aromatase protein, CXCR4 is much more promiscuous and is able to accommodate ligands of several different classes due to its relative flexibility (192). Moreover, our group has already identified key pharmacophores that are essential for CXCR4 inhibitory activity, notably the amide and sulfamide pharmacophores (117). Therefore, due to the fact that we had a rough idea in regard to the general compound structure for our modulators, we

resorted to virtual high-throughput screening as our preferred hit discovery method instead because we believed that we could get several more hits that had the potential to bind well to CXCR4 due to its flexible binding pocket.

We began this study by assembling the necessary building blocks (i.e. sulfochlorides, carboxylic acid groups) that were readily available in a virtual compound library. These sulfochlorides and carboxylic acids were first filtered and selected for their drug-like properties (i.e. obeying the Lipinski rule of five); those which showed unfavorable drug-like characteristics were removed from the screening and only those who progressed were then assembled to generate potential CXCR4 modulators that were simultaneously docked into the CXCR4 receptor. After the top 30 hits were systematically screened and tested, we sought to investigate the effects of modifying the top hits in a way to generate an extensive structure activity relationship (SAR) report. In this study, some of the screening assays that we used included: (i) a primary binding affinity screening whereby we measured the ability of our compounds to bind to the CXCR4 receptor; (ii) a Matrigel invasion assay to assess the anti-invasiveness of our analogs; (iii) an *in vivo* xylene-induced ear edema inflammation model where we measured the anti-inflammatory properties of our compounds; (iv) an MTT assay to measure cytotoxicity; (v) *in vivo* pharmacokinetics study to assess stability. All of these screening assays are essential in properly characterizing the feasibility of our analogs as CXCR4 modulators in that they assess both *in vitro* and *in vivo* efficacy and toxicity. Collectively, from this data, we were able to generate a detailed structure activity relationship (SAR) report.

In terms of binding affinity, the benzamide side chain showed favorable tolerance. The influence of electron-withdrawing and electron-donating groups on the binding activity did not demonstrate a notable difference; both could maintain or improve the binding affinity. When the 2'-position of the benzamide side chain was substituted, most of the derivatives exhibited better

affinity, which was basically stronger than the 3’ or 4’-position substituted compounds. A direct comparison between the 3’ and 4’-position substituted derivatives showed no obvious difference in binding affinity. Moreover, when an electron-donating substituent, such as a methyl group, was introduced to the 4’-position of the benzene sulfonamide side chain, binding affinity increased significantly. Further modification on the benzene sulfonamide structure is needed.

In terms of the Matrigel invasion test, the benzamide scaffold was still tolerated. Both electron-withdrawing and electron-donating groups enhanced the inhibitory potency. When the 2’-position was substituted with methyl, methoxyl or chlorine groups, these corresponding compounds displayed the most potent activity, better than 3’ or 4’-position modified compounds. In contrast, when substituted with fluorine, the 3’ and 4’-position substituted compounds demonstrated a greater effect. In the *in vivo* anti-inflammatory evaluation, when the 4’-position of benzamide side chain was substituted, the melting point increased significantly, especially with strong electron-withdrawing groups. These changes decreased the solubility of the target compounds and may also impact the bioavailability. Although compound **IIj** (4’-position substituted with fluorine) showed the strongest anti-inflammatory activity, its solubility was not favourable. Taking **IIj** as the lead compound, introducing groups containing nitrogen atoms to the benzene sulfonamide structure will be an advisable strategy for further optimization. The obtained compounds could be converted into salts to address solubility issues. Results from this study very exquisitely show how another hit-to-lead discovery approach, virtual high throughput screening, could be complemented with SAR studies for the characterization and optimization of a novel class of CXCR4 modulators. It made the most sense to use vHTS given the flexibility of the receptor as well as *a priori* data about desired pharmacophores.

Upon discovering a promising hit or lead compound, characterization of the compound’s mechanism of action, both *in vitro* and *in vivo*, becomes the next major hurdle. While screening

approaches such as *in silico* drug design and vHTS might offer preliminary mechanistic information, there needs to be a much more extensive study which demonstrates how the compound is eliciting its therapeutic (and sometimes toxic) effects. The work summarized in this entire work focuses on three major targets: aromatase, CXCR4 and histone deacetylases (HDACs). Signaling pathways involved in endogenous and pharmacological signaling with respect to the first two targets are already well documented; however, very little is known with respect to how HDAC inhibitors (HDACi's) actually exert their function. Emerging data suggests that the currently used HDACi's may differ significantly with regard to target selectivity. As masters of gene regulation, HDACs prove to be crucial to all aspects of cell growth and differentiation. Thus, HDAC inhibitors are expected to have several downstream targets which have an overall global impact on cellular homeostasis. However, a better understanding of the particular HDAC isoforms inhibited by HDACi's as well as downstream effectors that contribute to oncogenic development might potentially give rise to more personalized therapies.

Our research group is highly interested in triple negative breast cancer (TNBC) tumorigenesis and recently, we showed that downregulation of tumor suppressor microRNA-206 drives invasion and angiogenesis in TNBC (155). Given that TNBCs lack expression of certain receptor types (i.e. estrogen receptor, progesterone receptor, and Her2/neu receptor), there are limited therapies that exist to treat this type of cancer due to the fact that it remains poorly understood. One recent finding was that a particular HDAC isoform, HDAC9, was aberrantly expressed in several cancer subtypes (144-147). Thus, as a starting point in this study, we decided to panel several TNBC and non-TNBC cell lines and assess if there were any significant differences in HDAC expression among the HDAC isoforms. Interestingly, we observed that HDAC9 was significantly upregulated in TNBC's when compared to non-TNBC's. Furthermore, we showed a direct, inverse correlation between HDAC9 and tumor suppressor miR-206

expression. Finally, we showed that in tissue samples, HDAC9 expression was significantly greater than non-TNBC tissue samples via immunohistochemistry staining. Thus, this provided the preliminary rationale that HDAC9 might be promoting the invasiveness of TNBC tumors.

Next, we showed via an invasion assay that introduction of either a selective class II HDACi (TMP269) or HDAC9 siRNA both significantly reduced tumor invasiveness. Moreover, in a Matrigel plug *in vivo* angiogenesis assay, we demonstrated that both TMP269 and HDAC9 siRNA significantly reduced average hemoglobin content within the Matrigel plug, which is a readout of angiogenesis *in vivo*. Finally, through Western blot analysis, we showed that at the protein level, HDAC9 siRNA exposure to TNBC cells caused a restoration of miR-206, along with a downregulation of VEGF and MAPK3, markers of angiogenesis and proliferation, respectively. Collectively, through these studies, we were able to identify a distinct, novel mechanism of action through which HDACi's are able to exert their function; namely, through the inhibition of HDAC9, which in turn, will restore expression of tumor suppressor miR-206. This study highlights a more specific mechanism that may be manipulated which might help in the design of safer, more personalized therapies. Studies like these are instrumental in providing rationale for any drug discovery project because not only is efficacy demonstrated, but distinct pathways are elucidated in both *in vitro* and *in vivo* models.

It is only after appropriate stringent pharmacological and toxicological testing in selected cellular and organismal models where the test compound may then progress into human clinical trials. One of the biggest focuses of our research group is in epigenetic inhibitors for cancer, particularly in breast cancer and glioblastoma (GBM). Currently, we are conducting a Phase II clinical trial where we are assessing another HDACi, belinostat, in combination with standard of care, on the improvement and quality-of-life of GBM patients. Our group is currently developing a novel, state-of-the-art imaging technique, spectroscopic MRI imaging (sMRI), which we intend

to use as a visual means for assessing patient response to our novel therapy (178). Phase I clinical trials are the first type of human trials where the maximum tolerable dose is determined for progression into Phase II clinical trials. Phase I clinical trials do not measure efficacy; thus, a much smaller number of patients are needed to assess toxicity. We utilized a 3+3 approach, in which we first administered belinostat at a dose of 750 mg/m^2 to three patients and monitored patient response. Unfortunately, two out of the three patients experienced severe thrombocytopenia, and as a result, we de-escalated the dose down to 500 mg/m^2 where no patients experienced toxicity. Thus, 500 mg/m^2 belinostat was determined as the maximal tolerated dose for progression into Phase II clinical trials.

In this ongoing clinical trial Phase, we currently have about 30 patients who are either receiving placebo + standard of care, or 500 mg/m^2 belinostat + standard of care. Patients are also receiving sMRI scans after selected intervals to visualize metabolically active tumors. Additionally, patients are asked to fill out quality-of-life surveys, which include depression surveys (IDS-SR) and neurocognitive assessments (HVLT-R). Our overall goal is to link changes in patient response to changes in patient quality-of-life. Unfortunately, given the high comorbidity of depression in GBM patients, we suspect that by reducing tumor inflammation via belinostat, this might help restore the patient's mood and cognition. Currently, our clinical studies are demonstrating the potential for belinostat to act as a potent antidepressant as well as a tumoricidal agent. Not only did belinostat administration reduce tumor burden, it also acted as a mood enhancer in a rat glioma model. In the clinical setting, the belinostat arm showed a trend for higher survival compared to the control group. While the trend approached statistical significance, a larger sample size is needed to conclusively determine if belinostat indeed extends progression free survival. Furthermore, our state-of-the-art sMRI technology was successful in identifying tumor progression versus pseudoprogression, highlighting its utility as a noninvasive imaging means not

requiring injection of contrast agents. Lastly, a preliminary comparison of IDS-SR depression survey scores between control and belinostat-treated patients revealed that belinostat-treated patients show a statistically significant improvement in depressive symptoms throughout the course of treatment. Collectively, these clinical trial studies provide an excellent foundation for the basis of clinical design and specifically in providing a balance for stringent therapy versus quality-of-life.

6.2. Conclusion

In summary, this work as a whole very intricately describes the challenging yet rewarding process of drug discovery, which involves: target discovery, hit discovery, hit-to-lead optimization, mechanistic and toxicological preclinical testing, and finally, human clinical trials. It is apparent that given what is known about a target and/or existing leads, no drug discovery project will ever follow the same process. If there is a strong rationale for a particular chemical scaffold, as was the case for the aromatase inhibitor project, then that may drive that discovery project in one way; however, if certain pharmacophores and a relatively flexible structure could be tolerated in potentially different orientations then a high throughput screening approach might be better, as was the case for the CXCR4 modulator project. Rigorous and extensive testing in both preclinical and clinical testing ensure that a successful therapeutic reaches the population with minimized toxicity and proven efficacy. Additionally, the PhD candidate responsible for this dissertation has received additional training in clinical and translational research offered at Emory University via a certificate program. These interdisciplinary projects, in addition to the certificate training, provide a broad, comprehensive overview of the drug development industry and adequately prepares the student for a career as a drug development researcher.

References

1. Henning S. The Evolution of Drug Discovery: From Traditional Medicines to Modern Drugs. By Enrique Raviña. ChemMedChem. 2011;6(9):1746-7. doi: doi:10.1002/cmdc.201100321.

2. Seneca. CHAPTER 1 - Definition, Typology and Occurrence of Alkaloids. In: Aniszewski T, editor. Alkaloids - Secrets of Life. Amsterdam: Elsevier; 2007. p. 1-59.

3. Brown AC, Fraser TR. On the Connection between Chemical Constitution and Physiological Action; with special reference to the Physiological Action of the Salts of the Ammonium Bases derived from Strychnia, Brucia, Thebaia, Codeia, Morphia, and Nicotia. Journal of Anatomy and Physiology. 1868;2(2):224-42. PubMed PMID: 17230757; PMCID: PMC1318606.

4. Newman DJ, Cragg GM. Natural Products as Sources of New Drugs from 1981 to 2014. Journal of Natural Products. 2016;79(3):629-61. doi: 10.1021/acs.jnatprod.5b01055.

5. DiMasi JA, Grabowski HG, Hansen RW. Innovation in the pharmaceutical industry: New estimates of R&D costs. Journal of Health Economics. 2016;47:20-33. doi: https://doi.org/10.1016/j.jhealeco.2016.01.012.

6. K P. Drug Discovery and Development - Present and Future. Croatia: Intech; 2011.

7. Pereira DA, Williams JA. Origin and evolution of high throughput screening. British Journal of Pharmacology. 2007;152(1):53-61. doi: 10.1038/sj.bjp.0707373. PubMed PMID: PMC1978279.

8. International Human Genome Sequencing C. Finishing the euchromatic sequence of the human genome. Nature. 2004;431:931. doi: 10.1038/nature03001 https://www.nature.com/articles/nature03001#supplementary-information.

9. Hughes JP, Rees S, Kalindjian SB, Philpott KL. Principles of early drug discovery. British Journal of Pharmacology. 2010;162(6):1239-49. doi: 10.1111/j.1476-5381.2010.01127.x.

10. Penrod NM, Cowper-Sal_lari R, Moore JH. Systems genetics for drug target discovery. Trends in pharmacological sciences. 2011;32(10):623-30. doi: 10.1016/j.tips.2011.07.002. PubMed PMID: PMC3185183.

11. Hopkins AL, Groom CR. The druggable genome. Nature Reviews Drug Discovery. 2002;1:727. doi: 10.1038/nrd892 https://www.nature.com/articles/nrd892#supplementary-information.

12. Butcher SP. Target discovery and validation in the post-genomic era. Neurochem Res. 2003;28(2):367-71. Epub 2003/03/01. PubMed PMID: 12608710.

13. Yang Y, Adelstein SJ, Kassis AI. Target discovery from data mining approaches. Drug Discovery Today. 2009;14(3):147-54. doi: https://doi.org/10.1016/j.drudis.2008.12.005.

14. Yuan C, Hu J, Parathath S, Grauer L, Cassella CB, Bagdasarov S, Goldberg IJ, Ramasamy R, Fisher EA. Human Aldose Reductase Expression Prevents Atherosclerosis Regression in Diabetic Mice. Diabetes. 2018. Epub 2018/06/13. doi: 10.2337/db18-0156. PubMed PMID: 29891593.

15. Gashaw I, Ellinghaus P, Sommer A, Asadullah K. What makes a good drug target? Drug Discovery Today. 2011;16(23):1037-43. doi: https://doi.org/10.1016/j.drudis.2011.09.007.

16. Mittal R, Jhaveri VM, Kay SS, Blackwelder P, Patel K. Pseudomonas aeruginosa invades human aortic endothelial cells and induces cell damage in vitro. Cardiovasc Hematol Disord Drug Targets. 2018. Epub 2018/06/12. doi: 10.2174/1871529X18666180611094928. PubMed PMID: 29886837.

17. Cassidy WM, Reynolds TB. Serum lactic dehydrogenase in the differential diagnosis of acute hepatocellular injury. J Clin Gastroenterol. 1994;19(2):118-21. Epub 1994/09/01. PubMed PMID: 7963356.

18. Wang B, Li J, Wang S, Hao Y, Zhao X, Chen J. Lactobacillus plantarum ameliorates tumour necrosis factor-induced bacterial translocation in Caco-2 cells by regulation of TLR4 expression. J Med Microbiol. 2018. Epub 2018/06/08. doi: 10.1099/jmm.0.000762. PubMed PMID: 29877788.

19. Whiting D, Chung WO, Johnson JD, Paranjpe A. Characterization of the Cellular Responses of Dental Mesenchymal Stem Cells to the Immune System. J Endod. 2018. Epub 2018/06/10. doi: 10.1016/j.joen.2018.03.018. PubMed PMID: 29884336.

20. Szymański P, Markowicz M, Mikiciuk-Olasik E. Adaptation of High-Throughput Screening in Drug Discovery—Toxicological Screening Tests. International Journal of Molecular Sciences. 2012;13(1):427-52. doi: 10.3390/ijms13010427. PubMed PMID: PMC3269696.

21. Broach JRT, J. High-throughput screening for drug discovery. Nature. 1996;384(6604 SUPPL.):14-6.

22. Dandapani S, Rosse G, Southall N, Salvino JM, Thomas CJ. Selecting, Acquiring, and Using Small Molecule Libraries for High-Throughput Screening. Current protocols in chemical biology. 2012;4:177-91. doi: 10.1002/9780470559277.ch110252. PubMed PMID: PMC4687755.

23. Brasier ART, J.E.; Habener, J.F. Optimized use of the firefly luciferase assay as a reporter gene in mammalian cell lines. BioTechniques. 1989;7(10):1116-22.

24. Kain SRA, M.; Kondepudi, A.; Yang, T.T.; Ward, W.W.; Kitts, P. Green fluorescent protein as a reporter of gene expression and protein localization. Biotechniques. 1995;19(4):650-5.

25. Lionta E, Spyrou G, Vassilatis DK, Cournia Z. Structure-Based Virtual Screening for Drug Discovery: Principles, Applications and Recent Advances. Current Topics in Medicinal Chemistry. 2014;14(16):1923-38. doi: 10.2174/1568026614666140929124445. PubMed PMID: PMC4443793.

26. Jorgensen WL. The many roles of computation in drug discovery. Science. 2004;303(5665):1813-8.

27. Benod C, Carlsson J, Uthayaruban R, Hwang P, Irwin JJ, Doak AK, Shoichet BK, Sablin EP, Fletterick RJ. Structure-based Discovery of Antagonists of Nuclear Receptor LRH-1. The Journal of Biological Chemistry. 2013;288(27):19830-44. doi: 10.1074/jbc.M112.411686. PubMed PMID: PMC3707686.

28. Sastry GMA, M.; Day, T.; Annabhimoju, R.; Sherman, W. Protein and ligand preparation: parameters, protocols, and influence on virtual screening enrichments. Journal of Computer-Aided Molecular Design. 2013;27(3):221-34.

29. Athanasiadis EC, Z.; Spyrou, G. ChemBioServer: a web-based pipeline for filtering, clutering and visualization of chemical compounds used in drug discovery. Bioinformatics. 2012;28(22):3002-3.

30. Sadowski J, Rudolph C, Gasteiger J. The generation of 3D models of host-guest complexes. Analytica Chimica Acta. 1992;265(2):233-41. doi: https://doi.org/10.1016/0003-2670(92)85029-6.

31. Kalliokoski T, Salo HS, Lahtela-Kakkonen M, Poso A. The Effect of Ligand-Based Tautomer and Protomer Prediction on Structure-Based Virtual Screening. Journal of Chemical Information and Modeling. 2009;49(12):2742-8. doi: 10.1021/ci900364w.

32. Friesner RA, Banks JL, Murphy RB, Halgren TA, Klicic JJ, Mainz DT, Repasky MP, Knoll EH, Shelley M, Perry JK, Shaw DE, Francis P, Shenkin PS. Glide: A New Approach for Rapid,

Accurate Docking and Scoring. 1. Method and Assessment of Docking Accuracy. Journal of Medicinal Chemistry. 2004;47(7):1739-49. doi: 10.1021/jm0306430.

33. Venkatachalam CM, Jiang X, Oldfield T, Waldman M. LigandFit: a novel method for the shape-directed rapid docking of ligands to protein active sites. Journal of Molecular Graphics and Modelling. 2003;21(4):289-307. doi: https://doi.org/10.1016/S1093-3263(02)00164-X.

34. Cheng T, Li Q, Zhou Z, Wang Y, Bryant SH. Structure-Based Virtual Screening for Drug Discovery: a Problem-Centric Review. The AAPS Journal. 2012;14(1):133-41. doi: 10.1208/s12248-012-9322-0. PubMed PMID: PMC3282008.

35. Lavecchia A.; Di Giovanni C. Virtual Screening Strategies in Drug Discovery: A Critical Review. Current Medicinal Chemistry. 2013;20(23):2839-60.

36. Ravindranathan K, Tirado-Rives J, Jorgensen WL, Guimarães CRW. Improving MM-GB/SA Scoring through the Application of the Variable Dielectric Model. Journal of chemical theory and computation. 2011;7(12):3859-65. doi: 10.1021/ct200565u. PubMed PMID: PMC3351111.

37. Benet LZ, Hosey CM, Ursu O, Oprea TI. BDDCS, the Rule of 5 and Drugability. Advanced drug delivery reviews. 2016;101:89-98. doi: 10.1016/j.addr.2016.05.007. PubMed PMID: PMC4910824.

38. Hann MM, Oprea TI. Pursuing the leadlikeness concept in pharmaceutical research. Current Opinion in Chemical Biology. 2004;8(3):255-63. doi: https://doi.org/10.1016/j.cbpa.2004.04.003.

39. Keserű GM, Makara GM. Hit discovery and hit-to-lead approaches. Drug Discovery Today. 2006;11(15):741-8. doi: https://doi.org/10.1016/j.drudis.2006.06.016.

40. Hamada Y, Kiso Y. The application of bioisosteres in drug design for novel drug discovery: focusing on acid protease inhibitors. Expert Opinion on Drug Discovery. 2012;7(10):903-22. doi: 10.1517/17460441.2012.712513.

41. Swinney DC, Anthony J. How were new medicines discovered? Nature Reviews Drug Discovery. 2011;10:507. doi: 10.1038/nrd3480 https://www.nature.com/articles/nrd3480#supplementary-information.

42. Gaines T, Camp D, Bai R, Liang Z, Yoon Y, Shim H, Mooring SR. Synthesis and evaluation of 2,5 and 2,6 pyridine-based CXCR4 inhibitors. Bioorganic & Medicinal Chemistry. 2016;24(21):5052-60. doi: https://doi.org/10.1016/j.bmc.2016.08.018.

43. Nogueira RC, Oliveira-Costa JF, de Sá MS, dos Santos RR, Soares MBP. Early toxicity screening and selection of lead compounds for parasitic diseases. Current Drug Targets. 2009;10(3):291-8. doi: 10.2174/138945009787581212.

44. Doshi U, Li AP. Luciferin IPA–Based Higher Throughput Human Hepatocyte Screening Assays for CYP3A4 Inhibition and Induction. Journal of Biomolecular Screening. 2011;16(8):903-9. doi: 10.1177/1087057111414900.

45. Festing S, Wilkinson R. The ethics of animal research. Talking Point on the use of animals in scientific research. EMBO Reports. 2007;8(6):526-30. doi: 10.1038/sj.embor.7400993. PubMed PMID: PMC2002542.

46. Hefti FF. Requirements for a lead compound to become a clinical candidate. BMC Neuroscience. 2008;9(Suppl 3):S7-S. doi: 10.1186/1471-2202-9-S3-S7. PubMed PMID: PMC2604885.

47. Rashid OM, Takabe K. Animal models for exploring the pharmacokinetics of breast cancer therapies. Expert opinion on drug metabolism & toxicology. 2015;11(2):221-30. doi: 10.1517/17425255.2015.983073. PubMed PMID: PMC4583421.

48. Hutchinson JN, Muller WJ. Transgenic mouse models of human breast cancer. Oncogene. 2000;19:6130. doi: 10.1038/sj.onc.1203970.

49. Stewart TA, Pattengale PK, Leder P. Spontaneous mammary adenocarcinomas in transgenic mice that carry and express MTV/myc fusion genes. Cell. 1984;38(3):627-37. doi: 10.1016/0092-8674(84)90257-5.

50. Richmond A, Su Y. Mouse xenograft models vs GEM models for human cancer therapeutics. Disease Models & Mechanisms. 2008;1(2-3):78-82. doi: 10.1242/dmm.000976. PubMed PMID: PMC2562196.

51. Antonello ZA, Nucera C. Orthotopic mouse models for the preclinical and translational study of targeted therapies against metastatic human thyroid carcinoma with BRAF(V600E) or wild-type BRAF. Oncogene. 2014;33(47):5397-404. doi: 10.1038/onc.2013.544. PubMed PMID: PMC4524291.

52. Holbein MEB. Understanding FDA Regulatory Requirements for Investigational New Drug Applications for Sponsor-Investigators. Journal of investigative medicine : the official publication of the American Federation for Clinical Research. 2009;57(6):688-94. doi: 10.231/JIM.0b013e3181afdb26. PubMed PMID: PMC4435682.

53. Le Tourneau C, Lee JJ, Siu LL. Dose Escalation Methods in Phase I Cancer Clinical Trials. JNCI Journal of the National Cancer Institute. 2009;101(10):708-20. doi: 10.1093/jnci/djp079. PubMed PMID: PMC2684552.

54. Woodcock VK, Clive S, Wilson RH, Coyle VM, Stratford MRL, Folkes LK, Eastell R, Barton C, Jones P, Kazmi-Stokes S, Turner H, Halford S, Harris AL, Middleton MR. A first-in-human phase I study to determine the maximum tolerated dose of the oral Src/ABL inhibitor AZD0424. British Journal Of Cancer. 2018;118:770. doi: 10.1038/bjc.2017.484 https://www.nature.com/articles/bjc2017484#supplementary-information.

55. Simon R. Optimal two-stage designs for phase II clinical trials. Contemporary Clinical Trials. 1989;10(1):1-10.

56. Sedgwick P. What are the four phases of clinical research trials? BMJ : British Medical Journal. 2014;348. doi: 10.1136/bmj.g3727.

57. Umscheid CA, Margolis DJ, Grossman CE. Key Concepts of Clinical Trials: A Narrative Review. Postgraduate Medicine. 2011;123(5):194-204. doi: 10.3810/pgm.2011.09.2475. PubMed PMID: PMC3272827.

58. Eypasch E, Lefering R, Kum CK, Troidl H. Probability of adverse events that have not yet occurred: a statistical reminder. BMJ : British Medical Journal. 1995;311(7005):619-20. PubMed PMID: PMC2550668.

59. Comparative Efficacy Trials (Phase III Studies). Encyclopedia of Quantitative Risk Analysis and Assessment.

60. Lesaffre E. Superiority, equivalence, and non-inferiority trials. Bulletin of the NYU hospital for joint diseases. 2008;66(2):150-4. Epub 2008/06/10. PubMed PMID: 18537788.

61. Suresh KP. An overview of randomization techniques: An unbiased assessment of outcome in clinical research. Journal of Human Reproductive Sciences. 2011;4(1):8-11. doi: 10.4103/0974-1208.82352. PubMed PMID: PMC3136079.

62. Kernan WN, Viscoli CM, Makuch RW, Brass LM, Horwitz RI. Stratified Randomization for Clinical Trials. Journal of Clinical Epidemiology. 1999;52(1):19-26. doi: https://doi.org/10.1016/S0895-4356(98)00138-3.

63. Day SJ, Altman DG. Blinding in clinical trials and other studies. BMJ. 2000;321(7259):504. doi: 10.1136/bmj.321.7259.504.

64. Van Norman GA. Drugs, Devices, and the FDA: Part 1: An Overview of Approval Processes for Drugs. JACC: Basic to Translational Science. 2016;1(3):170-9. doi: https://doi.org/10.1016/j.jacbts.2016.03.002.

65. Howlader NAK, M.; Neyman, N.; Aminou, R.; Waldron, W.; Altekruse, S.F.; Kosary, C.L.; Ruhl, J.; Tatalovich, Z.; Cho, H.; Mariotto, A.; Eisner, M.P.; Lewis, D.R.; Chen, H.S.; Feuer, E.J.; Cronin, K.A. . SEER Cancer Statistics Review, 1975-20092012.

66. Chumsri S, Brodie A. Aromatase inhibitors and breast cancer. Hormone molecular biology and clinical investigation. 2012;9(2):119-26. Epub 2012/04/01. doi: 10.1515/hmbci-2012-0001. PubMed PMID: 25436703.

67. Nichols HB, DeRoo LA, Scharf DR, Sandler DP. Risk-benefit profiles of women using tamoxifen for chemoprevention. Journal of the National Cancer Institute. 2015;107(1):354. Epub 2014/12/06. doi: 10.1093/jnci/dju354. PubMed PMID: 25475563; PMCID: PMC4296193.

68. Ma X, Liu Y, Wang Q, Chen Y, Liu M, Li X, Xiang R, Wei Y, Duan Y, Han J. Tamoxifen induces the development of hernia in mice by activating MMP-2 and MMP-13 expression. Biochimica et biophysica acta. 2015;1852(5):1038-48. Epub 2015/02/24. doi: 10.1016/j.bbadis.2015.02.006. PubMed PMID: 25703139.

69. Kim Y, Kim OJ, Kim J. Cerebral venous thrombosis in a breast cancer patient taking tamoxifen: Report of a case. International journal of surgery case reports. 2015;6c:77-80. Epub 2014/12/22. doi: 10.1016/j.ijscr.2014.11.068. PubMed PMID: 25528030; PMCID: PMC4334637.

70. Gunaldi M, Erkisi M, Afsar CU, Ercolak V, Paydas S, Kara IO, Sahin B, Gulec UK, Secilmis A. Evaluation of endometrial thickness and bone mineral density based on CYP2D6 polymorphisms in Turkish breast cancer patients receiving tamoxifen treatment. Pharmacology. 2014;94(3-4):183-9. Epub 2014/11/08. doi: 10.1159/000363304. PubMed PMID: 25378122.

71. Sohl CD, Guengerich FP. Kinetic analysis of the three-step steroid aromatase reaction of human cytochrome P450 19A1. J Biol Chem. 2010;285(23):17734-43. Epub 2010/04/14. doi: 10.1074/jbc.M110.123711. PubMed PMID: 20385561; PMCID: PMC2878537.

72. Goss PE, Strasser K. Aromatase inhibitors in the treatment and prevention of breast cancer. Journal of Clinical Oncology. 2001;19(3):881-94.

73. Jeong S, Woo MM, Flockhart DA, Desta Z. Inhibition of drug metabolizing cytochrome P450s by the aromatase inhibitor drug letrozole and its major oxidative metabolite 4,4'-methanol-bisbenzonitrile in vitro. Cancer chemotherapy and pharmacology. 2009;64(5):867-75. Epub 2009/02/10. doi: 10.1007/s00280-009-0935-7. PubMed PMID: 19198839; PMCID: PMC2774495.

74. Ariazi EA, Leitao A, Oprea TI, Chen B, Louis T, Bertucci AM, Sharma CG, Gill SD, Kim HR, Shupp HA, Pyle JR, Madrack A, Donato AL, Cheng D, Paige JR, Jordan VC. Exemestane's 17-hydroxylated metabolite exerts biological effects as an androgen. Molecular cancer therapeutics. 2007;6(11):2817-27. Epub 2007/11/09. doi: 10.1158/1535-7163.Mct-07-0312. PubMed PMID: 17989318.

75. Grimm SW, Dyroff MC. Inhibition of human drug metabolizing cytochromes P450 by anastrozole, a potent and selective inhibitor of aromatase. Drug metabolism and disposition: the biological fate of chemicals. 1997;25(5):598-602. Epub 1997/05/01. PubMed PMID: 9152599.

76. CYP2C9 CC, CYP2D6 CA. The effect of cytochrome P450 metabolism on drug response, interactions, and adverse effects. Am Fam Physician. 2007;76:391-6.

77. Gaillard S, Stearns V. Aromatase inhibitor-associated bone and musculoskeletal effects: new evidence defining etiology and strategies for management. Breast cancer research : BCR. 2011;13(2):205. Epub 2011/04/05. doi: 10.1186/bcr2818. PubMed PMID: 21457526; PMCID: PMC3219175.

78. Eastell R, Adams JE, Coleman RE, Howell A, Hannon RA, Cuzick J, Mackey JR, Beckmann MW, Clack G. Effect of anastrozole on bone mineral density: 5-year results from the anastrozole, tamoxifen, alone or in combination trial 18233230. Journal of clinical oncology : official journal of the American Society of Clinical Oncology. 2008;26(7):1051-7. Epub 2008/03/04. doi: 10.1200/jco.2007.11.0726. PubMed PMID: 18309940.

79. Perez EA, Josse RG, Pritchard KI, Ingle JN, Martino S, Findlay BP, Shenkier TN, Tozer RG, Palmer MJ, Shepherd LE, Liu S, Tu D, Goss PE. Effect of letrozole versus placebo on bone mineral density in women with primary breast cancer completing 5 or more years of adjuvant tamoxifen: a companion study to NCIC CTG MA.17. Journal of clinical oncology : official journal of the American Society of Clinical Oncology. 2006;24(22):3629-35. Epub 2006/07/11. doi: 10.1200/jco.2005.05.4882. PubMed PMID: 16822845.

80. Yue W, Wang JP, Hamilton CJ, Demers LM, Santen RJ. In situ aromatization enhances breast tumor estradiol levels and cellular proliferation. Cancer research. 1998;58(5):927-32. Epub 1998/03/21. PubMed PMID: 9500452.

81. Partridge AH, LaFountain A, Mayer E, Taylor BS, Winer E, Asnis-Alibozek A. Adherence to initial adjuvant anastrozole therapy among women with early-stage breast cancer. Journal of clinical oncology : official journal of the American Society of Clinical Oncology. 2008;26(4):556-62. Epub 2008/01/09. doi: 10.1200/jco.2007.11.5451. PubMed PMID: 18180462.

82. Geisler J, Helle H, Ekse D, Duong NK, Evans DB, Nordbo Y, Aas T, Lonning PE. Letrozole is superior to anastrozole in suppressing breast cancer tissue and plasma estrogen levels. Clinical cancer research : an official journal of the American Association for Cancer Research. 2008;14(19):6330-5. Epub 2008/10/03. doi: 10.1158/1078-0432.Ccr-07-5221. PubMed PMID: 18829517.

83. Bajetta E, Zilembo N, Noberasco C, Martinetti A, Mariani L, Ferrari L, Buzzoni R, Greco M, Bartoli C, Spagnoli I, Danesini GM, Artale S, Paolini J. The minimal effective exemestane dose for endocrine activity in advanced breast cancer. European journal of cancer (Oxford, England : 1990). 1997;33(4):587-91. Epub 1997/04/01. PubMed PMID: 9274439.

84. Bisagni G, Cocconi G, Scaglione F, Fraschini F, Pfister C, Trunet PF. Letrozole, a new oral non-steroidal aromastase inhibitor in treating postmenopausal patients with advanced breast cancer. A pilot study. Annals of oncology : official journal of the European Society for Medical Oncology. 1996;7(1):99-102. Epub 1996/01/01. PubMed PMID: 9081401.

85. Evans TR, Di Salle E, Ornati G, Lassus M, Benedetti MS, Pianezzola E, Coombes RC. Phase I and endocrine study of exemestane (FCE 24304), a new aromatase inhibitor, in postmenopausal women. Cancer research. 1992;52(21):5933-9. Epub 1992/11/01. PubMed PMID: 1394219.

86. Goss PE, Qi S, Cheung AM, Hu H, Mendes M, Pritzker KP. Effects of the steroidal aromatase inhibitor exemestane and the nonsteroidal aromatase inhibitor letrozole on bone and lipid metabolism in ovariectomized rats. Clinical cancer research : an official journal of the American Association for Cancer Research. 2004;10(17):5717-23. Epub 2004/09/10. doi: 10.1158/1078-0432.Ccr-04-0438. PubMed PMID: 15355898.

87. Ghosh D, Griswold J, Erman M, Pangborn W. Structural basis for androgen specificity and oestrogen synthesis in human aromatase. Nature. 2009;457(7226):219-23. Epub 2009/01/09. doi: 10.1038/nature07614. PubMed PMID: 19129847; PMCID: PMC2820300.

88. Lombardi P. Exemestane, a new steroidal aromatase inhibitor of clinical relevance. Biochimica et biophysica acta. 2002;1587(2-3):326-37. Epub 2002/06/27. PubMed PMID: 12084475.

89. Morton D, Dick AR, Ghosh D, Davies HM. Convenient method for the functionalization of the 4- and 6-positions of the androgen skeleton. Chemical communications (Cambridge, England). 2012;48(47):5838-40. Epub 2012/05/11. doi: 10.1039/c2cc31973j. PubMed PMID: 22572866; PMCID: PMC3357189.

90. Ghosh D, Lo J, Morton D, Valette D, Xi J, Griswold J, Hubbell S, Egbuta C, Jiang W, An J, Davies HM. Novel aromatase inhibitors by structure-guided design. J Med Chem. 2012;55(19):8464-76. Epub 2012/09/07. doi: 10.1021/jm300930n. PubMed PMID: 22951074; PMCID: PMC3469775.

91. Long BJ, Tilghman SL, Yue W, Thiantanawat A, Grigoryev DN, Brodie AM. The steroidal antiestrogen ICI 182,780 is an inhibitor of cellular aromatase activity. The Journal of steroid biochemistry and molecular biology. 1998;67(4):293-304. Epub 1999/01/12. PubMed PMID: 9883986.

92. Haynes BP, Dowsett M, Miller WR, Dixon JM, Bhatnagar AS. The pharmacology of letrozole. The Journal of steroid biochemistry and molecular biology. 2003;87(1):35-45. doi: https://doi.org/10.1016/S0960-0760(03)00384-4.

93. Bhatnagar AS. The discovery and mechanism of action of letrozole. Breast Cancer Research and Treatment. 2007;105(Suppl 1):7-17. doi: 10.1007/s10549-007-9696-3. PubMed PMID: PMC2001216.

94. Ettinger B, Pressman A, Sklarin P, Bauer DC, Cauley JA, Cummings SR. Associations between low levels of serum estradiol, bone density, and fractures among elderly women: the study of osteoporotic fractures. The Journal of clinical endocrinology and metabolism. 1998;83(7):2239-43. Epub 1998/07/14. doi: 10.1210/jcem.83.7.4708. PubMed PMID: 9661589.

95. Vaananen HK, Harkonen PL. Estrogen and bone metabolism. Maturitas. 1996;23 Suppl:S65-9. Epub 1996/05/01. PubMed PMID: 8865143.

96. Felson DT, Zhang Y, Hannan MT, Kiel DP, Wilson P, Anderson JJ. The Effect of Postmenopausal Estrogen Therapy on Bone Density in Elderly Women. New England Journal of Medicine. 1993;329(16):1141-6. doi: 10.1056/NEJM199310143291601.

97. Tang ML, Zhong C, Liu ZY, Peng P, Liu XH, Sun X. Discovery of novel sesquistilbene indanone analogues as potent anti-inflammatory agents. European journal of medicinal chemistry. 2016;113:63-74. Epub 2016/02/29. doi: 10.1016/j.ejmech.2016.02.021. PubMed PMID: 26922229.

98. Suthar SK, Sharma M. Recent developments in chimeric NSAIDs as safer anti-inflammatory agents. Medicinal research reviews. 2015;35(2):341-407. Epub 2014/10/17. doi: 10.1002/med.21331. PubMed PMID: 25319808.

99. Wallace JL. NSAID gastropathy and enteropathy: distinct pathogenesis likely necessitates distinct prevention strategies. Br J Pharmacol. 2012;165(1):67-74. Epub 2011/06/02. doi: 10.1111/j.1476-5381.2011.01509.x. PubMed PMID: 21627632; PMCID: PMC3252967.

100. Wallace JL, McKnight W, Reuter BK, Vergnolle N. NSAID-induced gastric damage in rats: requirement for inhibition of both cyclooxygenase 1 and 2. Gastroenterology. 2000;119(3):706-14. Epub 2000/09/13. PubMed PMID: 10982765.

101. Das D, Maeda K, Hayashi Y, Gavande N, Desai DV, Chang SB, Ghosh AK, Mitsuya H. Insights into the mechanism of inhibition of CXCR4: identification of Piperidinylethanamine analogs as anti-HIV-1 inhibitors. Antimicrobial agents and chemotherapy. 2015;59(4):1895-904. Epub 2015/01/15. doi: 10.1128/aac.04654-14. PubMed PMID: 25583709; PMCID: PMC4356787.

102. Gudmundsson KS, Sebahar PR, Richardson LD, Miller JF, Turner EM, Catalano JG, Spaltenstein A, Lawrence W, Thomson M, Jenkinson S. Amine substituted N-(1H-benzimidazol-2ylmethyl)-5,6,7,8-tetrahydro-8-quinolinamines as CXCR4 antagonists with potent activity

against HIV-1. Bioorganic & medicinal chemistry letters. 2009;19(17):5048-52. Epub 2009/07/31. doi: 10.1016/j.bmcl.2009.07.037. PubMed PMID: 19640718.

103. Zachariassen ZG, Thiele S, Berg EA, Rasmussen P, Fossen T, Rosenkilde MM, Vabeno J, Haug BE. Design, synthesis, and biological evaluation of scaffold-based tripeptidomimetic antagonists for CXC chemokine receptor 4 (CXCR4). Bioorg Med Chem. 2014;22(17):4759-69. Epub 2014/08/02. doi: 10.1016/j.bmc.2014.07.004. PubMed PMID: 25082513.

104. Hummel S, Van Aken H, Zarbock A. Inhibitors of CXC chemokine receptor type 4: putative therapeutic approaches in inflammatory diseases. Current opinion in hematology. 2014;21(1):29-36. Epub 2013/11/28. doi: 10.1097/moh.0000000000000002. PubMed PMID: 24275689.

105. Donzella GA, Schols D, Lin SW, Este JA, Nagashima KA, Maddon PJ, Allaway GP, Sakmar TP, Henson G, De Clercq E, Moore JP. AMD3100, a small molecule inhibitor of HIV-1 entry via the CXCR4 co-receptor. Nature medicine. 1998;4(1):72-7. Epub 1998/01/14. PubMed PMID: 9427609.

106. Lefrancois M, Lefebvre MR, Saint-Onge G, Boulais PE, Lamothe S, Leduc R, Lavigne P, Heveker N, Escher E. Agonists for the Chemokine Receptor CXCR4. ACS medicinal chemistry letters. 2011;2(8):597-602. Epub 2011/08/16. doi: 10.1021/ml200084n. PubMed PMID: 21841963; PMCID: PMC3155278.

107. Scozzafava A, Mastrolorenzo A, Supuran CT. Non-peptidic chemokine receptors antagonists as emerging anti-HIV agents. Journal of enzyme inhibition and medicinal chemistry. 2002;17(2):69-76. Epub 2002/11/08. doi: 10.1080/14756360290024227. PubMed PMID: 12420752.

108. Hendrix CW, Flexner C, MacFarland RT, Giandomenico C, Fuchs EJ, Redpath E, Bridger G, Henson GW. Pharmacokinetics and safety of AMD-3100, a novel antagonist of the CXCR-4

chemokine receptor, in human volunteers. Antimicrobial agents and chemotherapy. 2000;44(6):1667-73. Epub 2000/05/19. PubMed PMID: 10817726; PMCID: PMC89930.

109. Zhang H, Kang D, Huang B, Liu N, Zhao F, Zhan P, Liu X. Discovery of non-peptide small molecular CXCR4 antagonists as anti-HIV agents: Recent advances and future opportunities. European journal of medicinal chemistry. 2016;114:65-78. Epub 2016/03/15. doi: 10.1016/j.ejmech.2016.02.051. PubMed PMID: 26974376.

110. Liles WC, Rodger E, Broxmeyer HE, Dehner C, Badel K, Calandra G, Christensen J, Wood B, Price TH, Dale DC. Augmented mobilization and collection of CD34+ hematopoietic cells from normal human volunteers stimulated with granulocyte-colony-stimulating factor by single-dose administration of AMD3100, a CXCR4 antagonist. Transfusion. 2005;45(3):295-300. Epub 2005/03/09. doi: 10.1111/j.1537-2995.2005.04222.x. PubMed PMID: 15752146.

111. Hatse S, Princen K, Bridger G, De Clercq E, Schols D. Chemokine receptor inhibition by AMD3100 is strictly confined to CXCR4. FEBS letters. 2002;527(1-3):255-62. Epub 2002/09/11. PubMed PMID: 12220670.

112. Shu HK, Yoon Y, Hong S, Xu K, Gao H, Hao C, Torres-Gonzalez E, Nayra C, Rojas M, Shim H. Inhibition of the CXCL12/CXCR4-axis as preventive therapy for radiation-induced pulmonary fibrosis. PloS one. 2013;8(11):e79768. Epub 2013/11/19. doi: 10.1371/journal.pone.0079768. PubMed PMID: 24244561; PMCID: PMC3820649.

113. Liang Z, Zhan W, Zhu A, Yoon Y, Lin S, Sasaki M, Klapproth JM, Yang H, Grossniklaus HE, Xu J, Rojas M, Voll RJ, Goodman MM, Arrendale RF, Liu J, Yun CC, Snyder JP, Liotta DC, Shim H. Development of a unique small molecule modulator of CXCR4. PloS one. 2012;7(4):e34038. Epub 2012/04/10. doi: 10.1371/journal.pone.0034038. PubMed PMID: 22485156; PMCID: PMC3317778.

114. Zhan W, Liang Z, Zhu A, Kurtkaya S, Shim H, Snyder JP, Liotta DC. Discovery of small molecule CXCR4 antagonists. J Med Chem. 2007;50(23):5655-64. Epub 2007/10/26. doi: 10.1021/jm070679i. PubMed PMID: 17958344.

115. Zhu A, Zhan W, Liang Z, Yoon Y, Yang H, Grossniklaus HE, Xu J, Rojas M, Lockwood M, Snyder JP, Liotta DC, Shim H. Dipyrimidine amines: a novel class of chemokine receptor type 4 antagonists with high specificity. J Med Chem. 2010;53(24):8556-68. Epub 2010/11/26. doi: 10.1021/jm100786g. PubMed PMID: 21105715; PMCID: PMC3003753.

116. Mooring SR, Liu J, Liang Z, Ahn J, Hong S, Yoon Y, Snyder JP, Shim H. Benzenesulfonamides: a unique class of chemokine receptor type 4 inhibitors. ChemMedChem. 2013;8(4):622-32. Epub 2013/03/08. doi: 10.1002/cmdc.201200582. PubMed PMID: 23468189; PMCID: PMC3752296.

117. Bai R, Shi Q, Liang Z, Yoon Y, Han Y, Feng A, Liu S, Oum Y, Yun CC, Shim H. Development of CXCR4 modulators by virtual HTS of a novel amide-sulfamide compound library. European journal of medicinal chemistry. 2017;126:464-75. Epub 2016/12/04. doi: 10.1016/j.ejmech.2016.11.026. PubMed PMID: 27914361; PMCID: PMC5253094.

118. Lipinski CA, Lombardo F, Dominy BW, Feeney PJ. Experimental and computational approaches to estimate solubility and permeability in drug discovery and development settings. Adv Drug Deliv Rev. 2001;46(1-3):3-26. Epub 2001/03/22. PubMed PMID: 11259830.

119. Jorgensen WL. Efficient drug lead discovery and optimization. Accounts of chemical research. 2009;42(6):724-33. Epub 2009/03/26. doi: 10.1021/ar800236t. PubMed PMID: 19317443; PMCID: PMC2727934.

120. Morelli X, Bourgeas R, Roche P. Chemical and structural lessons from recent successes in protein-protein interaction inhibition (2P2I). Curr Opin Chem Biol. 2011;15(4):475-81. Epub 2011/06/21. doi: 10.1016/j.cbpa.2011.05.024. PubMed PMID: 21684802.

121. Bai R, Liang Z, Yoon Y, Liu S, Gaines T, Oum Y, Shi Q, Mooring SR, Shim H. Symmetrical bis-tertiary amines as novel CXCR4 inhibitors. European journal of medicinal chemistry. 2016;118:340-50. Epub 2016/05/15. doi: 10.1016/j.ejmech.2016.04.040. PubMed PMID: 27179215; PMCID: PMC4894032.

122. Lalrinzuali K, Vabeiryureilai M, Jagetia GC. Investigation of the Anti-Inflammatory and Analgesic Activities of Ethanol Extract of Stem Bark of Sonapatha Oroxylum indicum In Vivo. International journal of inflammation. 2016;2016:8247014. Epub 2016/03/01. doi: 10.1155/2016/8247014. PubMed PMID: 26925290; PMCID: PMC4746378.

123. Eddouks M, Chattopadhyay D, Zeggwagh NA. Animal models as tools to investigate antidiabetic and anti-inflammatory plants. Evidence-based complementary and alternative medicine : eCAM. 2012;2012:142087. Epub 2012/08/18. doi: 10.1155/2012/142087. PubMed PMID: 22899950; PMCID: PMC3414199.

124. Barbero S, Bonavia R, Bajetto A, Porcile C, Pirani P, Ravetti JL, Zona GL, Spaziante R, Florio T, Schettini G. Stromal cell-derived factor 1alpha stimulates human glioblastoma cell growth through the activation of both extracellular signal-regulated kinases 1/2 and Akt. Cancer research. 2003;63(8):1969-74. Epub 2003/04/19. PubMed PMID: 12702590.

125. Liang Z, Brooks J, Willard M, Liang K, Yoon Y, Kang S, Shim H. CXCR4/CXCL12 axis promotes VEGF-mediated tumor angiogenesis through Akt signaling pathway. Biochemical and biophysical research communications. 2007;359(3):716-22. Epub 2007/06/15. doi: 10.1016/j.bbrc.2007.05.182. PubMed PMID: 17559806; PMCID: PMC1986788.

126. Liang Z, Wu T, Lou H, Yu X, Taichman RS, Lau SK, Nie S, Umbreit J, Shim H. Inhibition of breast cancer metastasis by selective synthetic polypeptide against CXCR4. Cancer research. 2004;64(12):4302-8. Epub 2004/06/19. doi: 10.1158/0008-5472.Can-03-3958. PubMed PMID: 15205345.

127. Demetrius L. Of mice and men. When it comes to studying ageing and the means to slow it down, mice are not just small humans. EMBO Reports. 2005;6 Spec No:S39-44. Epub 2005/07/05. doi: 10.1038/sj.embor.7400422. PubMed PMID: 15995660; PMCID: PMC1369270.

128. Gregory PD, Wagner K, Hörz W. Histone Acetylation and Chromatin Remodeling. Experimental Cell Research. 2001;265(2):195-202. doi: https://doi.org/10.1006/excr.2001.5187.

129. Deckert J, Struhl K. Histone Acetylation at Promoters Is Differentially Affected by Specific Activators and Repressors. Molecular and Cellular Biology. 2001;21(8):2726-35. doi: 10.1128/mcb.21.8.2726-2735.2001.

130. Marks PA, Richon VM, Kelly WK, Chiao JH, Miller T, Pelicci. Histone deacetylase inhibitors: Development as cancer therapy. Novartis Foundation Symposium2004. p. 269-84.

131. Kelly WK, O'Connor OA, Marks PA. Histone deacetylase inhibitors: from target to clinical trials. Expert Opinion on Investigational Drugs. 2002;11(12):1695-713. doi: 10.1517/13543784.11.12.1695.

132. Arts J, de Schepper S, Van Emelen K. Histone deacetylase inhibitors: from chromatin remodeling to experimental cancer therapeutics. Curr Med Chem. 2003;10(22):2343-50. Epub 2003/10/08. PubMed PMID: 14529477.

133. Sengupta N, Seto E. Regulation of histone deacetylase activities. Journal of Cellular Biochemistry. 2004;93(1):57-67. doi: 10.1002/jcb.20179.

134. Dokmanovic M, Marks PA. Prospects: Histone deacetylase inhibitors. Journal of Cellular Biochemistry. 2005;96(2):293-304. doi: 10.1002/jcb.20532.

135. Phiel CJ, Zhang F, Huang EY, Guenther MG, Lazar MA, Klein PS. Histone Deacetylase Is a Direct Target of Valproic Acid, a Potent Anticonvulsant, Mood Stabilizer, and Teratogen. Journal of Biological Chemistry. 2001;276(39):36734-41.

136. Richon VM, Emiliani S, Verdin E, Webb Y, Breslow R, Rifkind RA, Marks PA. A class of hybrid polar inducers of transformed cell differentiation inhibits histone deacetylases. Proceedings of the National Academy of Sciences. 1998;95(6):3003.

137. Butler LM, Webb Y, Agus DB, Higgins B, Tolentino TR, Kutko MC, LaQuaglia MP, Drobnjak M, Cordon-Cardo C, Scher HI, Breslow R, Richon VM, Rifkind RA, Marks PA. Inhibition of transformed cell growth and induction of cellular differentiation by pyroxamide, an inhibitor of histone deacetylase. Clinical cancer research : an official journal of the American Association for Cancer Research. 2001;7(4):962-70. Epub 2001/04/20. PubMed PMID: 11309347.

138. Meinke PT, Colletti SL, Doss G, Myers RW, Gurnett AM, Dulski PM, Darkin-Rattray SJ, Allocco JJ, Galuska S, Schmatz DM, Wyvratt MJ, Fisher MH. Synthesis of Apicidin-Derived Quinolone Derivatives: Parasite-Selective Histone Deacetylase Inhibitors and Antiproliferative Agents. Journal of Medicinal Chemistry. 2000;43(25):4919-22. doi: 10.1021/jm0001976.

139. Chiu HW, Yeh YL, Wang YC, Huang WJ, Chen YA, Chiou YS, Ho SY, Lin P, Wang YJ. Suberoylanilide hydroxamic acid, an inhibitor of histone deacetylase, enhances radiosensitivity and suppresses lung metastasis in breast cancer in vitro and in vivo. PloS one. 2013;8(10):e76340. Epub 2013/10/17. doi: 10.1371/journal.pone.0076340. PubMed PMID: 24130769; PMCID: PMC3794942.

140. Tate CR, Rhodes LV, Segar HC, Driver JL, Pounder FN, Burow ME, Collins-Burow BM. Targeting triple-negative breast cancer cells with the histone deacetylase inhibitor panobinostat. Breast cancer research : BCR. 2012;14(3):R79. Epub 2012/05/23. doi: 10.1186/bcr3192. PubMed PMID: 22613095; PMCID: PMC3446342.

141. Millward M, Price T, Townsend A, Sweeney C, Spencer A, Sukumaran S, Longenecker A, Lee L, Lay A, Sharma G, Gemmill RM, Drabkin HA, Lloyd GK, Neuteboom ST, McConkey DJ, Palladino MA, Spear MA. Phase 1 clinical trial of the novel proteasome inhibitor marizomib

with the histone deacetylase inhibitor vorinostat in patients with melanoma, pancreatic and lung cancer based on in vitro assessments of the combination. Investigational new drugs. 2012;30(6):2303-17. Epub 2011/11/15. doi: 10.1007/s10637-011-9766-6. PubMed PMID: 22080430.

142. Clocchiatti A, Florean C, Brancolini C. Class IIa HDACs: from important roles in differentiation to possible implications in tumourigenesis. Journal of Cellular and Molecular Medicine. 2011;15(9):1833-46. doi: 10.1111/j.1582-4934.2011.01321.x.

143. Yuan J, Adamski R, Chen J. Focus on histone variant H2AX: To be or not to be. FEBS letters. 2010;584(17):3717-24. doi: 10.1016/j.febslet.2010.05.021.

144. Milde T, Oehme I, Korshunov A, Kopp-Schneider A, Remke M, Northcott P, Deubzer HE, Lodrini M, Taylor MD, von Deimling A, Pfister S, Witt O. HDAC5 and HDAC9 in Medulloblastoma: Novel Markers for Risk Stratification and Role in Tumor Cell Growth. Clinical Cancer Research. 2010;16(12):3240.

145. Moreno DA, Scrideli CA, Cortez MAA, De Paula Queiroz R, Valera ET, Da Silva Silveira V, Yunes JA, Brandalise SR, Tone LG. research paper: Differential expression of HDAC3, HDAC7 and HDAC9 is associated with prognosis and survival in childhood acute lymphoblastic leukaemia. British Journal of Haematology. 2010;150(6):665-73. doi: 10.1111/j.1365-2141.2010.08301.x.

146. Yang R, Wu Y, Wang M, Sun Z, Zou J, Zhang Y, Cui H. HDAC9 promotes glioblastoma growth via TAZ-mediated EGFR pathway activation. Oncotarget. 2015;6(10):7644-56. doi: 10.18632/oncotarget.3223.

147. Zhao YX, Wang YS, Cai QQ, Wang JQ, Yao WT. Up-regulation of HDAC9 promotes cell proliferation through suppressing p53 transcription in osteosarcoma. International journal of

clinical and experimental medicine. 2015;8(7):11818-23. Epub 2015/09/18. PubMed PMID: 26380023; PMCID: PMC4565406.

148. Schneider BP, Winer EP, Foulkes WD, Garber J, Perou CM, Richardson A, Sledge GW, Carey LA. Triple-Negative Breast Cancer: Risk Factors to Potential Targets. Clinical Cancer Research. 2008;14(24):8010.

149. Dent R, Trudeau M, Pritchard KI, Hanna WM, Kahn HK, Sawka CA, Lickley LA, Rawlinson E, Sun P, Narod SA. Triple-Negative Breast Cancer: Clinical Features and Patterns of Recurrence. Clinical Cancer Research. 2007;13(15):4429.

150. Rakha EA, Ellis IO. Triple-negative/basal-like breast cancer: review. Pathology. 2009;41(1):40-7. doi: https://doi.org/10.1080/00313020802563510.

151. Sung H, Jeon S, Lee KM, Han S, Song M, Choi JY, Park SK, Yoo KY, Noh DY, Ahn SH, Kang D. Common genetic polymorphisms of microRNA biogenesis pathway genes and breast cancer survival. BMC cancer. 2012;12:195. Epub 2012/05/30. doi: 10.1186/1471-2407-12-195. PubMed PMID: 22639842; PMCID: PMC3487887.

152. Liu J, Liu J, Wei M, He Y, Liao B, Liao G, Li H, Huang J. Genetic Variants in the MicroRNA Machinery Gene GEMIN4 Are Associated with Risk of Prostate Cancer: A Case-control Study of the Chinese Han Population. DNA and Cell Biology. 2012;31(7):1296-302. doi: 10.1089/dna.2011.1600.

153. Zhang X, Yang H, Lee JJ, Kim E, Lippman SM, Khuri FR, Spitz MR, Lotan R, Hong WK, Wu X. MicroRNA-related genetic variations as predictors for risk of second primary tumor and/or recurrence in patients with early-stage head and neck cancer. Carcinogenesis. 2010;31(12):2118-23. Epub 2010/09/08. doi: 10.1093/carcin/bgq177. PubMed PMID: 20819778; PMCID: PMC3105587.

154. Cascione L, Gasparini P, Lovat F, Carasi S, Pulvirenti A, Ferro A, Alder H, He G, Vecchione A, Croce CM, Shapiro CL, Huebner K. Integrated microRNA and mRNA signatures associated with survival in triple negative breast cancer. PloS one. 2013;8(2):e55910. Epub 2013/02/14. doi: 10.1371/journal.pone.0055910. PubMed PMID: 23405235; PMCID: PMC3566108.

155. Liang Z, Bian X, Shim H. Downregulation of microRNA-206 promotes invasion and angiogenesis of triple negative breast cancer. Biochemical and biophysical research communications. 2016;477(3):461-6. Epub 2016/06/19. doi: 10.1016/j.bbrc.2016.06.076. PubMed PMID: 27318091; PMCID: PMC4955785.

156. Shim H, Lau SK, Devi S, Yoon Y, Cho HT, Liang Z. Lower expression of CXCR4 in lymph node metastases than in primary breast cancers: Potential regulation by ligand-dependent degradation and HIF-1α. Biochemical and biophysical research communications. 2006;346(1):252-8. doi: https://doi.org/10.1016/j.bbrc.2006.05.110.

157. Livak KJ, Schmittgen TD. Analysis of Relative Gene Expression Data Using Real-Time Quantitative PCR and the 2−ΔΔCT Method. Methods. 2001;25(4):402-8. doi: https://doi.org/10.1006/meth.2001.1262.

158. Liang Z, Wu H, Xia J, Li Y, Zhang Y, Huang K, Wagar N, Yoon Y, Cho HT, Scala S, Shim H. Involvement of miR-326 in chemotherapy resistance of breast cancer through modulating expression of multidrug resistance-associated protein 1. Biochemical Pharmacology. 2010;79(6):817-24. doi: https://doi.org/10.1016/j.bcp.2009.10.017.

159. Liang Z, Yoon Y, Votaw J, Goodman MM, Williams L, Shim H. Silencing of CXCR4 blocks breast cancer metastasis. Cancer research. 2005;65(3):967-71. Epub 2005/02/12. PubMed PMID: 15705897; PMCID: PMC3734941.

160. Bolden JE, Peart MJ, Johnstone RW. Anticancer activities of histone deacetylase inhibitors. Nature reviews Drug discovery. 2006;5(9):769-84. Epub 2006/09/07. doi: 10.1038/nrd2133. PubMed PMID: 16955068.

161. Schuurbiers OC, Kaanders JH, van der Heijden HF, Dekhuijzen RP, Oyen WJ, Bussink J. The PI3-K/AKT-pathway and radiation resistance mechanisms in non-small cell lung cancer. Journal of thoracic oncology : official publication of the International Association for the Study of Lung Cancer. 2009;4(6):761-7. Epub 2009/05/01. doi: 10.1097/JTO.0b013e3181a1084f. PubMed PMID: 19404218.

162. Bussink J, van der Kogel AJ, Kaanders JH. Activation of the PI3-K/AKT pathway and implications for radioresistance mechanisms in head and neck cancer. The Lancet Oncology. 2008;9(3):288-96. Epub 2008/03/01. doi: 10.1016/s1470-2045(08)70073-1. PubMed PMID: 18308254.

163. Mukherjee R, McGuinness DH, McCall P, Underwood MA, Seywright M, Orange C, Edwards J. Upregulation of MAPK pathway is associated with survival in castrate-resistant prostate cancer. Br J Cancer. 2011;104(12):1920-8. Epub 2011/05/12. doi: 10.1038/bjc.2011.163. PubMed PMID: 21559022; PMCID: PMC3111196.

164. Xu H, Chen J, Xu H, Qin Z. Geographic Variations in the Incidence of Glioblastoma and Prognostic Factors Predictive of Overall Survival in US Adults from 2004–2013. Frontiers in Aging Neuroscience. 2017;9:352. doi: 10.3389/fnagi.2017.00352. PubMed PMID: PMC5681990.

165. Stupp R, Hegi ME, Mason WP, van den Bent MJ, Taphoorn MJ, Janzer RC, Ludwin SK, Allgeier A, Fisher B, Belanger K, Hau P, Brandes AA, Gijtenbeek J, Marosi C, Vecht CJ, Mokhtari K, Wesseling P, Villa S, Eisenhauer E, Gorlia T, Weller M, Lacombe D, Cairncross JG, Mirimanoff RO. Effects of radiotherapy with concomitant and adjuvant temozolomide versus radiotherapy alone on survival in glioblastoma in a randomised phase III study: 5-year analysis of

the EORTC-NCIC trial. The Lancet Oncology. 2009;10(5):459-66. Epub 2009/03/10. doi: 10.1016/s1470-2045(09)70025-7. PubMed PMID: 19269895.

166. Seto E, Yoshida M. Erasers of Histone Acetylation: The Histone Deacetylase Enzymes. Cold Spring Harbor Perspectives in Biology. 2014;6(4):a018713. doi: 10.1101/cshperspect.a018713. PubMed PMID: PMC3970420.

167. Groselj B, Sharma NL, Hamdy FC, Kerr M, Kiltie AE. Histone deacetylase inhibitors as radiosensitisers: effects on DNA damage signalling and repair. British Journal Of Cancer. 2013;108:748. doi: 10.1038/bjc.2013.21.

168. Dinarello CA, Fossati G, Mascagni P. Histone deacetylase inhibitors for treating a spectrum of diseases not related to cancer. Molecular medicine (Cambridge, Mass). 2011;17(5-6):333-52. Epub 2011/05/11. doi: 10.2119/molmed.2011.00116. PubMed PMID: 21556484; PMCID: PMC3105126.

169. Du R, Lu KV, Petritsch C, Liu P, Ganss R, Passegue E, Song H, Vandenberg S, Johnson RS, Werb Z, Bergers G. HIF1alpha induces the recruitment of bone marrow-derived vascular modulatory cells to regulate tumor angiogenesis and invasion. Cancer cell. 2008;13(3):206-20. Epub 2008/03/11. doi: 10.1016/j.ccr.2008.01.034. PubMed PMID: 18328425; PMCID: PMC2643426.

170. Lewis CE, Pollard JW. Distinct role of macrophages in different tumor microenvironments. Cancer research. 2006;66(2):605-12. Epub 2006/01/21. doi: 10.1158/0008-5472.Can-05-4005. PubMed PMID: 16423985.

171. Covington HE, 3rd, Maze I, LaPlant QC, Vialou VF, Ohnishi YN, Berton O, Fass DM, Renthal W, Rush AJ, 3rd, Wu EY, Ghose S, Krishnan V, Russo SJ, Tamminga C, Haggarty SJ, Nestler EJ. Antidepressant actions of histone deacetylase inhibitors. The Journal of neuroscience

: the official journal of the Society for Neuroscience. 2009;29(37):11451-60. Epub 2009/09/18. doi: 10.1523/jneurosci.1758-09.2009. PubMed PMID: 19759294; PMCID: PMC2775805.

172. Rooney AG, Carson A, Grant R. Depression in cerebral glioma patients: a systematic review of observational studies. Journal of the National Cancer Institute. 2011;103(1):61-76. Epub 2010/11/26. doi: 10.1093/jnci/djq458. PubMed PMID: 21106962.

173. Mann BS, Johnson JR, Cohen MH, Justice R, Pazdur R. FDA approval summary: vorinostat for treatment of advanced primary cutaneous T-cell lymphoma. The oncologist. 2007;12(10):1247-52. Epub 2007/10/27. doi: 10.1634/theoncologist.12-10-1247. PubMed PMID: 17962618.

174. Eyupoglu IY, Hahnen E, Buslei R, Siebzehnrubl FA, Savaskan NE, Luders M, Trankle C, Wick W, Weller M, Fahlbusch R, Blumcke I. Suberoylanilide hydroxamic acid (SAHA) has potent anti-glioma properties in vitro, ex vivo and in vivo. Journal of neurochemistry. 2005;93(4):992-9. Epub 2005/04/29. doi: 10.1111/j.1471-4159.2005.03098.x. PubMed PMID: 15857402.

175. Krauze AV, Myrehaug SD, Chang MG, Holdford DJ, Smith S, Shih J, Tofilon PJ, Fine HA, Camphausen K. A Phase 2 Study of Concurrent Radiation Therapy, Temozolomide, and the Histone Deacetylase Inhibitor Valproic Acid for Patients With Glioblastoma. International journal of radiation oncology, biology, physics. 2015;92(5):986-92. Epub 2015/07/22. doi: 10.1016/j.ijrobp.2015.04.038. PubMed PMID: 26194676; PMCID: PMC4510472.

176. Wang C, Eessalu TE, Barth VN, Mitch CH, Wagner FF, Hong Y, Neelamegam R, Schroeder FA, Holson EB, Haggarty SJ, Hooker JM. Design, synthesis, and evaluation of hydroxamic acid-based molecular probes for in vivo imaging of histone deacetylase (HDAC) in brain. American journal of nuclear medicine and molecular imaging. 2013;4(1):29-38. Epub 2014/01/01. PubMed PMID: 24380043; PMCID: PMC3867727.

177. Lee HZ, Kwitkowski VE, Del Valle PL, Ricci MS, Saber H, Habtemariam BA, Bullock J, Bloomquist E, Li Shen Y, Chen XH, Brown J, Mehrotra N, Dorff S, Charlab R, Kane RC, Kaminskas E, Justice R, Farrell AT, Pazdur R. FDA Approval: Belinostat for the Treatment of Patients with Relapsed or Refractory Peripheral T-cell Lymphoma. Clinical cancer research : an official journal of the American Association for Cancer Research. 2015;21(12):2666-70. Epub 2015/03/25. doi: 10.1158/1078-0432.Ccr-14-3119. PubMed PMID: 25802282.

178. Cordova JS, Shu H-KG, Liang Z, Gurbani SS, Cooper LAD, Holder CA, Olson JJ, Kairdolf B, Schreibmann E, Neill SG, Hadjipanayis CG, Shim H. Whole-brain spectroscopic MRI biomarkers identify infiltrating margins in glioblastoma patients. Neuro-Oncology. 2016;18(8):1180-9. doi: 10.1093/neuonc/now036. PubMed PMID: PMC4933486.

179. Barajas RF, Phillips JJ, Parvataneni R, Molinaro A, Essock-Burns E, Bourne G, Parsa AT, Aghi MK, McDermott MW, Berger MS, Cha S, Chang SM, Nelson SJ. Regional variation in histopathologic features of tumor specimens from treatment-naive glioblastoma correlates with anatomic and physiologic MR Imaging. Neuro-Oncology. 2012;14(7):942-54. doi: 10.1093/neuonc/nos128. PubMed PMID: PMC3379808.

180. Wen PY, Macdonald DR, Reardon DA, Cloughesy TF, Sorensen AG, Galanis E, Degroot J, Wick W, Gilbert MR, Lassman AB, Tsien C, Mikkelsen T, Wong ET, Chamberlain MC, Stupp R, Lamborn KR, Vogelbaum MA, van den Bent MJ, Chang SM. Updated response assessment criteria for high-grade gliomas: response assessment in neuro-oncology working group. Journal of clinical oncology : official journal of the American Society of Clinical Oncology. 2010;28(11):1963-72. Epub 2010/03/17. doi: 10.1200/jco.2009.26.3541. PubMed PMID: 20231676.

181. Stadlbauer A, Buchfelder M, Doelken MT, Hammen T, Ganslandt O. Magnetic resonance spectroscopic imaging for visualization of the infiltration zone of glioma. Central European

neurosurgery. 2011;72(2):63-9. Epub 2010/07/17. doi: 10.1055/s-0030-1253410. PubMed PMID: 20635312.

182. Stadlbauer A, Nimsky C, Buslei R, Pinker K, Gruber S, Hammen T, Buchfelder M, Ganslandt O. Proton magnetic resonance spectroscopic imaging in the border zone of gliomas: correlation of metabolic and histological changes at low tumor infiltration--initial results. Investigative radiology. 2007;42(4):218-23. Epub 2007/03/14. doi: 10.1097/01.rli.0000255812.61435.67. PubMed PMID: 17351427.

183. Wei L, Hong S, Yoon Y, Hwang SN, Park JC, Zhang Z, Olson JJ, Hu XP, Shim H. Early prediction of response to Vorinostat in an orthotopic rat glioma model. NMR in biomedicine. 2012;25(9):1104-11. Epub 2012/02/04. doi: 10.1002/nbm.2776. PubMed PMID: 22302519; PMCID: PMC3356508.

184. Yankelevitch-Yahav R, Franko M, Huly A, Doron R. The forced swim test as a model of depressive-like behavior. Journal of visualized experiments : JoVE. 2015(97). Epub 2015/04/14. doi: 10.3791/52587. PubMed PMID: 25867960; PMCID: PMC4401172.

185. Maudsley A, Domenig C, editors. Signal normalization for MR spectroscopic imaging using an interleaved water-reference. International Society for Magnetic Resonance in Medicine; 2008.

186. Maudsley AA, Domenig C, Govind V, Darkazanli A, Studholme C, Arheart K, Bloomer C. Mapping of brain metabolite distributions by volumetric proton MR spectroscopic imaging (MRSI). Magnetic resonance in medicine. 2009;61(3):548-59. Epub 2008/12/30. doi: 10.1002/mrm.21875. PubMed PMID: 19111009; PMCID: PMC2724718.

187. Cordova JS, Gurbani SS, Olson JJ, Liang Z, Cooper LA, Shu HG, Schreibmann E, Neill SG, Hadjipanayis CG, Holder CA, Shim H. A systematic pipeline for the objective comparison of whole-brain spectroscopic MRI with histology in biopsy specimens from grade III glioma.

Tomography (Ann Arbor, Mich). 2016;2(2):106-16. Epub 2016/08/05. doi: 10.18383/j.tom.2016.00136. PubMed PMID: 27489883; PMCID: PMC4968944.

188. Persons JB, Thase ME, Crits-Christoph P. The role of psychotherapy in the treatment of depression: review of two practice guidelines. Archives of general psychiatry. 1996;53(4):283-90. Epub 1996/04/01. PubMed PMID: 8634003.

189. Trivedi MH, Kern JK, Grannemann BD, Altshuler KZ, Sunderajan P. A computerized clinical decision support system as a means of implementing depression guidelines. Psychiatric services (Washington, DC). 2004;55(8):879-85. Epub 2004/08/05. doi: 10.1176/appi.ps.55.8.879. PubMed PMID: 15292537.

190. Moreau P, Facon T, Touzeau C, Benboubker L, Delain M, Badamo-Dotzis J, Phelps C, Doty C, Smit H, Fourneau N, Forslund A, Hellemans P, Leleu X. Quisinostat, bortezomib, and dexamethasone combination therapy for relapsed multiple myeloma. Leukemia & lymphoma. 2016;57(7):1546-59. Epub 2016/01/14. doi: 10.3109/10428194.2015.1117611. PubMed PMID: 26758913.

191. Hanahan D, Weinberg RA. Hallmarks of cancer: the next generation. Cell. 2011;144(5):646-74. Epub 2011/03/08. doi: 10.1016/j.cell.2011.02.013. PubMed PMID: 21376230.

192. Qin L, Kufareva I, Holden LG, Wang C, Zheng Y, Zhao C, Fenalti G, Wu H, Han GW, Cherezov V, Abagyan R, Stevens RC, Handel TM. Crystal structure of the chemokine receptor CXCR4 in complex with a viral chemokine(). Science (New York, NY). 2015;347(6226):1117-22. doi: 10.1126/science.1261064. PubMed PMID: PMC4362693.